PHOTOINDUCED ELECTRON TRANSFER AND ITS APPLICATIONS IN SOME $Ru(bpy)_3^{2+}$ BASED DONOR-ACCEPTOR SYSTEMS

THESIS SUBMITTED TO
THE UNIVERSITY OF KERALA
FOR THE DEGREE OF
DOCTOR OF PHILOSOPHY
IN CHEMISTRY
UNDER THE FACULTY OF SCIENCE

By

AJAYAKUMAR, G.

UNDER THE SUPERVISION OF

Dr. K. R. GOPIDAS

PHOTOSCIENCES AND PHOTONICS
CHEMICAL SCIENCES AND TECHNOLOGY DIVISION
NATIONAL INSTITUTE FOR INTERDISCIPLINARY SCIENCE AND TECHNOLOGY (CSIR)
TRIVANDRUM - 695019
KERALA, INDIA

DECEMBER 2008

STATEMENT

I hereby declare that the matter embodied in the thesis entitled, **"Photoinduced Electron Transfer and Its Applications in Some $Ru(bpy)_3^{2+}$ Based Donor-Acceptor Systems"** are results of investigations carried out by me at the Photosciences and Photonics Section, Chemical Sciences and Technology Division of the National Institute for Interdisciplinary Science and Technology (CSIR), Trivandrum, under the supervision of Dr. K. R. Gopidas and the same has not been submitted elsewhere for a degree.

In keeping with the general practice of reporting scientific observations, due acknowledgement has been made wherever the work described is based on the findings of other investigators.

Ajayakumar, G.

NATIONAL INSTITUTE FOR INTERDISCIPLINARY SCIENCE AND TECHNOLOGY

(Formerly Regional Research Laboratory)

Council of Scientific & Industrial Research (CSIR)
Industrial Estate P.O.,Trivandrum – 695 019
Kerala, INDIA.

Dr. K. R. Gopidas
Scientist F
E-mail: gopidaskr@rediffmail.com

Tel : 0471-2515 390
Fax : 0471-2490186

December 22, 2008

CERTIFICATE

This is to certify that the work embodied in the thesis entitled, **"Photoinduced Electron Transfer and Its Applications in Some $Ru(bpy)_3^{2+}$ Based Donor-Acceptor Systems"** has been carried out by Mr. Ajayakumar, G., under my supervision and the same has not been submitted elsewhere for a degree.

K. R. Gopidas

(Thesis Supervisor)

ACKNOWLEDGEMENTS

It is with immense pleasure that I express my deep sense of gratitude to my research supervisor Dr. K. R. Gopidas, for suggesting the research topic and for his guidance, constant support and encouragement that led to the successful completion of this work.

I express my sincere thanks to Professor M. V. George for his inspiration, motivation and moral support during the course of this work.

I wish to thank Dr. B. C. Pai and Professor T. K. Chandrashekar, present and former Directors, NIIST, Trivandrum, for providing me with necessary facilities for carrying out this work.

My sincere thanks are also due to:

- *Dr. Suresh Das, Dr. A. Ajayaghosh, Dr. K. George Thomas, Dr. D. Ramaiah and Dr. A. Srinivasan, the scientists of Photosciences and Photonics Group, for all their help and support.*
- *Dr. C. H. Suresh, CMS section for his help and advice.*
- *Dr. K. P. Jaya (Mrs. K. R. Gopidas) for her care, motivation and affection.*
- *Mr. Robert Philip and Mrs. Sarada Nair, Photosciences and Photonics Group, for their help and support.*
- *Mrs. Soumini Mathew for NMR analysis , Mrs. S. Viji for HRMS analysis, Ms. Priya A. Nair for IR and GC-MS analysis and Mr. B. Adarsh for NMR analysis.*
- *My seniors, Dr. S. Sumalekshmy and Dr. Bijitha Balan for their help and support.*
- *My colleagues K. Sreenath, C.V. Suneesh, V. K. Ratheeshkumar, Deepthi. L. Sivadas, A. M. Rakhi, K. Retheesh, M. V. Vinayak, Tony George Thomas and all other members of Photosciences and Photonics Group for their valuable help and affection.*
- *All friends in other divisions of NIIST, Trivandrum for their help and support.*
- *Council of Scientific and Industrial Research (CSIR) and Department of Science and Technology (DST), Government of India, for the financial assistance.*

I am deeply grateful to my brother Sreekumar, G., for his invaluable care and support.

Finally, I thank the Almighty for everything.

Ajayakumar, G.

PREFACE

Study of photoinduced electron transfer (PET) between donor (D) and acceptor (A) systems is an extremely active area of research and it plays the pivotal role in the design of artificial photosynthetic systems. Understanding the dynamics of PET helps scientists to design potential systems for artificial photosynthesis, which ultimately aims in mimicking green plants and other photosynthetic organisms that are using sunlight to make high energy chemicals. Ruthenium complexes containing derivatives of 2,2'-bipyridines (bpy) as ligands have been extensively used by chemists for PET reactions because of their unique photophysical and electrochemical properties. In the present thesis, the synthesis, photophysical investigations and some applications in metal ion sensing of a novel class of $Ru(bpy)_3^{2+}$ based donor-acceptor systems are described.

The first chapter provides an overview of the photophysics of $Ru(bpy)_3^{2+}$ based systems with particular emphasis on PET studies. A brief discussion of the PET events occurring in various covalently linked donor-acceptor systems (dyads, triads, tetrads etc.) in general, and $Ru(bpy)_3^{2+}$ based systems in particular, is presented. Potential applications of some $Ru(bpy)_3^{2+}$ based systems reported for ion sensing also are included in this chapter.

In Chapter 2 of the thesis we present the synthesis, photophysical and electron transfer studies of a few $Ru(bpy)_3^{2+}$-Phenothiazine (abbreviated as Ru-Ptz) dyads. These dyads have one, two or three Ptz ligands (**Ru-Ptz**, **Ru-Ptz$_2$** and **Ru-Ptz$_3$**, respectively) covalently linked to the bpy moieties through an amide linkage. Rates of forward

electron transfer are gradually increased with respect to the number of Ptz units. The PET rates observed are one order higher than the similar class of $Ru(bpy)_3^{2+}$-$(CH_2)_n$-Ptz dyads. These dyads exhibit CS state lifetimes in the 10-30 ns range, which is about 100 times higher compared to previously reported $Ru(bpy)_3^{2+}$ based dyads. In order to explain these two favorable aspects of photoinduced charge separation, a particular structural orientation of the **Ru-Ptz** system is assumed.

The third chapter describes the synthesis and PET studies of some higher order donor-acceptor systems. As a continuation of the results summarised in the second chapter we have investigated Ru-Ptz systems containing one, two or three bpy-Ptz_2 ligands attached to Ru^{2+}. These systems contain two, four and six phenothiazine moieties and are designated as, **Ru-Ptz$_{2(S)}$**, **Ru-Ptz$_4$** and **Ru-Ptz$_6$**, respectively. Better forward electron transfer rates than the previous dyads are observed in these systems. We also present some secondary electron transfer studies in which the ET occurs from the CS state to electron acceptors such as dodecylviologen and pyromellitic diimide. The secondary electron transfer to the CS state from donors like trimethoxytriphenylamine also is discussed. Very long-lived products are obtained by the secondary electron transfer. Following to the long lived CS state observed for the **Ru-Ptz$_{2(S)}$** system, synthesis and PET studies of one $Ru(bpy)_3^{2+}$ based triad system **Ptz-Ru-NT** (NT = nitrotoluene) also has been completed.

In Chapter 4 of the thesis we present a study of the metal ion sensing ability of **Ru-Ptz** dyad. We show that **Ru-Ptz** can act as a “turn-ON” luminescence

chemodosimeter for Cu^{2+}. This study is based on our observation that Cu^{2+} oxidizes Ptz to phenothiazine-5-oxide (PtzO) in acetonitrile. Addition of Cu^{2+} in acetonitrile converts the non-luminescent **Ru-Ptz** to the luminescent $Ru(bpy)_3^{2+}$-PtzO, which forms the basis of Cu^{2+} detection by **Ru-Ptz**. None other than Cu^{2+} in the sixteen metal ions tested is capable of this reaction and hence **Ru-Ptz** is very selective towards Cu^{2+}. The metal ions sensing studies with other three derivatives (**Ru-Ptz$_2$**, **Ru-Ptz$_3$** and **Ru-Ptz$_{2(S)}$**) also are presented. The experiments on the selective detection of Fe^{3+} ions by **Ru-Ptz** in methanol also are discussed in this chapter.

CONTENTS

CHAPTER 1

Photoinduced Electron Transfer (PET) in $Ru(bpy)_3^{2+}$ Based Systems: An Overview

1.1. Introduction

Electron Transfer (ET) is a ubiquitous chemical process, which plays a central role in various crucial events in Chemistry and Biology.[1] It involves the transfer of an electron from a donor molecule (D) to an acceptor molecule (A) without making or breaking of chemical bonds. Electron transfer reactions occur both thermally and photochemically. The latter reactions, referred to as photoinduced electron transfer (PET) reactions, take place following light absorption by the donor or acceptor. Nature utilizes this process in the photosynthetic reaction centre in order to convert solar energy into chemical energy.[2] Extensive research activities have been going on in the area of PET for the last several decades.[3] Understanding the process of PET helps scientists to design potential systems for artificial photosynthesis, which ultimately aims in mimicking green plants and other photosynthetic organisms that are using sunlight to make high-energy chemicals.[4]

PET can be either intramolecular or intermolecular depending on whether the D and A units are linked or not (Schemes 1.1 and 1.2). PET results in the formation of product ions (donor radical cation $D^{\bullet+}$ and acceptor radical anion $A^{\bullet-}$) which are at

higher energy levels compared to the starting D and A. The term 'conversion of solar energy into chemical energy' actually means the generation of a high energy charge separated (CS) state by the way of light absorption. As shown in Schemes 1.1 and 1.2, the CS state is generally short lived and undergo 'back electron transfer' (BET) to generate the D-A system in their ground state thereby leading to wastage of the absorbed energy.

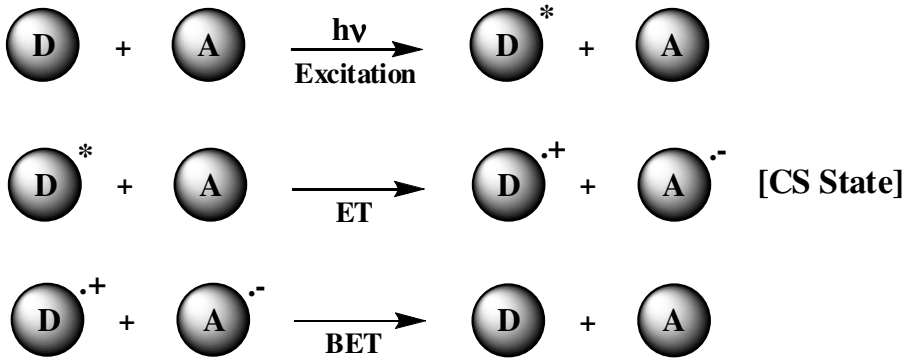

Scheme 1.1. Schematic of PET and BET in intermolecular D-A systems

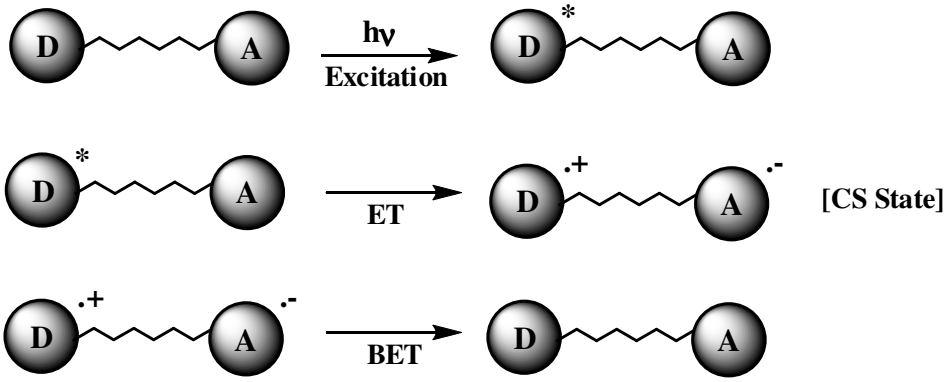

Scheme 1.2. Schematic of PET and BET in covalently linked D-A systems

In Schemes 1.1 and 1.2, BET represents the energy wasting back electron transfer reaction. In simple donor-acceptor systems, $D^{\bullet+}$ and $A^{\bullet-}$ are formed at close proximity which facilitates the BET reaction. BET reaction reduces the yield and lifetime of the charge separated state. This energy wasting step is the serious limitation of PET reactions of simple D-A systems. A large number of D-A systems have been studied in order to elucidate the charge separation and recombination mechanisms and also to assess the efficiency and practical applicability of such molecular systems. These studies have led to important advances in the theory and practice of electron-transfer reactions.[3] Studies on the photophysical and photochemical processes involved in the natural photosynthetic reaction center also have guided the efforts in this direction.

Photosynthetic reactions centers (RCs), considered as nature's solar batteries, are excellent models for understanding the dynamics of photoinduced electron transfer. They are integral membrane proteins, where rapid sequential electron transfers occur resulting in efficient charge separation across the membrane, establishing an electrochemical potential, ultimately leading to the energy conversion. One of the milestones in the exploration of the photosynthetic reaction center was the crystallization and structure determination of the RC protein from the purple bacterium *Rhodopseudomonas* (*Blastochloris*) *viridis*[5] by Huber, Michel and Deisenhofer in 1984. Structure of the RC in the related *Rhodobacter sphaeroides* (Figure 1.1) was established a few years later.[6] The purple bacterial RC remains as the best 'model system' for understanding basic structure and functions important for the efficient photochemistry

in both natural and artificial photosynthetic complexes. The RC in *Rhodobacter sphaeroides* consists of three 30-35 kDa protein subunits, L, M and H, and nine cofactors: four bacteriochlorophyll (Bchl) molecules (two of which make up a "special pair", P), two bacteriopheophytin ($H_{A/B}$) molecules, two quinine ($Q_{A/B}$) molecules, and one non-heme iron atom (Figure 1.1).

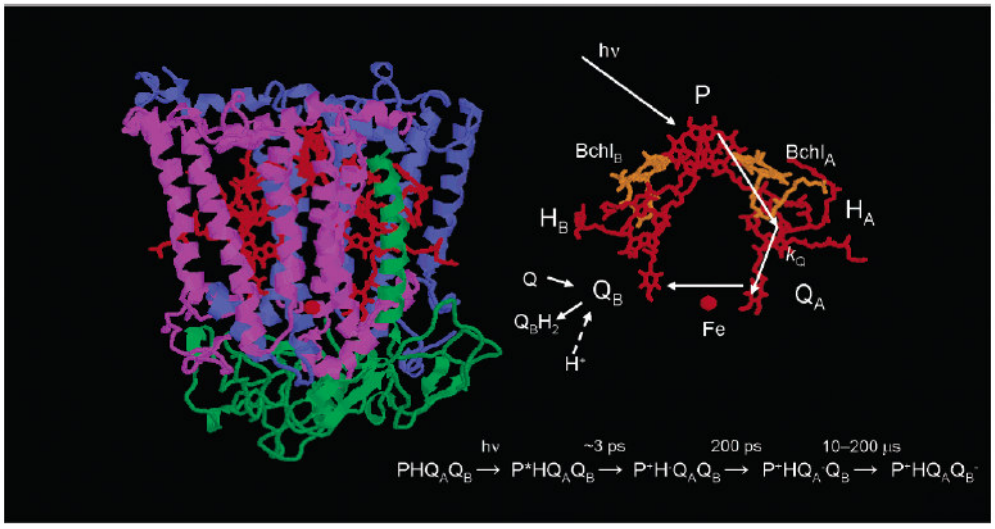

Figure 1.1. Reaction center from *Rb. sphaeroides* including three protein subunits, L (blue), M (purple), and H (green), the cofactors (red), and the electron-transfer pathway and proton uptake at Q_B.

Electron transfer is initiated in the RC following photo-excitation of P, which transfers an electron to H_A to form the radical pair $P^{\oplus}H_A^{\ominus}$ within 3 ps of photoexcitation of P. The electron is transferred from $H_A^{\ominus}$ to the primary quinone acceptor (Q_A) within ~200 ps, yielding the charge-separated state $P^{\oplus}H_AQ_A^{\ominus}$. In about 200 μs, the electron reaches the final quinone acceptor, Q_B. After a two-electron, two-proton reduction, Q_BH_2 is released from the RC. The free hydroquinone is oxidized by cytochrome bc_1

complex, thereby releasing quinol protons into the periplasm. This creates a trans-membrane proton gradient which is utilized for ATP synthesis. As a result of the series of sequential electron transfers, the final charge separated state is achieved with unit efficiency. Since in the final stage the oppositely charged counterparts are separated by a thick layer of protein, the energy wasting back electron transfer is completely avoided.

Considerable effort has been devoted in designing artificial modules that can mimic photosynthesis in the laboratory. This led to the development of multi-component systems containing donor and/or acceptor units attached to a photosensitizer aiming at the creation of long-lived CS states. A large number of covalently linked D-A systems such as dyads (D-A), triads (D-A_1-A_2 or D_1-D_2-A), and tetrads (D-A_1-A_2-A_3, D_1-D_2-D_3-A etc) have been synthesized and studied as part of this effort. A few of these systems will be reviewed in the following section.

1.2. Photoinduced Electron Transfer in Donor -Acceptor Dyads

A number of simple D-A dyads have been developed to understand the dynamics of electron transfer processes in natural photosynthesis. Compared to the higher order systems, the dyads are easy to synthesize. The major disadvantage in these systems is the rapid BET process. Example of a dyad synthesized and studied by Holten *et al*.[7] is presented in Figure 1.2. The dyad consists of a perylene-*bis*(imide) dye (PDI) connected to zinc porphyrin (Zn) via a diphenylethyne (pep) linker (**1**). Excitation of PDI leads to energy transfer to porphyrin, followed by electron transfer from the excited porphyrin to the PDI. The charge separated state PDI^--pep-Zn^+ generated was characterized by laser flash photolysis studies. In the non-polar solvent (toluene), the

charge-transfer product has a lifetime of >10 ns and decays to the ground state by charge recombination. In a polar solvent (acetonitrile), the PDI^{-}-pep-Zn^{+} charge-separated state decays much more rapidly (< 0.5 ns). It was reported that the initial energy transfer occurred with 80% efficiency and the electron transfer process was 99% efficient. The quantum yield of the charge separated state (Φ_{CS}) was 50% in toluene and 55% in acetonitrile.

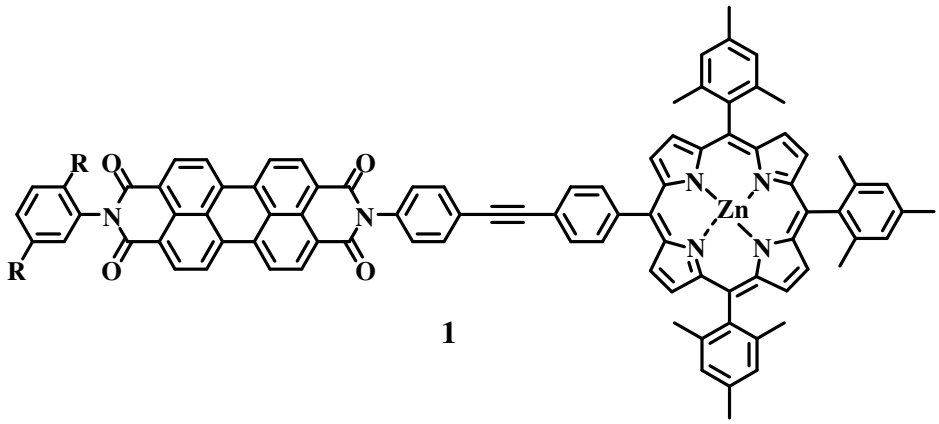

1

Figure 1.2

Majima *et al.* investigated the PET processes in dyads (**2**, Figure 1.3), where the donor tetrathiophene (4T) moiety is linked to monocyclic aromatic acceptors (Ph-R, where R is an electron withdrawing group).[8] They observed ultrafast (k_{CS} of 5×10^{12} s^{-1}) CS state formation in these systems. The high value of k_{CS} was attributed to the large electronic coupling matrix element between the donor and acceptor. Even though this class of systems exhibit very high quantum yield of charge separation (Φ_{CS} ~ 0.99), charge recombination rates also were fast because of enhanced super-exchange interaction through the amide spacer. The fast recombination in this system leads to the

formation of a triplet state (^{3}4T*-Ph-X) which was characterized by laser flash photolysis experiments.

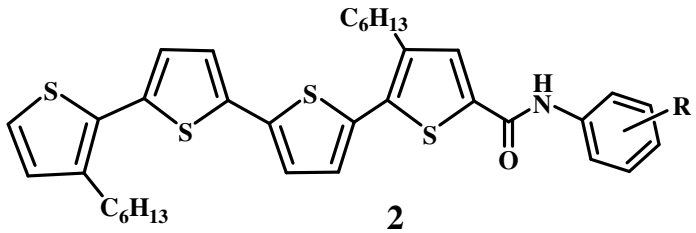

2

R = 4-H
4-CN
3,4-$(CN)_2$
4-NO_2
3,5-$(NO_2)_2$

Figure 1.3

Photoinduced electron transfer in platinum(II) terpyridinyl acetylide - porphyrin dyads were studied by Hammarstrom *et al*.[9] A series of dyads with zinc or magnesium porphyrins attached to platinum terpyridine acetylide complex via a *para*-phenylene bisacetylene spacer (**3**, Figure 1.4) were synthesized. Excitation of the porphyrin unit leads to very rapid electron transfer (2-20 ps) to the platinum complex. The subsequent recombination of the charge transfer state was more rapid. Charge recombination resulting in the regeneration of the ground state reactants followed the same kinetics as the decay of the porphyrin excited state. This prevented any observation of the CS state. Femtosecond transient absorption studies in those systems could not give any evidences of ET products. Only transient absorptions corresponding to the S_1 (singlet) and T_1 (triplet) states of the porphyrin moiety were observed. By changing the substituents in the terpyridine ligand and the metal complexed to porphyrin, it was shown that the redox potentials and the excited-state properties of the system could be varied.

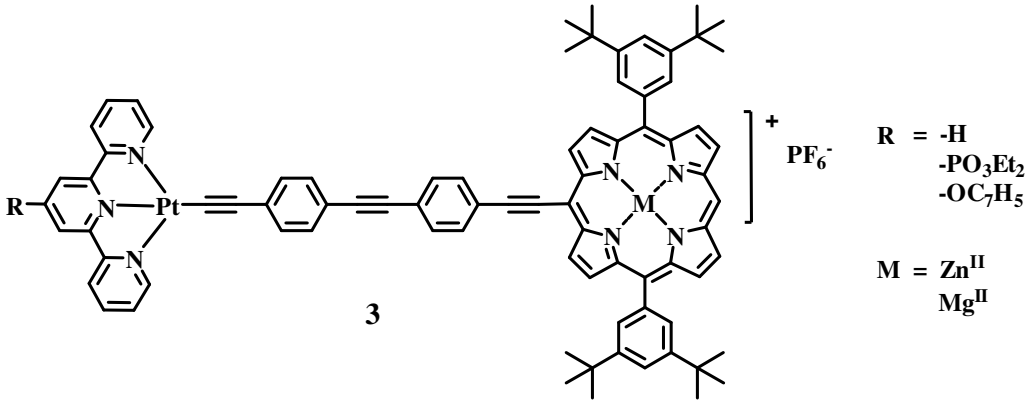

3

Figure 1.4

Directly linked porphyrin-ferrocene dyads designed by Nakashima *et al.*[10] also have shown ultrafast photoinduced charge separation (**4**, Figure 1.5). Here the ferrocene (Fc) moiety is covalently linked to the *meso* position of 3,5-di-*tert*-butylphenyl zinc porphyrin (BPZnP-Fc), pentafluorophenyl zinc porphyrin (FPZnP-Fc), or 3,5-di-*tert*-butylphenyl free-base porphyrin (BPH_2P-Fc) units. In these systems PET could occur from the S_2 or S_1 state of porphyrin. Charge separation and recombination were confirmed by transient absorption spectra, and lifetimes of the CS states (~ 20 ps) were estimated from the decay rate of the porphyrin radical anion absorptions. The k_{CS} were found to be $>10^{13}$ s^{-1} from the S_2 state and 6.3×10^{12} s^{-1} from the S_1 state.

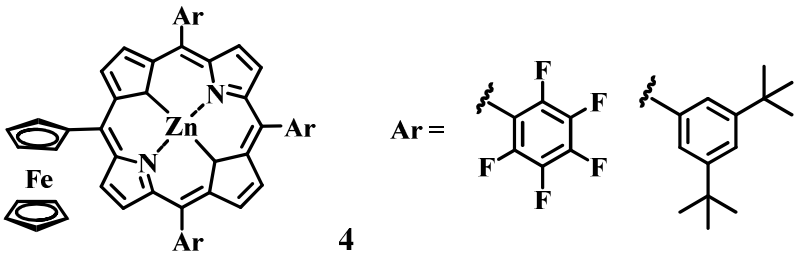

4

Figure 1.5

Even though a large number of dyad systems reported in literature exhibit very good PET rates, most of them suffer from the problem of high rates of charge recombination. The CS states in these cases could be observed only in ultra low time scales (≤ ps). Within the entire family of D-A dyads, systems possessing high PET and low BET rates are very few in number. Dyads based on the fullerene (C_{60}) motifs are examples of such systems possessing unusually low charge recombination rates.

In the Zinc chlorin-C_{60} dyad[11] (**5**, Figure 1.6), efficient PET occurs from the ^{1}Zn-Chlorin* to the C_{60} acceptor. Charge separation occurs within 10 ps, with a quantum yield of 12%. The charge recombination, however, was surprisingly slow (230 μs at 25 °C). The authors attributed the longer lifetime of the CS state to inverted region effects. Electron transfer rates in the inverted region are expected to be very small.

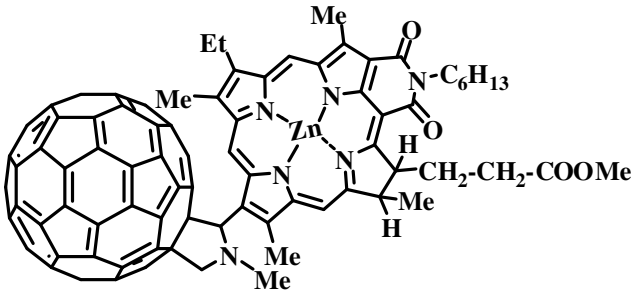

5

Figure 1.6

This system was reinvestigated by Verhoeven *et al.*[13] who suggested that the long lifetime could be due to the possible intersystem crossing of the singlet charge transfer state (^{1}CT) to a longer lived triplet (^{3}CT) state. The low quantum yield and higher lifetime of the CT state could be supported by this hypothesis without emphasizing the 'invert-region effect'. The small reorganization energy and favourable

acceptor properties of fullerene derivatives have attracted great interest in recent years, giving rise to the generation of a number of C_{60} based donor-acceptor dyads and triads.[14]

Fukuzumi *et al.*[15] have reported a simple dyad system, namely 9-mesityl-10-methylacridinium ion (Acr^+-Mes, **6**, Figure 1.7) in which an electron donor (mesityl) group is directly connected at the 9-position of the acceptor acridinium ion, possessing exceptional PET properties. The CS state ($Acr^{\bullet}$-$Mes^{\bullet+}$), characterized by laser flash photolysis experiments was very long-lived; with lifetimes from microseconds in solution to many hours and even years at low temperature in solid matrix with an excellent quantum efficiency of ~98%. Here also the large dependence of the BET rate with temperature (as in the case of Zinc chlorin-C_{60} system **5**) led the authors to the conclusion that charge recombination could be occurring in the inverted Marcus region with extremely low rate compared to the ultrafast forward electron transfer. It is claimed that the dyad is surpassing the natural photosynthetic system both in the lifetime and yield of the charge separated state.

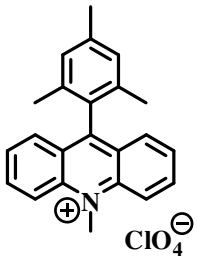

6

Figure 1.7

Verhoeven *et al*. have reinvestigated[13,16] the PET properties of **6** and pointed out that the exceptionally long-lived transients observed in the laser flash photolysis most probably could be the triplet-triplet (T_1-T_n) absorption of the acridinium chromophore. This species could arise from the ^{1}CS state ^{1}(Acr$^{\bullet}$-Mes$^{\bullet+}$) by BET and hence the claim of long-lived CS state formation in this case remains controversial.

1.3. PET in $Ru(bpy)_3^{2+}$ Based D-A Systems

1.3.1. Ruthenium *tris*(bipyridyl) Systems

Tris(2,2'-bipyridyl)dichlororuthenium(II), abbreviated as $Ru(bpy)_3^{2+}$ and known as the 'king of inorganic complexes', is one of the most extensively used systems in the study of photoinduced electron transfer and artificial photosynthesis. As one of the few transition metal complexes that emits strongly in solution at room temperature and exhibits powerful photosensitization capabilities for electron- and energy-transfer processes, it has gained a great amount of attention for the past thirty years.[17] Solar water splitting studies using $Ru(bpy)_3^{2+}$ has been an area of particular interest.[18]

Structure and absorption spectrum of $Ru(bpy)_3^{2+}$ is shown in Figure 1.8. $Ru(bpy)_3^{2+}$ possesses an octahedral (Oh) geometry with a d^6 electronic configuration like in the case of Fe^{2+}. When coordinated with the bipyridine (bpy) ligands, the molecular orbitals are localized on the metal or on the ligands. Different electronic transitions are possible between these molecular orbitals, which are: (1) Metal to ligand charge transfer (MLCT), where an electron is transferred from the metal orbitals to the bipyridine orbitals, (2) Ligand to metal charge transfer (LMCT), (3) Metal centered

(MC) transitions between orbitals localized on the metal and (4) Ligand centered transitions (LC) between orbitals mainly localized on ligands. Among the different transitions possible in $Ru(bpy)_3^{2+}$ complexes (Figure 1.8 b), generally the lowest energy transition is the ^{1}MLCT transition corresponding to the t_{2g} (π_M) molecular orbital to the π^* molecular orbital of the ligand (Scheme 1.3), which is observed as the broad band centered around 450 nm. The ligand centered transitions from the π orbital to π^* orbital corresponds to the high intensity absorption in the UV region. The absorptions observing around 350 nm corresponds to the metal centered transitions, which are very weak in terms of the intensity. The high energy LMCT bands are not observed in the absorption spectrum of $Ru(bpy)_3^{2+}$, but for the oxidized form $Ru(bpy)_3^{3+}$ the LMCT state is the lowest energy state.

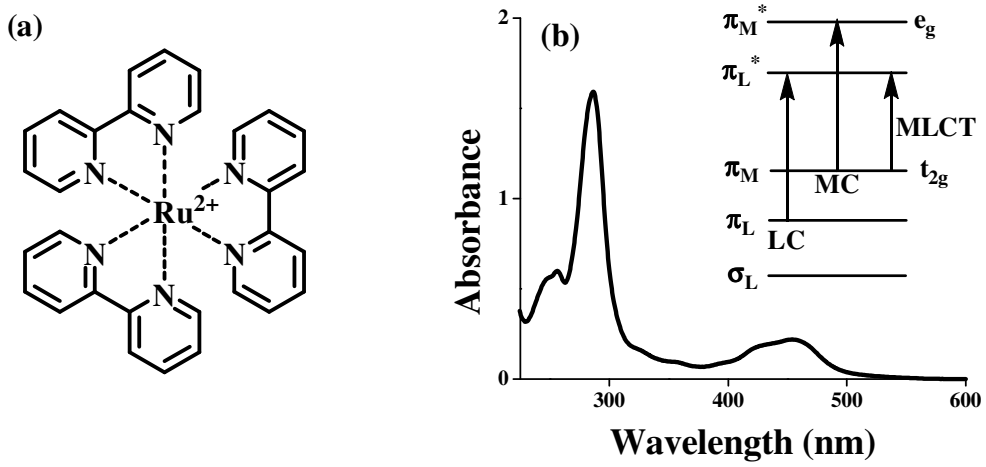

Figure 1.8. (a) Structure and (b) absorption spectrum of $Ru(bpy)_3^{2+}$. Inset in (b) shows energy levels in $Ru(bpy)_3^{2+}$.

$$[Ru^{II}(bpy)_3]^{2+} \xrightarrow{h\nu} [(bpy)_2Ru^{III}(bpy^{\cdot-})]^{2+} \quad [MLCT]$$

$$(d\pi)^6 \qquad\qquad (d\pi)^5(\pi^*)^1$$

Scheme 1.3

The excited state energy in the $Ru(bpy)_3^{2+}$ systems is proposed to be localized in one of the three bipyridine ligands at a time and the exchange of this energy between the ligands occur in an ultrafast time scale (of the order of a few femtoseconds). The emission observed from $Ru(bpy)_3^{2+}$ systems are explained to be from the lowest energy triplet state (^{3}MLCT), which is formed by the rapid intersystem crossing ($\tau \approx 100$ fs) from the ^{1}MLCT state with almost 100% efficiency. The decay of the ^{3}MLCT state is highly dependent on temperature and oxygen present in the medium. In water, $*Ru(bpy)_3^{2+}$ shows a variation of luminescence lifetime from 0.6 μs to 5 μs with a change from room temperature to 77 K. The luminescence quantum yield shows an analogous change from 0.04 to 0.4 under the same conditions. At room temperature, $*Ru(bpy)_3^{2+}$ possesses sufficient lifetime in the excited state to participate in bimolecular and intramolecular photochemical processes. It is interesting to note that the excited state energy of the ruthenium polypyridyl systems can be altered using different bipyridine ligands. When different ligands are used, the lowest MLCT state will be localized on that ligand which is easiest to reduce. The electron withdrawing and donating nature of the ligands can be tuned by varying the substituents attached to the bipyridine ligands.

A fundamental requirement for participating in electron transfer reactions is the stability of the oxidized and/or reduced forms, i.e. the reversibility of the oxidation and/or reduction processes in the ground state. Due to the high energy content, $*Ru(bpy)_3^{2+}$ can act as reductant and oxidant. Apart from the inherent decay pathways, electron transfer and energy transfer are the main modes of deactivation of the excited state. The deactivation by electron transfer can be either the oxidative electron transfer where $*Ru(bpy)_3^{2+}$ transfers an electron to an acceptor or the reductive electron transfer where the electron transfer is from a donor to $*Ru(bpy)_3^{2+}$ (Scheme 1.4).

$$*Ru(bpy)_3^{2+} + A \longrightarrow Ru(bpy)_3^{3+} + A^{\bullet -} \quad \textbf{(Oxidative Quenching)}$$

$$*Ru(bpy)_3^{2+} + D \longrightarrow Ru(bpy)_3^{+} + D^{\bullet +} \quad \textbf{(Reductive Quenching)}$$

Scheme 1.4

Depending on the nature of the quencher, either of the above mechanisms can be operative.

1.3.2. $Ru(bpy)_3^{2+}$ Based Dyads

A unique combination of photophysical and redox properties makes derivatives of Ru-$(bpy)_3^{2+}$ as ideal candidates for use as photosensitizers for PET reactions.[17] A large number of Ru(II) polypyridyl based donor-acceptor systems have been reported[19] in literature, which include dyads and triads where, readily reducible organic moieties (such as methyl Viologen, MV^{2+}) or readily oxidizable moieties (such as phenothiazine,

Ptz) are attached to $Ru(bpy)_3^{2+}$ to give Ru(II)-A, Ru(II)-D and D- Ru(II)-A systems. Few examples of such systems are discussed here.

Highlighting the concept of artificial photosynthesis, several systems have been made based on manganese(II) and tyrosine covalently linked to $Ru(bpy)_3^{2+}$.[20] The aim was to investigate the feasibility of electron transfer from Mn(II) or tyrosine to photo-oxidized Ru(III). Hammarstrom *et al*. studied the PET processes in **7** (Figure 1.9) in the presence of MV^{2+}. They observed that the Ru(III) formed as a result of PET to MV^{2+} is involved in a slow intramolecular electron transfer with the Mn(II) centre with a rate constant of 1.8×10^5 s^{-1}. But the inherent disadvantage of this system is the energy transfer from $^*Ru(bpy)_3^{2+}$ to the manganese moiety. It also suffers from the serious limitation of decomposition of the Mn(II) from the complex during the photoinduced processes. However, the PET occurring in **7** is assessed to be an important step for further development of artificial systems mimicking the donor side in photosystem II.

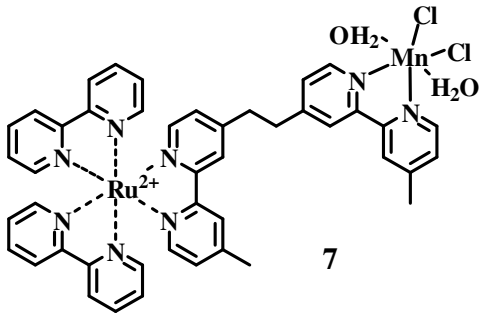

7

Figure 1.9

A number of different acceptors have been linked to the $Ru(bpy)_3^{2+}$ chromophore. Among these, viologens are the most widely used[21]. Quinones[22] and naphthalenediimides[23] also have been used as acceptors. All these systems offer

different possibilities in terms of synthesis, redox and spectroscopic properties, and stability. Mallouk *et al*. have investigated a series of dyads where $Ru(bpy)_3^{2+}$ is covalently linked to viologen acceptor[24] (**8**, Figure 1.10). PET properties were studied by picosecond laser flash photolysis experiments, which showed spectral features attributable to a ruthenium bipyridyl MLCT state and a Ru(III)-$MV^{\bullet+}$ charge separated state. The MLCT state is characterized by a broad absorbance maximum around 370 nm and bleaching of the ground-state absorbance at 450 nm, whereas the latter is characterized by a sharp absorbance peak at 400 nm and bleaching at 450 nm. Lifetimes of the CS state were in the range of 60-120 ps.

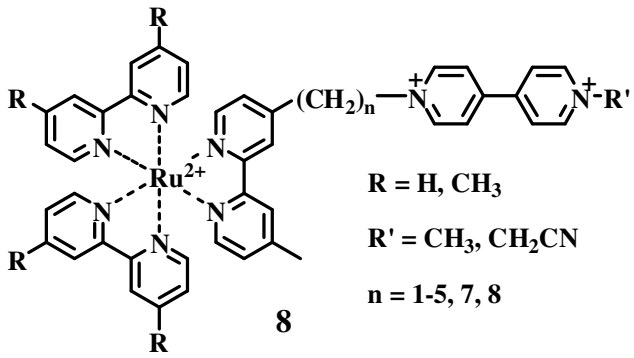

8

Figure 1.10

Mallouk *et al*. also studied the distance dependence of electron transfer[21h] in **8** where n = 1-5, 7, 8. They observed that the rate of intramolecular PET in the series varied exponentially with the number of carbon atoms in the spacer chain up to n = 5, and thereafter remained constant. It was concluded that a "through bond" electron transfer operates in systems with short spacers; while a "through solvent" ET pathway operates in the case of systems with long spacers. PET rates were in the range of 6 ×

10^{10} to 2.5×10^{7} s^{-1} corresponding to an increase in spacer length, n = 1 to 8. The BET rates, however, did not show much distance dependence and the CS states decayed in 25-300 ps.

Kinetic analysis of the PET processes occurring in the $Ru(bpy)_3^{2+}$-Viologen dyads with an amide linkage and with various substituents in the bipyridine ligand (**9**, Figure 1.11) were performed later by Kelley *et al.*[21c] Forward electron transfer rates of the order of 2×10^{8} to 5×10^{8} s^{-1} were obtained. One important observation here was that for a given donor-acceptor distance, the rate constants for the forward electron transfer were 60 to 400 times smaller for complexes bearing electron withdrawing substituents in the bipyridine. This was attributed to a possible redistribution of electron density between the substituted bipyridine ligands remote to the viologen and the ligand to which the viologen is connected. CS state lifetimes in these systems varied in the rage of 150-1000 ps.

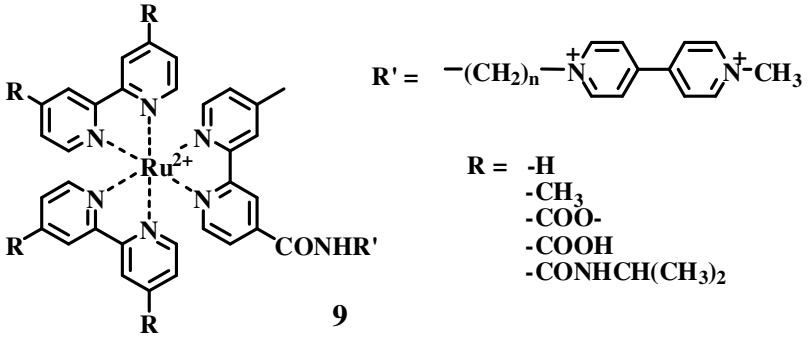

9

Figure 1.11

Kelley *et al.*[21b] and Elliott *et al.*[25] have studied the PET processes in a few $Ru(bpy)_3^{2+}$-$(CH_2)_n$-diquat (DQ^{2+}) systems (**10**, Figure 1.12). The kinetics of ET from the MLCT state of $Ru(bpy)_3^{2+}$ to the DQ^{2+} were analyzed. A fast ligand-to-ligand ET

occurs in these systems, allowing equilibrium to be established between adjacent and remote MLCT state populations, and relatively slow ET takes place from remote MLCT states to DQ^{2+}. Depending on the number of methylene groups in DQ^{2+} acceptor and the methyl substituents in the remote bipyridine ligands, forward electron transfer rates ranged from 3×10^9 to 7×10^{10} s^{-1}. From the recovery of the bleach at 450 nm, following the excitation at 355 nm, repopulation of the ground state by BET was estimated to be < 5 ns.

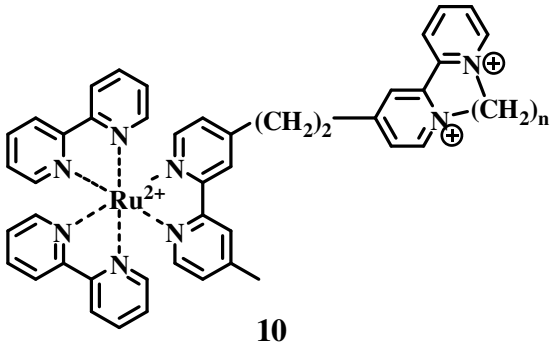

10

Figure 1.12

An example for the switching back of the electron transfer in presence of an external potential bias was presented by Hammarstrom *et al.*[26] in **11**, where $Ru(bpy)_3^{2+}$ is covalently connected to MV^{2+} (Figure 1.13). Here, $MV^{\bullet+}$ or MV^0 were generated by the reduction of viologen electrochemically, prior to the excitation. Transient absorption spectroscopy on the nano to femto-second timescale showed that quenching of the excited $*[Ru(bpy)_3]^{2+}$ by $MV^{\bullet+}$ or MV^0 generates the reduced ruthenium complex. This happens both in the bimolecular reaction and in the $Ru(bpy)_3^{2+}$-MV^{n+} dyad, which is in contrast to the well-known oxidative quenching observed with MV^{2+}. The observation

of reduced $Ru(bpy)_3^+$ generated by PET was illustrated here for the first time by transient absorption spectroscopy. Ru^+ was characterized by the transient absorptions at 370 nm and 502 nm region with lifetimes of a few picoseconds. This demonstrates the potential of the dyad as a redox-switchable photodiode which could be further explored as a molecular switch operative in sub-picosecond timescale.

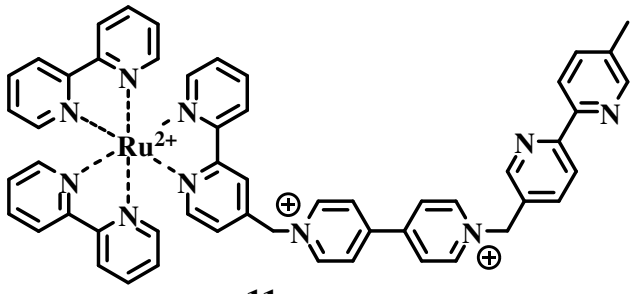

11

Figure 1.13

Efficient oxidative quenching was observed in a series of conformationally rigid dyads where $Ru(bpy)_3^{2+}$ is linked to naphthalenediimide (NDI) directly or through a phenyl spacer (**12**, Figure 1.14), investigated by Akermark *et al*.[27] Rapid forward electron transfer was observed and the excited state is converted to the CS state with almost 100% efficiency. Forward electron transfer rates were 5×10^9 and 8×10^8 s^{-1}, respectively, for the two systems. The ^{3}NDI state was generated by the energy transfer from the $*Ru(bpy)_3^{2+}$ to the NDI, and this triplet state was characterized by the transient absorption in the 400 nm region (τ = 38 ns). It was proposed that ET occurs during the quenching of this state by ruthenium (II). Ru^{3+} and $NDI^{\bullet-}$ were characterized by the bleach at 460 nm and by absorptions at 474 nm and 675 nm respectively. Back electron

transfer rates also were estimated; charge separated states with lifetimes lying between 200 ps and 5 ns were observed in these derivatives.

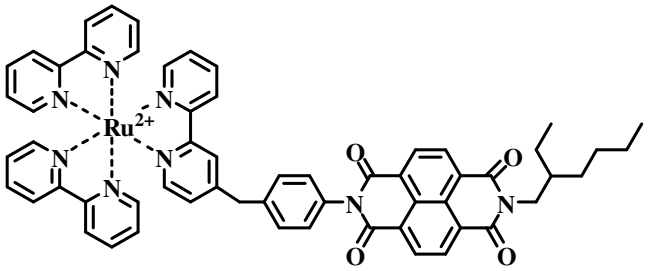

12

Figure 1.14

A number of D-A dyad systems exhibiting very good PET properties have been reported with $Ru(bpy)_3^{2+}$ connected to myoglobin[28], phthalocyanines[29] or Zn-porphyrins.[30] In the $Ru(bpy)_3^{2+}$-(Zn-Porphyrin)[30] system **13** (Figure 1.15), it has been shown that intramolecular PET can occur from the Zn-porphyrin S_2 state (S_2 corresponds to the Soret band of porphyrin, centered around 435 nm) to the $Ru(bpy)_3^{2+}$ moiety ($k_{ET} = 6 \times 10^{11}$ s^{-1}). PET can also occur in this system from the Zn-porphyrin S_1 state, but the rate is 100 times slower. The depopulation of the S_2 state was investigated by femtosecond transient absorption studies. Lifetime of the S_2 state in the absence of $Ru(bpy)_3^{2+}$ moiety, measured from the bleaching recovery at 435 nm, was 1.6 ps. When the $Ru(bpy)_3^{2+}$ was attached, S_2 lifetime was reduced to 0.8 ps suggesting the involvement of the S_2 state in the PET process. Even though existence of Ru(I) (near to 500 nm) could be established from the picosecond transient absorption studies, lifetime of the CS state was not mentioned in the report.

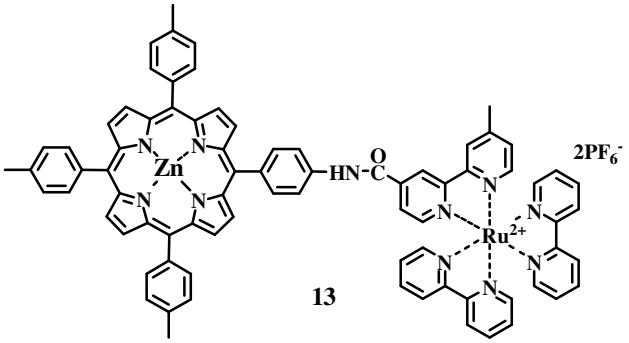

13

Figure 1.15

The small reorganization energy and favorable acceptor properties of C_{60} have made it an exceptional candidate in electron transfer chemistry in recent years, especially in the design of simple D-A systems.[14b-d] It can serve as a molecular model for functionalization of carbon nanotubes using near-identical chemical transformations, which is an important topic in current nanomaterial science. Grennberg *et al.* have studied a series of $Ru(bpy)_3^{2+}$-C_{60} dyads[31] with short linker units (**14**, Figure 1.16). In **14**, the main quenching mechanism is a fast direct energy transfer ($k_{obs} > 1 \times 10^{12}$ s^{-1}) leading to population of $^3C_{60}$. No evidence for electron transfer was found, despite the very short donor-acceptor distance that could kinetically favor the PET process.

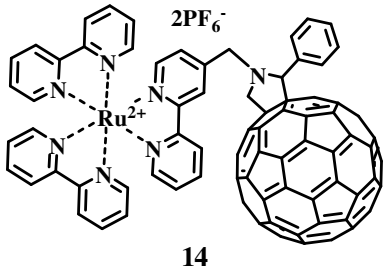

14

Figure 1.16

A solvent dependent intramolecular electron transfer was observed in peptide chain-linked $Ru(bpy)_3^{2+}$-C_{60} dyad **15** (Figure 1.17) investigated by Maggini *et al.*[32] In **15**, PET occurred from $Ru(bpy)_3^{2+}$ to C_{60} only in aprotic solvents. It is suggested that in aprotic solvents the linker peptide exists in a helical conformation and allows efficient interactions between the $Ru(bpy)_3^{2+}$ and C_{60} chromophores. In protic solvents unfolding of the helix occurs which hampers suitable spatial orientations of the chromophores for electron transfer.

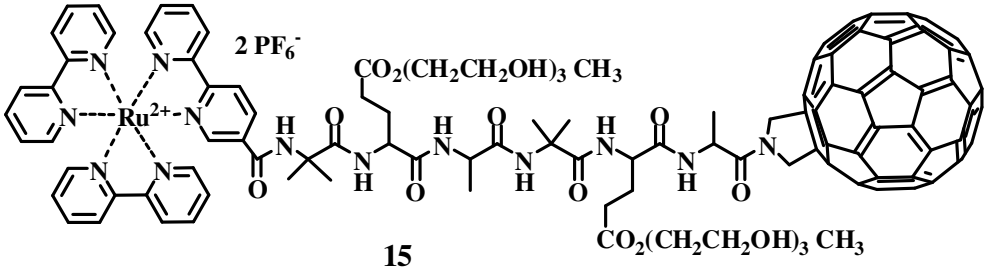

15

Figure 1.17

Energy transfer from the $Ru(bpy)_3^{2+}$ to C_{60} did not take place in **15**. Even though the charge separated state, Ru^{3+}-$C_{60}^{\bullet-}$ could be characterized by transient absorption studies, exact lifetime of the CS state was not mentioned in the report.

Phenothiazine (Ptz) is one of the most extensively studied donor moiety in $Ru(bpy)_3^{2+}$ based dyads and triads.[19g,21a,e,22d,28] Kelley *et al.*[33] studied several dyads where phenothiazine is attached *via* variable-length methylene chains to the $Ru(bpy)_3^{2+}$ chromophore. An example is shown here (**16**, Figure 1.18), where two phenothiazine donors are attached to one $Ru(bpy)_3^{2+}$ moiety. Several dyads of this type were studied with an emphasis on the role of the solvent, electron-transfer distance, number of Ptz-

containing ligands, and driving force for electron transfer. PET rates in these systems, calculated using luminescence data, varied in the range 1.2×10^5 s^{-1} to 5.5×10^7 s^{-1}, depending on the reaction conditions and substituents in the bipyridine ligands. Driving forces of the PET processes in these systems were in the range of -0.04 to + 0.20 eV in acetonitrile. Transient absorption data were not reported for these systems most probably because of the very small CS state lifetimes.

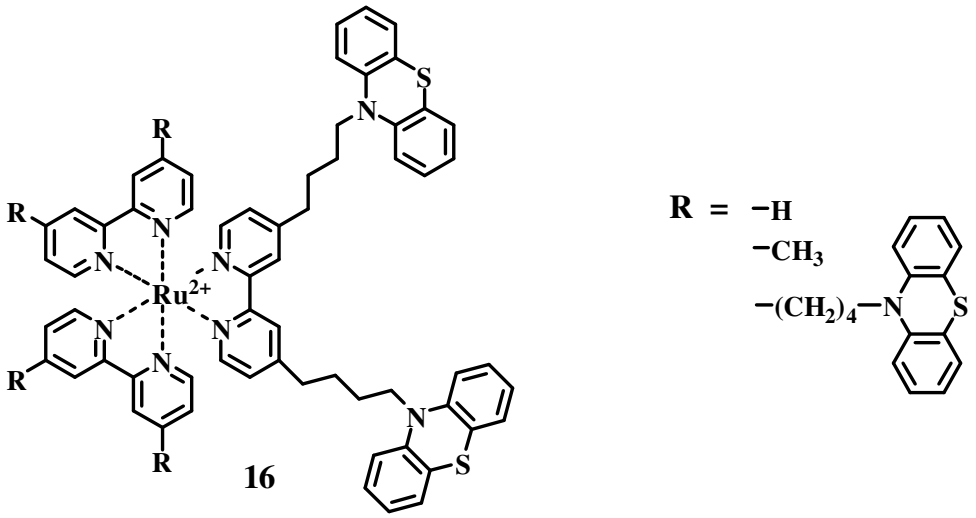

Figure 1.18

Vos *et al.*[34] have reported dyad **17** (Figure 1.19), where a Ptz is linked to a negatively charged bridging ligand which is not part of the luminescent ^{3}MLCT state. These investigations were prompted by the notion that by decreasing the coupling between the donor and the excited state, the rate of charge recombination, leading to the decay of the charge separated state, might decrease. It is claimed to be the first attempt on studying the effect of an intervening negatively charged bridge on the formation of the CS state. The PET process occurring in the system could be monitored by time-

resolved spectroscopy only in the presence of MV^{2+} as sacrificial acceptor. Intermolecular PET takes place from $Ru(bpy)_3^{2+}$ to MV^{2+} and the $Ru(bpy)_3^{3+}$ formed gets back the electron from the attached Ptz. The long-lived transient absorption due to $Ptz^{\bullet+}$ grows in at 530 nm with a lifetime of 170 ns which then decays following second order kinetics.

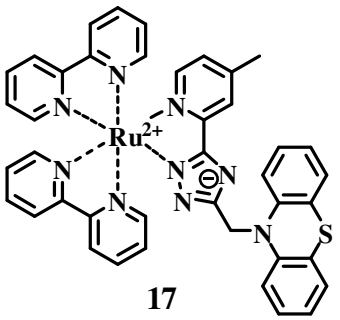

17

Figure 1.19

Evidences of $Ptz^{\bullet+}$-$Ru^{II}(bpy)_2(bpy^{\bullet-})$ charge transfer state, with significant contribution from both the reduced ruthenium and the oxidized Ptz moieties could be obtained from transient absorption studies of the dyad **18** (Figure 1.20) investigated by Hammarstrom *et al.*[19f] The charge transfer-recombination processes and excited state population in the dyad could not be directly resolved in this study. They have calculated that a quasi equilibrium was established (within 7 ns), with 82% of the population in the Ptz-*Ru^{II} state and 18% in the CS state. Within 90 ns the excited state and the CS state decayed together by the intrinsic deactivation and the charge recombination mechanisms, respectively. Separate analysis of the CS state could not be done. By

approximating the transient lifetime of the Ptz-*Ru^{II} state as equal to that of *$Ru(bpy)_3^{2+}$ the charge recombination rate was calculated to be 5.7×10^7 s^{-1}.

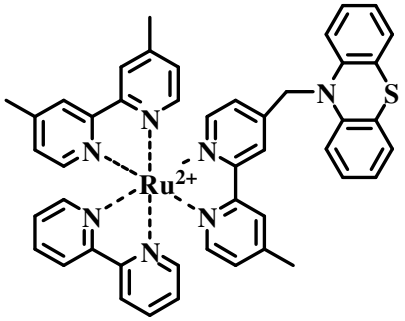

18

Figure 1.20

1.4. PET in Higher Order Donor-Acceptor Systems

Compared to the simple D-A dyads, the donor-chromophore-acceptor (D-C-A) triads are often capable of generating longer-lived (hundreds of nanoseconds) CS states with good quantum yields. Quantum yields and lifetimes of the CS state in D-C-A triad assemblies are expected to be strongly dependent on the structure of the assembly and the energetics of the various electron transfer steps. Triad **19**, consisting of a porphyrin (P) bearing a quinone (Q) electron acceptor and a carotenoid (C) secondary donor (Figure 1.21) was studied by Gust *et al*.[35] Excitation of P leads to electron transfer from *P to Q resulting in the formation of C-$P^{\bullet+}$-$Q^{\bullet-}$. The final CS state $C^{\bullet+}$-P-$Q^{\bullet-}$ is formed by electron transfer from C to $P^{\bullet+}$ and this process could be well monitored by transient absorption studies. Compared to simple P-Q dyads, CS state lifetime was at least three orders of magnitude longer in the triad. Wasielewski *et al*.[36] have reported comparable

results with triads consisting of a porphyrin bearing a quinone acceptor and a dimethylaniline-based secondary donor. Pioneering work by Meyer *et al.*[19g] resulted in the development of $Ru(bpy)_3^{2+}$ based triads where the CS state lifetimes were as high as 165 ns. A variety of other successful triads for substantial stabilization of the charge separation have been reported in recent years. [37]

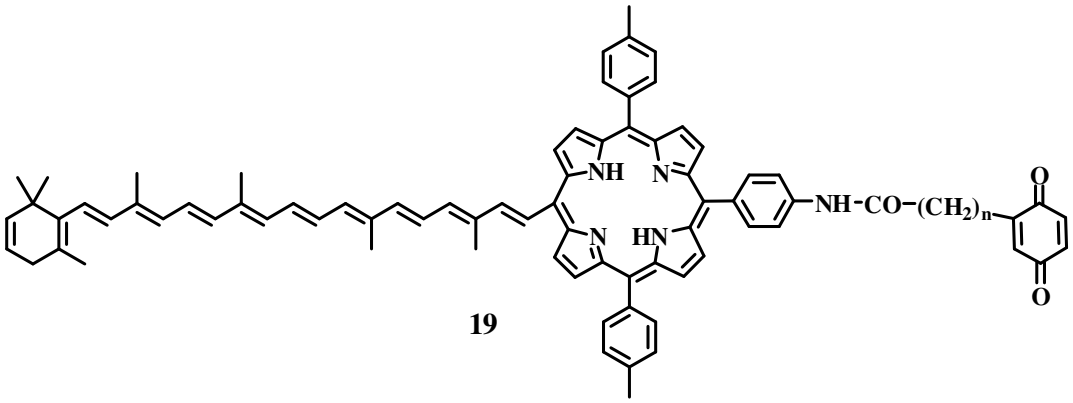

19

Figure 1.21

1.5. $Ru(bpy)_3^{2+}$ Based Triad Assemblies

Meyer *et al.*[19g] studied the electron transfer events following MLCT excitation of $Ru(bpy)_3^{2+}$ in the complex $[Ru(Me(bpy)\text{-}3DQ^{2+})(Me(bpy)\text{-}Ptz)_2]^{4+}$ (**20,** Figure 1.22). The absence of bleaching at 450 nm and absorptions centered around 516 ($Ptz^{\bullet+}$), 395 and 514 nm ($DQ^{\bullet+}$) in the transient absorption spectrum have confirmed the PET events taking place in the system. From transient absorption studies they obtained a quantum yield of charge separation, $\Phi_{cs} = 0.26 \pm 0.04$ and lifetime of charge separated state, $\tau_{CS} = 165 \pm 14$ ns for **20**.

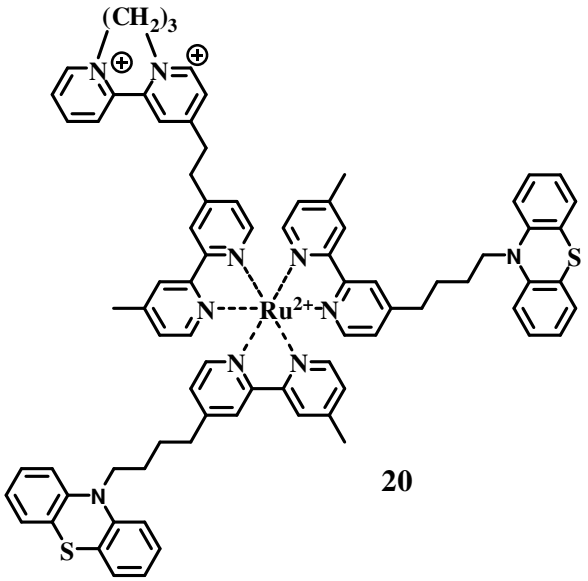

20

Figure 1.22

Kelley *et al.* have performed detailed time resolved emission studies on a series of $Ru[(Me(bpy)\text{-}3DQ)(Me(bpy)\text{-}Ptz)_2]^{4+}$ complexes.[34a] The results were compared with that of analogous $Ru(bpy)_3^{2+}$-DQ^{2+} complexes. It was concluded that the initial step is the oxidative quenching of the MLCT state by the DQ^{2+}, followed by electron transfer from Ptz to Ru(III). The extent of charge separation was found to depend on solvent polarity, being more efficient in dichloromethane than in acetonitrile. Studies using the model dyad $Ru(bpy)_3^{2+}$-DQ^{2+} revealed that the BET in acetonitrile following the first electron transfer is very fast and this is responsible for the low yield of CS state in this solvent.

Further studies by Kelley *et al.*[38] showed that the quantum yield of CS state formation depended on the length of the methylene chain separating the Ptz and $Ru(bpy)_3^{2+}$ moieties. Rate constants of electron transfer from Ptz to Ru(III) decreased as

the length of the bridging chain varied from 4 to 8 methylene units. This result was interpreted in terms of the fraction of Ptz moieties close to the Ru centre. Quantum yield of charge separation was highest (Φ_{CS} = 0.40) when four methylene groups were present in the linker. This value is comparable to that observed in $Ru(bpy)_3^{2+}$-DQ^{2+} dyad. Also it was concluded that the BET rates were independent of the length of the methylene chain linking Ptz to $Ru(bpy)_3^{2+}$.

Recently, Elliot *et al*.[39] have investigated the conformational changes prior to the photoinduced events in the above systems. They have proved the existence of a ground state association between RuL_3^{2+} and Ptz prior to photo-excitation. This association resulted in an enhanced donor-acceptor coupling, and a higher ET rate. The association mechanism is turned off once the Ptz is oxidized in the PET process to $Ptz^{\bullet+}$, due to the electrostatic repulsion between Ru^+ and $Ptz^{\bullet+}$. The repulsion enhances the distance and reduces the coupling between the redox centres leading to low BET rates. This explains the high quantum yield of CS state in these systems.

Photophysics of a similar class of triads, $Ru[((CH_3)_2\text{-bpy})(bpyCH_2Ptz)(bpyCH_2MV)]^{4+}$ (**21**, Figure 1.23) which has four positional isomers, were explored in detail by Meyer *et al*.[21g] Following laser excitation at 460 or 532 nm, the redox-separated states $Ru^{2+}[(bpy\text{-}[CH_3]_2)(bpyCH_2Ptz^{\bullet+})(bpyCH_2MV^{\bullet+})]$ were generated rapidly (< 5 ns). Quenching of MLCT emission by electron transfer occurred with near unit efficiency for all four isomers. ET rates were in the range of 4.5×10^6 - 8.7×10^7 s^{-1} for the four isomers. In two of the isomers, efficiency of CS state formation was nearly

25% and the highest lifetime showed was 160 ns.

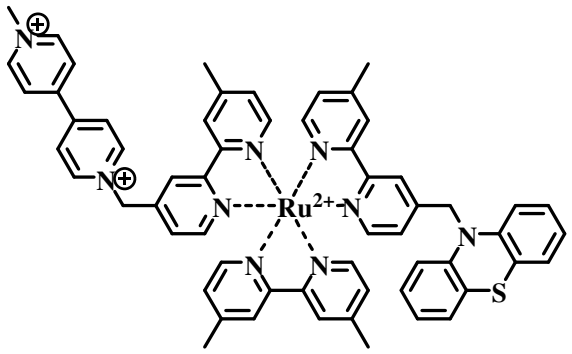

21

Figure 1.23

Meyer *et al*. have also studied[22d] intramolecular electron transfer quenching in $[Ru(bpy\text{-}AQ)_2(bpy\text{-}Ptz)]^{2+}$ where AQ stands for anthraquinone (**22**, Figure 1.24). PET leads to the formation of the CS state $[Ru^{2+}(bpy\text{-}AQ)(bpy\text{-}AQ^{\bullet-})(bpy\text{-}Ptz^{\bullet+})]$ in 40% yield. The CS state was characterized by absorptions corresponding to $Ptz^{\bullet+}$ (510 nm) and $AQ^{\bullet-}$ (590 nm) in the laser flash photolysis studies. From the PET results of the $[Ru^{2+}(bpy)_2(bpy\text{-}CH_2\text{-}Ptz)]$ system, it was interpreted that initial ET occured from phenothiazine to Ru(II), generating the CS state, $[Ru^{+}(bpy\text{-}AQ)_2(bpy\text{-}Ptz^{\bullet+})]$. This was followed by the ET from Ru^{+} to AQ resulting in the CS state, $[Ru^{2+}(bpy\text{-}AQ)(bpy\text{-}AQ^{\bullet-})(bpy\text{-}Ptz^{\bullet+})]$ with a lifetime of 150 ns. Here the generation of the $[Ru^{3+}(bpy\text{-}AQ^{\bullet-})(bpy\text{-}AQ)(bpy\text{-}Ptz)]$ state and thereby the rapid charge recombination between Ru^{3+} and $AQ^{\bullet-}$ could be avoided. The ΔG^{o} value for the BET process (-1.56 eV) was in the Marcus inverted region, supporting the observation of long- lived CS state.

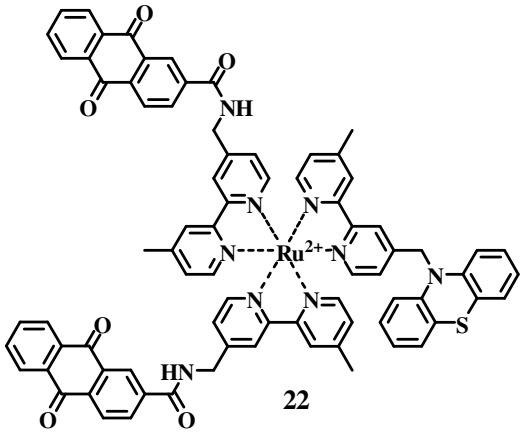

22

Figure 1.24

In the Ptz-Ru^{II}-BQ triad (BQ = benzoquinone, **23**, Figure 1.25) investigated by Hammarstrom *et al*.,[19f] the initial charge separation from Ru(II) to BQ was followed by a rapid ($k > 5 \times 10^9$ s^{-1}) electron transfer from the Ptz moiety to give the fairly long-lived $Ptz^{\bullet+}$-Ru^{II}-$BQ^{\bullet-}$ state (τ_{CS} = 80 ns) in unusually high yield (> 90%). The CS state, however, was not stable and a coupling between the $Ptz^{\bullet+}$ and $BQ^{\bullet-}$ moieties was proposed.

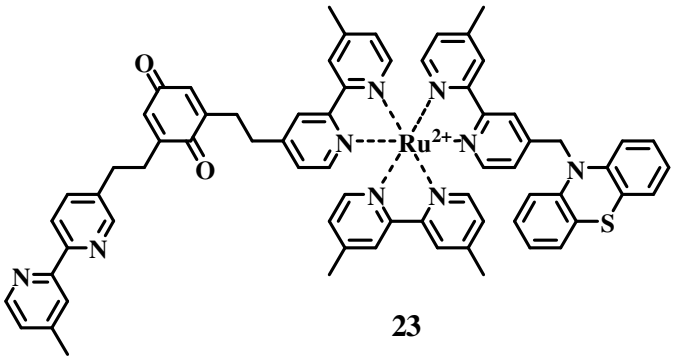

23

Figure 1.25

Motivated by the impressive solar energy harvesting devices developed by Grätzel and coworkers with ruthenium polypyridyl sensitizers anchored to porous

colloidal TiO_2 films, much efforts have been devoted in designing PET assemblies supported on solid surfaces.[40] As in natural photosynthesis, these materials convert light into useful energy. Here the electronically excited sensitizer injects an electron into the solid semiconductor to form a charge-separated pair with the hole localized on the sensitizer. Recombination of the electron and hole to give ground state products represents a detrimental process which may reduce the efficiency of a regenerative solar cell. It is therefore worthwhile to explore the performance of a more complex molecular sensitizer with a covalently bound electron donor and to develop a clear picture of the interfacial electron transfer processes which dictate charge separation efficiencies.

Two such systems (**24** and **25**) are illustrated in Figure 1.26. These are based on covalent assembly of hetero super molecules involving a TiO_2 nanocrystal, a ruthenium complex, and a Ptz donor[41] or a MV^{2+} acceptor.[42] It was observed that visible light excitation (532 nm) resulted in the formation of the excited state of the ruthenium complex component, $^1Ru(bpy)_3^{2+}$. In the former assembly, the $^1Ru(bpy)_3^{2+}$ or $^3Ru(bpy)_3^{2+}$ can inject an electron into the TiO_2 nanocrystal and this was followed by a second electron transfer from Ptz to Ru(III). In the latter system, under positive applied potentials, initial ET takes place from $^1Ru(bpy)_3^{2+}$ to TiO_2 and the second ET occurs from the TiO_2 layer to the MV^{2+}. In both the cases longer lived CS states (in the order of micro seconds) were obtained. An intramolecular electron-transfer efficiency of 90% was observed in a similar supramolecular assembly composed of Ru(II) *tris*-bipyridine, tyrosine, and dipicolylamine attached to TiO_2, reported by Sundstrom *et al*.[43]

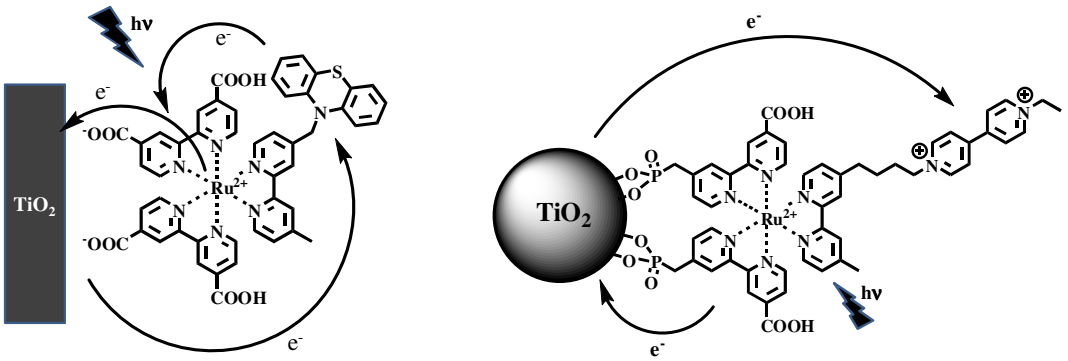

24 **25**

Figure 1.26

1.6. PET in Tetrads and Pentads

In order to address the energy wasting effects of BET, many higher order systems (tetrads, pentads and polyads) capable of sequential electron transfer were designed. Sequential electron transfers lead to large separation distances between the radical cation and radical anion centres, thereby reducing charge recombination probability. Fukuzumi *et al*. have achieved extremely long-lived charge-separated states ranging from hundreds of milliseconds to a few seconds in tetrads.[44] For example, tetrad **26** (Fc-ZnP-H_2P-C_{60}, Figure 1.27) gave the final CS state $Fc^{\bullet+}$-ZnP-H_2P-$C_{60}^{\bullet-}$, which exhibited a lifetime of 380 ms in benzonitrile solution, with a quantum yield of 0.17.

Porphyrin-donor-bridge-acceptor tetrad reported by Braslavsky *et al.*[45] and tetrads containing Zinc porphyrin (PZn) and methyl viologen (MV^{2+}) as the terminal chromophores and dimethoxynaphthalene (DMN) and naphthaquinone (NQ) as intermediate chromophores studied by Paddon-Row *et al.*[46] offered very good photoinduced charge separation. The former system exhibited CS state with 200 ns

lifetime and quantum yield of 0.13, while the latter showed CS state lifetimes of 250-450 ns in different solvents. A few examples of pentad systems offering better PET results were reported by D'Souza *et al*.[47] and Gust *et al*.[48,49]

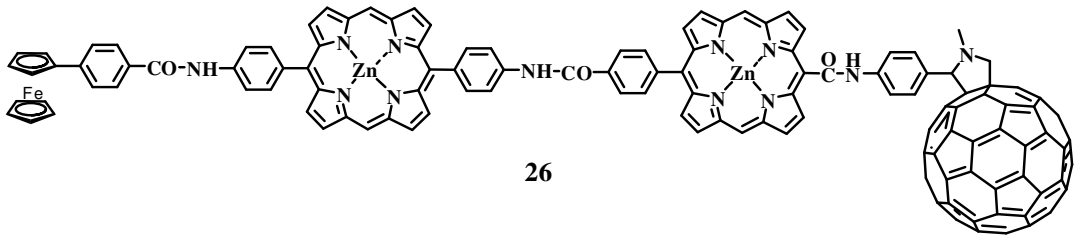

26

Figure 1.27

1.7. Ru(II)-polypyridyl Systems in Metal ion Sensing

A few Ru-polypyridyl based systems have metal ion sensing properties. Schmittel *et al*.[50] claimed that the Ru(II)phenanthroline derivative **27** containing an aza-crown moiety (Figure 1.28) can complex with different metal ions to produces different type of signals and hence it can be termed as a "lab on a molecule". The system **27** works as a selective chemosensor for Pb^{2+} as the Pb^{2+} complexation leads to an anodic shift of the Ru^{2+}/Ru^{3+} redox potential along with quenching of the luminescence. It works as an electro-chemiluminescence (ECL) based sensor selective for Hg^{2+} since only Hg^{2+} showed an enhancement in its ECL spectrum. Efficient luminescence quenching coupled with changes in the absorption spectrum leads to sensing of Cu^{2+} by **27**. This system is reported to be one of the first examples for the quadrupole-channel sensing in selective and quantitative multi-ion analysis.

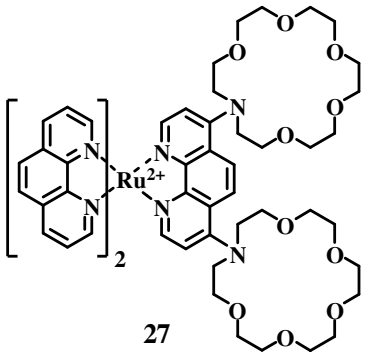

27

Figure 1.28

Grätzel *et al*. have shown that Ru(II) complexes **28** and **29** (Figure 1.29) can detect Hg^{2+} ions in the solution phase or when anchored on to TiO_2 films.[51] Upon addition of Hg^{2+} solution, the colour of **28** changes from red to orange and the colour of **29** changes from green to pink. UV-Vis and FT-IR absorption studies have shown that $HgCl_2$ has complexed with the dyes leading to a change in the MLCT absorption by ~ 50 nm. When adsorbed on to TiO_2 films, presence of Hg^{2+} leads to an enhancement in the luminescence and also an anodic shift of the Ru^{2+}/Ru^{3+} redox potential. Sensing by the complexes on TiO_2 films can be made reversible by dipping the films in potassium iodide solution.

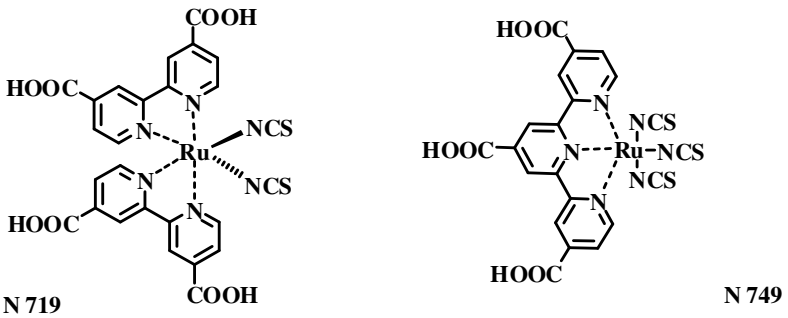

N 719 **28** **29** **N 749**

Figure 1.29

Ghosh *et al*. have reported that ruthenium(II) complex **30** (Figure 1.30) is capable of detecting anions such as $F^{\ominus}$, $CH_3COO^{\ominus}$, and $H_2PO_4^{\ominus}$ in acetonitrile solution.[52] Binding of the anions to **30** was confirmed by absorption, emission and ^1H NMR titration studies. Significant changes in the absorption spectrum of the receptor in the 300-600 nm region was observed upon binding with the anions. Emission spectral studies showed that the emission intensity was completely quenched or "*switched off*" in the presence of excess of $F^{\ominus}$, $CH_3COO^{\ominus}$, and $H_2PO_4^{\ominus}$. ^1H NMR titration experiments confirmed the formation of 1:1 hydrogen bonded adducts between the anions and **30**.

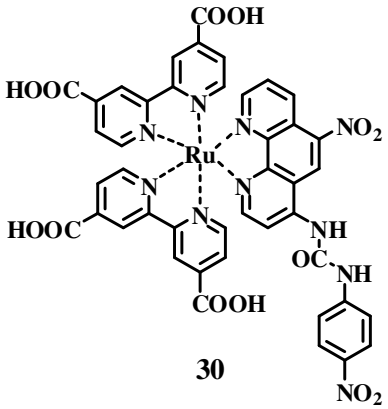

30

Figure 1.30

Zhao *et al*.[53] have reported that *bis*(2,2'-bipyridine)(4-methyl-2,2'-bipyridine-4'-carboxylic acid)ruthenium(II) (**31**) could be used as a fluorescent chemosensor to recognize Cu(II) in EtOH/H_2O (1:1, v/v) solution. The response of the sensor was based on the fluorescence quenching of complex by binding with Cu(II) as shown in Scheme 1.5. The fluorescence response was linear in the range of 5.0×10^{-8} to 1.0×10^{-4} M Cu^{2+} and the detection limit was 4.2×10^{-8} M. In the pH range of 4.0 - 8.0 the complex showed excellent selectivity for Cu(II) over other transition metal cations.

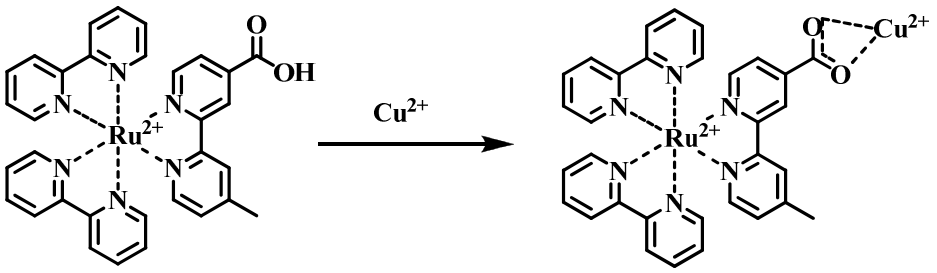

31

Scheme 1.5

Alsfasser *et al*. designed $Ru(bpy)_3^{2+}$ based systems **32** and **33** for the selective detection of Cu^{2+} in aqueous medium (Figure 1.31).[54] In **32**, the receptor moiety is a pentadentate acylated cyclen (1,4,7,10-tetraazacyclododecane) ligand capable of binding Cu^{2+} (1:1) in the pH range 2 - 12, leading to emission quenching. The emission properties of **32** in aqueous solution are almost independent of the pH. In the case of **33**, Cu^{2+} binds to the 2,2'-bipyridyl subunit and quenches its emission. Complex formation in this case is reversibly dependent on pH, with complex formation below pH 10 and dissociation at higher pH values. It is reported to be the first example for a receptor which exhibits reversibility at high pH.

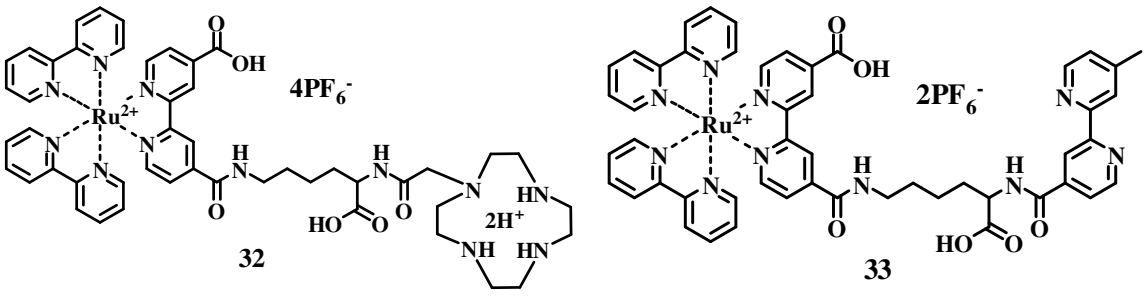

Figure 1.31

1.8. Origin of the present work

A major objective of this study is to design $Ru(bpy)_3^{2+}$ based dyads having CS state lifetimes in the nanosecond time scales so that they can be studied by nanosecond laser flash photolysis. Two important aspects need to be considered while designing linked PET systems based on $Ru(bpy)_3^{2+}$. Let us consider the case of a $Ru(bpy)_3^{2+}$-A dyad, where the acceptor A is linked through one of the ligands. Excitation of $Ru(bpy)_3^{2+}$ chromophore leads to transfer of an electron to the ligands. The ligand carrying the acceptor will share 1/3 of this electron density and this fraction can be transferred very fast to A. Transfer of electron density to A from the other two ligands would be slow because of the larger distances involved, leading to a reduction in the overall rate constant. This can be enhanced in principle by substituting the ligand attached to A with electron withdrawing groups. The excited electron would then reside mostly in the ligand attached to A, facilitating the electron transfer to A. This however is not a good strategy because substitution of electron withdrawing groups would increase the oxidation potential of $Ru(bpy)_3^{2+}$ and hence decrease the driving force for PET. In the case of $Ru(bpy)_3^{2+}$-D systems electron density residing in the ligand carrying D would slow down through-bond electron transfer from D to Ru(III) due to electron-electron repulsion. In this case, substituting the other two ligands with electron withdrawing groups might favour through ligand-PET from D to Ru(III).

A second problem faced by $Ru(bpy)_3^{2+}$ based dyads is the strong bleaching around 400-550 nm and strong emission around 600-750 nm in the transient absorption

spectrum. Short-lived transient absorptions will be submerged under the bleaching and emission profiles. This aspect is most prominent if $k_{PET} < 10^8$ s^{-1}.

An examination of the literature showed that $Ru(bpy)_3^{2+}$-$(CH_2)_n$-MV^{2+} or $Ru(bpy)_3^{2+}$-$(CH_2)_n$-DQ^{2+} are the most well studied dyads of the $Ru(bpy)_3^{2+}$-A type. The free energy change for the electron transfers were ΔG^0_{PET} ~ -0.5 eV and ΔG^0_{BET} ~ -1.6 eV respectively in these dyads. For these systems $k_{BET} \geq k_{PET}$ and hence the CS states are not observable in the nanosecond time scale. Since the intrinsic CS state lifetime is less than 1000 ps, it would be difficult to obtain long-lived CS states by structural modifications of these types of systems. Among the $Ru(bpy)_3^{2+}$-D type dyads $Ru(bpy)_3^{2+}$-$(CH_2)_n$-Ptz dyads are the most widely studied. In these systems ΔG^0 for PET is nearly zero which results in low k_{PET} values. In the case of **18**, Hammerstrom *et al*. suggested that the charge recombination is somewhat slow ($k_{BET} \sim 5.7 \times 10^7$ s^{-1}).[19f] The CS state could not be observed because of the low yield of this state and the slower bleaching recovery. We reasoned that if we could increase the forward electron transfer rate constant then it might be possible to observe the CS state in the nanosecond time scale in this system. An attempt in this direction is made in the second chapter of this thesis.

We observed that k_{PET} could be increased in the $Ru(bpy)_3^{2+}$-$(CH_2)_n$-Ptz system by a simple structural modification. Ptz is attached to bpy through a $(CH_2)_3$-NH-CO- linker and this served two purposes. The electron withdrawing carbonyl group helped to lower the reduction potential of $Ru(bpy)_3^{2+}$ leading to an increase in the driving force of

the reaction. The rigidity of the amide linkage helps in bringing the Ptz and Ru spatially close to each other leading to fast through space electron transfer from Ptz to Ru(III). We observed that this modification has resulted in increasing k_{PET} and reducing k_{BET}, which in turn allowed us to observe the CS state in the nanosecond time scale. Results of these investigations are presented in Chapter 2 of this thesis.

We have extended the studies into Ru-D systems with two, four and six Ptz units, where the 4 and 4' position of the bipyridine ligands were substituted. Results of these investigations are summarized in Chapter 3 of this thesis. The intermolecular PET events of one of the dyads with electron acceptors like dodecyl viologen (DV^{2+}) and pyromellitic diimide (PMDI) and electron donor trimethoxy triphenylamine (TMTPA) were also investigated. Longer lived charge separations were observed under these conditions. In order to make use of the exceptionally long lived charge separation observed in the system with two Ptz donors connected to the same bipyridine ligand, we have also designed a triad assembly, by extending the dyad architecture. A weak acceptor, 4-nitrotoluene was chosen for the studies, as the facile initial ET between Ptz and Ru was not intended to be interfered.

In Chapter 4 of this thesis we present a study of the metal sensing ability of $Ru(bpy)_3^{2+}$-Ptz dyads. We show that the dyads could act as a "turn-ON" luminescence dosimeter for Cu^{2+}. This study is based on our observation that Ptz reacts with Cu^{2+} in acetonitrile to give $Ptz^{\bullet+}$. In the presence of excess Cu^{2+} the $Ptz^{\bullet+}$ reacts further to give phenothiazine-5-oxide (PtzO). Ptz quenches the luminescence of $Ru(bpy)_3^{2+}$ by an electron transfer mechanism and hence $Ru(bpy)_3^{2+}$-Ptz dyads are non-emissive. PtzO

cannot quench the emission of $Ru(bpy)_3^{2+}$ and hence $Ru(bpy)_3^{2+}$-PtzO systems are emissive. Thus addition of Cu^{2+} in acetonitrile converts the non-luminescent $Ru(bpy)_3^{2+}$-Ptz dyads to luminescent $Ru(bpy)_3^{2+}$-PtzO systems, which form the basis of Cu^{2+} detection by the dyads. Other metal ions tested are not capable of this reaction and hence these dyads are very selective towards Cu^{2+}. Details of this study are presented in Chapter 4.

1.9. References

(1) (a) *Electron Transfer in Chemistry*, Balzani, V. (Ed.), *Vol. 1-5*, Wiley-VCH, Weinheim, 2001. (b) Kuznetsov, A. M.; Ulstrup, J. *Electron Transfer in Chemistry and Biology*, Wiley, New York, 1998. (c) *Electron Transfer*, Wishart, J. F.; Nocera, D. G. (Eds.), ACS, Washington DC, 1998. (d) *Electron Transfer Reactions: Inorganic, Organometallic, and Biological Applications*, Isied, S. S. (Ed.), ACS, Washington DC, 1997.

(2) (a) Kavarnos, G. J. *Fundamentals of Photoinduced Electron Transfer*, VCH, New York, 1993. (b) *Photoinduced Electron Transfer*, Fox, M. A.; Chanon, M. (Eds), *Parts A-D*, Elsevier, Amsterdam, 1988. (c) *Photoinduced Electron Transfer*, Mattay, J. (Ed.), *Parts I-IV*, Springer Verlag, Heidelberg, 1990.

(3) (a) Crosby, G. A. *J. Chem. Educ.* **1983**, *60*, 791-796. (b) Adamson, A. W. *J. Chem. Educ.* **1983**, *60*, 797-802. (c) Meyer, T. J. *Acc. Chem. Res.* **1989**, *22*, 163-170. (d) Balzani, V.; Scandola, F. *Supramolecular Photochemistry*; Horwood, Chichester, U. K., 1991.

(4) (a) Julliard, M.; Chanon, M. *Chem. Rev.* **1983**, *83*, 425-506. (b) Kavarnos, G. J.; Turro, N. J. *Chem. Rev.* **1986**, *86*, 401-449. (c) Mikkelsen, K. V.; Ratner, M. A. *Chem. Rev.* **1987**, *87*, 113-153. (d) Andrieux, C. P.; Hapiot, P.; Saveant, J. M. *Chem. Rev.* **1990**, *90*, 723-738. (e) Evans, D. H. *Chem. Rev.* **1990**, *90*, 739-751. (f) Blondin, G.; Girerd, J. J. *Chem. Rev.* **1990**, *90*, 1359-1376. (g) Newton, M. D. *Chem. Rev.* **1991**, *91*, 767-792.

(5) Deisenhofer, J.; Epp, O.; Miki, K.; Huber, R.; Michel, H. *J. Mol. Biol.* **1984**, *180*, 385-398.

(6) (a) Allen, J. P.; Feher, G.; Yeates, T. O.; Komiya, H.; Rees, D. C. *Proc. Natl. Acad. Sci. U.S.A.* **1988**, *85*, 8487-8491. (b) Chang, C. H.; El-Kabbni, O.; Tiede, D. M.; Norris, J.; Schiffer, M. *Biochemistry* **1991**, *30*, 5353-5360.

(7) Prathapan, S.; Yang, S. I.; Seth, J.; Miller, M. A.; Bocian, D. F.; Holten, D.; Lindsey, J. S. *J. Phys. Chem. B* **2001**, *105,* 8237-8248.

(8) Oseki, Y.; Fujitsuka, M.; Cho, D. W.; Sugimoto, A.; Tojo, S.; Majima, T. *J. Phys. Chem. B* **2005**, *109,* 19257-19262.

(9) Monnereau, C.; Gomez, J.; Blart, E.; Odobel, F.; Wallin, S.; Fallberg, A.; Hammarstrom, L. *Inorg. Chem.* **2005**, *44,* 4806-4817.

(10) Kubo, M.; Mori, Y.; Otani, M.; Murakami, M.; Ishibashi, Y.; Yasuda, M.; Hosomizu, K.; Miyasaka, H.; Imahori, H.; Nakashima, S. *J. Phys. Chem. B* **2007**, *111,* 5136-5143.

(11) Ohkubo, K.; Kotani, H.; Shao, J.; Ou, Z.; Kadish, K. M.; Li, G.; Pandey, R. K., Fujitsuka, M.; Ito, O.; Imahori, H.; Fukuzumi, S. *Angew. Chem. Int. Ed. Engl.* **2004**, *43*, 853-853.

(12) Marcus, R. A. *J. Phys. Chem.* **1990**, *94*, 4152-4155.

(13) Verhoeven, J. W.; Ramesdonk, H. J.; Groenveld, M. M.; Benniston, A. C.; Harriman, A. *Chem. Phys. Chem*. **2005**, *6*, 2251-2260.

(14) (a) Guldi, D.; Prato, M. *Acc. Chem. Res.* **2000**, *33*, 695–703. (b) Martin, N.; Sanchez, L.; Illescas, B.; Perez, I. *Chem. Rev.* **1998**, *98*, 2527–2547. (c) Meijer, M. D.; van Klink, G. P. M.; van Koten, G. *Coord. Chem. Rev.* **2002**, *230*, 141–163. (d) Diekers, M.; Hirsch, A.; Pyo, S.; Rivera, J.; Echegoyen, L. *Eur. J. Org. Chem.* **1998**, *1998*, 1111–1121.

(15) Fukuzumi, S.; Kotani, H.; Ohkubo, K.; Ogo, S.; Tkachenko, N. V.; Lemmetyinen, H. *J. Am. Chem. Soc.* **2004**, *126*, 1600-1601.

(16) Verhoeven, J. W.; Ramesdonk, H. J.; Zhang, H.; Groenveld, M. M.; Benniston, A. C.; Harriman, A. *Int. J. Photoenergy* **2005**, *7*, 103.

(17) (a) Balzani, V.; Juris, A.; Venturi, M.; Campagna, S.; Serroni, S. *Chem. Rev.* **1996**, *96*, 759-833. (b) Juris, A.; Balzani, V.; Barigelletti, F.; Campagna, S.; Belser, P.; von Zelewsky, A. *Coord. Chem. Rev.* **1988**, *84*, 85-277. (c) Kalyanasundaram, K. *Photochemistry of Polypyridine and Porphyrin Complexes*; Academic Press: London, 1992. (d) Sauvage, J.-P.; Collin, J.-P.; Chambron, J.-C.; Guillerez, S.; Coudret, C.; Balzani, V.; Barigelletti, F.; De Cola, L.; Flamigni, L. *Chem. Rev.* **1994**, *94*, 993-1019.

(18) (a) Borgarello, E.; Kiwi, J.; Pelizzetti, E.; Visca, M.; Gratzel, M. *Nature* **1981**, *289*, 158-160. (b) Kim, Y. I.; Atherton, S. J.; Brigham, E. S.; Mallouk, T. E. *J. Phys. Chem.* **1993**, *97*, 11802-11810. (c) Kim, Y. I.; Salim, S.; Huq, M. J.; Mallouk, T. E. *J. Am. Chem. Soc.* **1991**, *113*, 9561-9563.

(19) (a) Baranoff, E.; Collin, J.-P.; Flamigni, L.; Sauvage, J.-P. *Chem. Soc. Rev.* **2004**, *33*, 147-155. (b) Ciofini, I.; Laine, P. P.; Bedioui, F.; Adamo, C. *J. Am. Chem. Soc.* **2004**, *126*, 10763-10777. (c) Schild, V.; von Loyen, D.; Durr, H.; Bouas-Laurent, H.; Turro, C.; Worner, M.; Pokhrel, M. R.; Bossmann, S. H. *J. Phys. Chem. A* **2002**, *106*, 9149-9158. (d) Rutherford, T. J.; Keene, F. R. *Inorg. Chem.* **1997**, *36*, 2872-2878. (e) Maxwell, K. A.; Sykora, M.; De Simone, J. M.; Meyer, T. J. *Inorg. Chem.* **2000**, *39*, 71-75. (f) Borgstrom, M.; Johansson, O.; Lomoth, R.; Baudin, H. B.; Wallin, S.; Sun, L.; Akermark, B.; Hammarstrom, L. *Inorg. Chem.* **2003**, *42*, 5173-5184. (g) Danielson, E.; Elliott, C. M.; Merkert, J. W.; Meyer, T. J. *J. Am. Chem. Soc*. **1987**, *109*, 2519-2520. (h) Coe, B. J.; Friesen, D. A.; Thompson, D. W.; Meyer, T. J. *Inorg. Chem.* **1996**, *35*, 4575-4584. (i) Laine, P.; Bedioui, F.; Amouyal, E.; Albin, V.; Berruyer-Penaud, F. *Chem. Eur. J.* **2002**, *8*, 3162-3176.

(20) (a) Abrahamsson, M. L. A.; Baudin, H. B.; Tran, A.; Philouze, C.; Berg, K. E.; Johansson, M. K. R.; Sun, L.; Akermark, B.; Styring, S.; Hammarstrom, L. *Inorg. Chem.* **2002**, *41*, 1534-1544. (b) Baudin, H. B.; Sun, L.; Davidov, R.; Sundahl, M.; Styring, S.; Akermark, B.; Almgren, M.; Hammarstrom, L. *J. Phys. Chem. A* **1998**, *102*, 2515-2518. (c) Sun, L.; Hammarstrom, L.; Norrby,

T.; Berglund, H.; Davydov, R.; Andersson, M.; Börje, A.; Korall, P.; Philouze, C.; Almgren, M.; Styring, S.; Akermark, B. *J. Chem. Soc., Chem. Commun.* **1997**, 607-608. (d) Sun, L.; Berglund, H.; Davydov, R.; Norrby, T.; Hammarstrom, L.; Korall, P.; Borje, A.; Philouze, C.; Berg, K.; Tran, A.; Andersson, M.; Stenhagen, G.; Martensoon, J.; Almgren, M.; Styring, S.; Akermark, B. *J. Am. Chem. Soc.* **1997**, *119*, 6996-7004. (e) Magnuson, A.; Frapart, Y.; Abrahamsson, M.; Horner, O.; Akermark, B.; Sun, L.; Girerd, J.-J.; Hammarstrom, L.; Styring, S. *J. Am. Chem. Soc.* **1999**, *121*, 89-96. (f) Sjodin, M.; Styring, S.; Sun, L.; Akermark, B.; Hammarstrom, L. *J. Am. Chem. Soc.* **2000**, *122*, 3932-3936.

(21) (a) Collin, J.-P.; Guillerez, S.; Sauvage, J.-P.; Barigelletti, F.; De Cola, L.; Flamigni, L.; Balzani, V. *Inorg. Chem.* **1991**, *30*, 4230-4238. (b) Cooley, L. F.; Headford, C. E. L.; Elliott, C. M.; Kelley, D. F. *J. Am. Chem. Soc.* **1988**, *110*, 6673-6682. (c) Kelly, L. A.; Rodgers, M. A. J. *J. Phys. Chem.* **1995**, *99*, 13132-13140. (d) Hu, Y.-Z.; Tsukiji, S.; Shinkai, S.; Oishi, S.; Hamachi, I. *J. Am. Chem. Soc.* **2000**, *122*, 241-253. (e) Larson, S. L.; Cooley, L. F.; Elliott, C. M.; Kelley, D. F. *J. Am. Chem. Soc.* **1992**, *114*, 9504-9509. (f) Mecklenburg, S. L.; Peek, B. M.; Erickson, B. W.; Meyer, T. J. *J. Am. Chem. Soc.* **1991**, *113*, 8540-8542. (g) Treadway, J. A.; Chen, P.; Rutherford, T. J.; Keene, F. R.; Meyer, T. J. *J. Phys. Chem. A* **1997**, *101*, 6824-6826. (h) Yonemoto, E. H.; Saupe, G. B.; Schmehl, R. H.; Hubig, S. M.; Riley, R. L.; Iverson, B. L.; Mallouk, T. E. *J. Am. Chem. Soc.* **1994**, *116*, 4786-4795.

(22) (a) Arounaguiri, S.; Maiya, B. G. *Inorg. Chem.* **1999**, *38*, 842-843. (b) Beer, P. D.; Timoshenko, V.; Maestri, M.; Passaniti, P.; Balzani, V. *Chem. Commun.* **1999**, 1755-1756. (c) Goulle, V.; Harriman, A.; Lehn, J.-M. *J. Chem. Soc., Chem. Commun.* **1993**, 1034-1036. (d) Opperman, K. A.; Mecklenburg, S. L.; Meyer, T. J. *Inorg. Chem.* **1994**, *33*, 5295-5301.

(23) Dixon, D. W.; Thornton, N. B.; Steullet, V.; Netzel, T. *Inorg. Chem.* **1999**, *38*, 5526-5534. (b) Hossain, D.; Haga, M.; Monjushiro, H.; Gholamkhass, B.; Nozaki, K.; Ohno, T. *Chem. Lett.* **1997**, 573-574.

(24) Yonemoto, E. H.; Riley, R. L.; Kim, Y.; Atherton, S. J.; Schmehl, R. H.; Mallouk, T. E. *J. Am. Chem. Soc*. **1992**, *114*, 8081-8087.

(25) Elliott, C. M.; Freitag, R. A.; Blaney, D. D. *J. Am. Chem. Soc*. **1985**, *107*, 4647-4655.

(26) Lomoth, R.; Haupl, T.; Johansson, O.; Hammarstrom, L. *Chem. Eur. J.* **2002**, *8*, 102-110.

(27) Johansson, O.; Borgstrom, M.; Lomoth, R.; Palmblad, M.; Bergquist, J.; Hammarstrom, L.; Sun, L.; Akermark, B. *Inorg*. *Chem*. **2003**, *42*, 2908-2918.

(28) Immoos, C. E.; Bilio, A. J. D.; Cohen, M. S.; Veer, W. V.; Gray. H. B.; Farmer, P. J. *Inorg. Chem*. **2004**, *43*, 3593-3596.

(29) Cabello, A. G.; Vazquez, P.; Torres, T.; Guldi, D. M. *J. Org. Chem.* **2003**, *68*, 8635-8642.

(30) LeGourrierec, D.; Andersson, M.; Davidsson, J.; Mukhtar, E.; Sun, L.; Hammarstrom, L. *J. Phys. Chem. A* **1999**, *103*, 557-559.

(31) Karlsson, S.; Modin, J.; Becker, H. C.; Hammarstrom, L.; Grennberg, H. *Inorg. Chem.* **2008**, *47*, 7286-7294.

(32) Polese, A.; Mondini, S.; Bianco, A.; Toniolo, C.; Scorrano, G.; Guldi, D. M., Maggini, M. *J. Am. Chem. Soc.* **1999**, *121,* 3446-3452.

(33) Larson, S. L.; Elliott, C. M.; Kelley, D. F. *Inorg. Chem.* **1996**, *35*, 2070-2076.

(34) Fanni, S.; Keyes, T. E.; Campagna, S.; Vos, J. G. *Inorg. Chem.* **1998**, *37*, 5933-5935.

(35) (a) Gust, D.; Mathis, P.; Moore, A. L.; Liddell, P. A.; Nemeth, G. A.; Lehman, W. R.; Moore, T. A.; Bensasson, R. V.; Land, E. J.; Chachaty, C. *Photochem. Photobiol.* **1983**, *37S*, S46. (b) Gust, D.; Moore, T. A. *Science* **1989**, *244*, 35-41.

(36) Wasielewski, M. R.; Niemczyk, M. P.; Svec, W. A.; Pewitt, E. B. *J. Am. Chem. Soc.* **1985**, *107*, 5662-5563.

(37) (a) Gust, D.; Moore, T. A. *Adv. Photochem.* **1991**, *16*, 1-65. (b) Wasielewski, M. R. *Chem. Rev.* **1992**, *92*, 435-461. (c) Gust, D.; Moore, T. A. *Top. Curr. Chem.* **1991**, *159,* 103-151.

(38) (a) Cooley, L. F.; Larson, S. C.; Elliott, C. M.; Kelley, D. F. *J. Phys. Chem.* **1991**, *95*, 10694-10700. (b) Larson, S. L.; Elliott, C. M.; Kelley, D. F. *J. Phys. Chem.* **1995**, *99*, 6530-6539.

(39) Weber, J. M.; Rawls, M. T.; MacKenzie, V. J.; Limoges, B. R.; Elliott, C. M. *J. Am. Chem. Soc.* **2007**, *129*, 313-320.

(40) (a) Desilvestro, J.; Gratzel, M.; Kavan, L.; Moser, J.; Augustynski, J. *J. Am. Chem. Soc*. **1985**, *107*, 2988-2990. (b) O'Regan, B.; Gratzel, M. *Nature* **1991**, *353*, 737-740. (c) Nazeerudin, M. K.; Kay, A.; Rodicio, I.; Humphry, B. R.; Mueller, E.; Liska, P.; Vlachopoulos, N.; Gratzel, M. *J. Am. Chem. Soc.* **1993**, *115*, 6382-6390.

(41) Argazzi, R.; Bignozzi, C. A. *J. Am. Chem. Soc.* **1995**, *117*, 11815-11816.

(42) Merrins, A.; Kleverlaan, C.; Will, G.; Rao, S. N.; Scandola, F.; Fitzmaurice, D. *J. Phys. Chem. B* **2001**, *105*, 2998-3004.

(43) Pan, J.; Xu, Y.; Benko, G.; Feyziyev, Y.; Styring, S.; Sun, L.; Akermark, B.; Polivka, T.; Sundstrom, V. *J. Phys. Chem. B* **2004**, *108*, 12904-12910.

(44) (a) Imahori, H.; Guldi, D. M.; Tamaki, K.; Yoshida, Y.; Luo, C.; Sakata, Y.; Fukuzumi, S. *J. Am. Chem. Soc.* **2001**, *123,* 6617-6628. (b) Guldi, D. M.; Imahori, H.; Tamaki, K.; Kashiwagi, Y.; Yamada, H.; Sakata, Y.; Fukuzumi, S. *J. Phys. Chem. A* **2004**, *108*, 541-548.

(45) Junza, V. M.; Rizzi, A.; Jolliffe, K. A.; Head, N. J.; Row, M. N. P.; Braslavsky, S. E. *Phys. Chem. Chem. Phys.* **2005**, *7*, 4114-4125.

(46) (a) Jolliffe, K. A.; Langford, S. J.; Ranasinghe, M. G.; Shephard, M. J.; Paddon-Row, M. N. *J. Org. Chem.* **1999**, *64*, 1238-1246. (b) Jolliffe, K. A.; Bell, T. D. M.; Ghiggino, K. P.; Langford, S. J.; Paddon-Row, M. N. *Angew. Chem. Int. Ed. Engl.* **1998**, *37*, 916-919. (c) Jolliffe, K. A.; Langford, S. J.; Oliver, A. M.; Shephard, M. J.; Paddon-Row, M. N. *Chem. Eur. J.* **1999**, *5*, 2518-2530.

(47) Schumacher, A. L.; Sandanayaka, A. S. D.; Hill, J. P.; Ariga, K.; Karr, P. A.; Araki, Y.; Ito, O.; D'Souza, F. *Chem. Eur. J.* **2007**, *13*, 4628-4635.

(48) Maniga, N. I.; Sumida, J. P.; Stone, S.; Moore, A. L.; Moore, T. A.; Gust, D. *J. Porphyrins Phthalocyanines* **1999**, *3*, 32–44.

(49) Gust, D.; Moore, T. A.; Moore, A. L.; Macpherson, A. N.; Lopez, A.; DeGraziano, J. M.; Gouni, I.; Bittersmann, E.; Seely, G. R.; Gao, F.; Nieman, R. A.; Ma, X. C.; Demanche, L.; Luttrull, D. K.; Lee, S.-J.; Kerrigan, P. K. *J. Am. Chem. Soc.* **1993**, *115*,11141–11152.

(50) Schmittel, M.; Lin, H.-W. *Angew. Chem. Int. Ed.* **2007**, *46*, 893-896.

(51) (a) Nazeeruddin, M. K.; Censo, D. D.; Baker, R. H.; Gratzel, M. *Adv. Funct. Mater.* **2006**, *16*, 189-194. (b) Coronado, E.; Mascaro, J. R. G.; Gastaldo, C. M.; Palomares, E.; Durrant, J. R.; Vilars, R.; Gratzel, M.; Nazeeruddin, M. K. *J. Am. Chem. Soc.* **2005**, *127*, 12351-12356.

(52) Ghosh, A.; Ganguly, B.; Das, A. *Inorg. Chem.* **2007**, *46*, 9912-9918.

(53) He, C.-L.; Ren, F.-L.; Zhang, X.-B.; Dong, Y.-Y.; Zhao, Y. *Anal. Sci.* **2006**, *22*, 1547-1551.

(54) Geißer, B.; Alsfasser, R. *Inorg. Chim. Acta* **2003**, *348*, 179-186.

CHAPTER 2

Long-lived Charge Separation in new Ru(bipyridine)$_3^{2+}$- D Dyads Containing One, Two and Three Phenothiazine Moieties

2.1. Abstract

Synthesis and photophysical properties of three Ru(bpy)$_3^{2+}$ - Ptz (bpy = 2,2'-bipyridine and Ptz = phenothiazine) dyads; ***Ru-Ptz****,* ***Ru-Ptz$_2$*** *and* ***Ru-Ptz$_3$****, where the number of Ptz groups increased from one to three, are presented. The MLCT absorption bands of these compounds were slightly red shifted compared to Ru(bpy)$_3^{2+}$. The emission, however, was highly quenched and this was attributed to electron transfer from the Ptz moiety to the excited Ru(bpy)$_3^{2+}$ to generate the charge separated state Ru(bpy)$_3^{+}$ - Ptz$^{\bullet+}$. Observed electron transfer rates ($k_{et} > 10^8\ s^{-1}$) were much faster than those previously reported ($k_{et} < 10^7\ s^{-1}$) for linked Ru(bpy)$_3^{2+}$ - Ptz systems. Compared to the previous systems, back electron transfer rates in these systems were about 100 times slower. This has enabled us to observe the charge separated state in nanosecond flash photolysis experiments. Transient absorptions assignable to Ru(bpy)$_3^{+}$ and Ptz$^{\bullet+}$, having lifetimes in the range of 10-30 ns were observed. In order to explain the fast charge separation and slow charge recombination rates, formation of a folded conformer where the Ptz group attached to one bpy residue comes closer to and associates with another bpy moiety was invoked.*

A scheme which explains the fast electron transfer and slow recombination in this pre-associated state is proposed.

2.2. Introduction

Attaining long-lived photoinduced charge separation (CS) in $Ru(bpy)_3^{2+}$ based dyads or triads is a challenging goal in electron transfer chemistry. Almost all of the $Ru(bpy)_3^{2+}$ based dyads reported so far have CS state lifetimes in the picosecond time range.[1] Extremely rapid back electron transfer (BET) coupled with masking of the transient absorption in the bleaching (400-550 nm) and emission (620-750 nm) regions make it difficult to observe the CS states in $Ru(bpy)_3^{2+}$ based D-A systems. For example, in $Ru(bpy)_3^{2+}$-A type dyads such as $(Ru(bpy)_3^{2+}$-$(CH_2)_n$-MV^{2+} and $Ru(bpy)_3^{2+}$-$(CH_2)_n$-$DQ^{2+})$[1a-c] (MV^{2+} = methyl viologen and DQ^{2+} = diquat), $k_{BET} \geq k_{PET}$ and hence the CS states have lifetimes less than one nanosecond. For useful applications of PET reactions, the ratio k_{PET} / k_{BET} should be greater than 10^3. This means that in the $Ru(bpy)_3^{2+}$ systems k_{PET} has to increase and k_{BET} has to decrease. Structural modifications of existing, well-studied D-A systems could be an effective approach to improve the k_{PET} / k_{BET} ratio. In this chapter we describe such an approach, which enabled us to observe the CS state of a $Ru(bpy)_3^{2+}$ based dyad in the nanosecond time window.

In $Ru(bpy)_3^{2+}$-CH_2-MV^{2+} k_{PET} is already very high (6×10^{10} s^{-1})[2] and this does not give much scope for improvement. In the case of $Ru(bpy)_3^{2+}$-$(CH_2)_n$-Ptz dyads, k_{PET} values were found to be very low (< 10^7 s^{-1})[3] and gives some scope for

improvement through structural modifications. ΔG^0 for PET in the $Ru(bpy)_3^{2+}$ - Ptz system is very close to zero and this could be one reason for the low k_{PET} value. k_{PET} could be increased by increasing the driving force for the PET reaction and/or decreasing the spatial separation between the D and A moieties. Hammarstrom *et al*. have reported that k_{BET} values are already low (= 5.7×10^7 s^{-1}) in $Ru(bpy)_3^{2+}$ - Ptz systems.[4] We reasoned that in the $Ru(bpy)_3^{2+}$ - Ptz systems transient absorptions due to the CS state may be observed in the nanosecond time scales if k_{PET} values could be increased by two orders of magnitude. We observed that this could be achieved by using an amide linker between the $Ru(bpy)_3^{2+}$ and Ptz and details of this investigations are presented in this chapter.

The synthesis, photophysical and PET processes of three $Ru(bpy)_3^{2+}$ - Ptz dyads are summarized in this chapter. These dyads have one, two or three Ptz donors covalently linked to the bpy moieties through the amide [-$(CH_2)_3$-NH-CO-] linkage. The amide group plays the crucial role; the electron withdrawing carbonyl group helped to lower the reduction potential of $Ru(bpy)_3^{2+}$ leading to an increase in the driving force of the reaction and the rigidity of the amide linkage helps in bringing the Ptz and Ru moieties spatially close to each other leading to fast through space electron transfer from Ptz to $Ru(bpy)_3^{2+}$. We observed that this modification has resulted in increasing k_{PET} and reducing k_{BET}, which in turn allowed us to observe the CS state in the nanosecond time scale. These dyads exhibited CS states, which have lifetimes in the 10 – 30 ns range, which is about 100 times more compared to $Ru(bpy)_3^{2+}$ - based

dyads reported earlier. Structures of the dyads studied are shown in Figure 2.1.

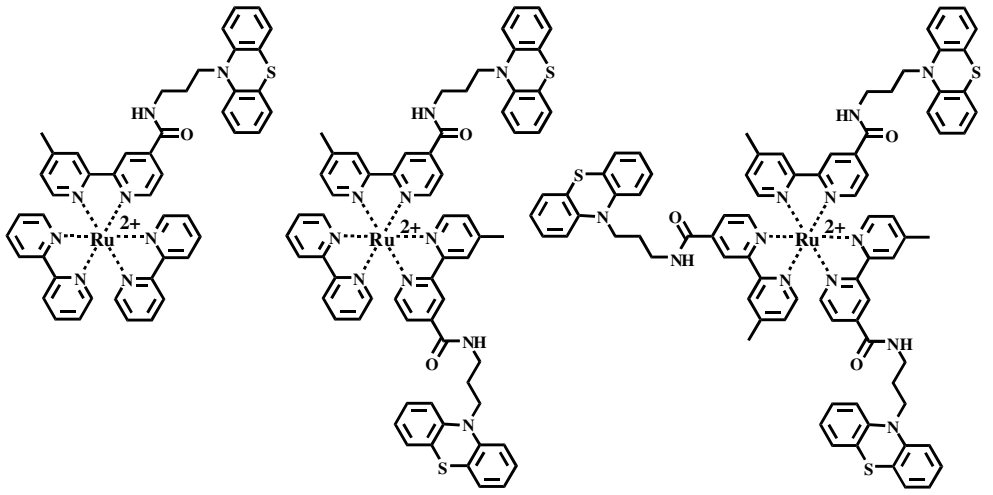

Figure 2.1. Structures of the $Ru(bpy)_3^{2+}$ - Ptz dyads studied.

2.3. Results and Discussion

2.3.1. Synthesis and Characterization of Ru-Ptz, $Ru\text{-}Ptz_2$ and $Ru\text{-}Ptz_3$

For the synthesis of **Ru-Ptz**, **$Ru\text{-}Ptz_2$** and **$Ru\text{-}Ptz_3$**, the phenothiazine-linked bipyridine ligand (bpy-Ptz ligand **1**, Figure 2.2) was required. The Ptz moiety was coupled to the bpy unit through the propyl-amide linkage.

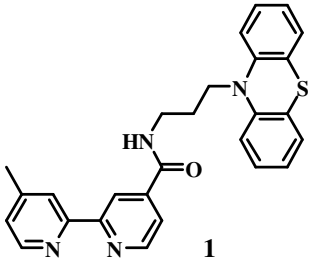

1

Figure 2.2

1 was synthesized as shown in Scheme 2.1. 4'-Methyl-2,2'-bipyridine-4-carboxylic acid,[5] **2**, was first converted to the acid chloride **3**, which was then coupled with *N*-(3-aminopropyl)phenothiazine to get **1**.

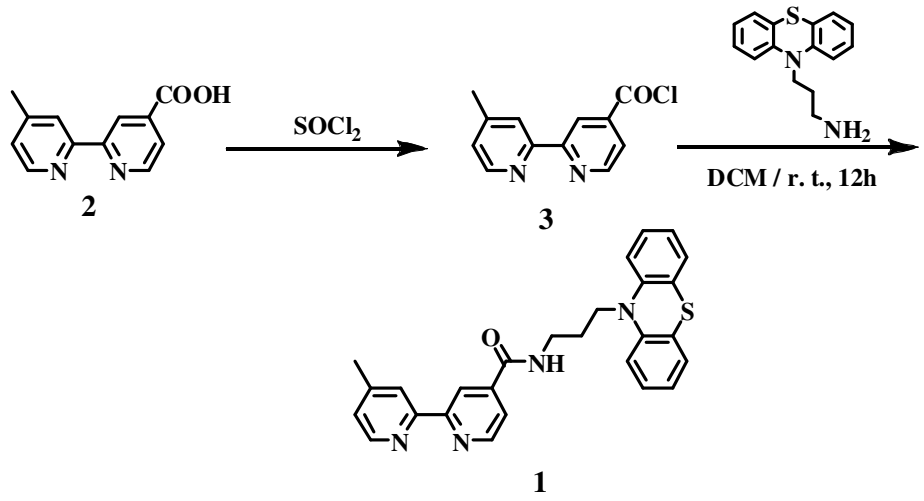

Scheme 2.1

Synthesis of **Ru-Ptz** was achieved by the reaction of the Ru *bis*bipyridyl complex **5** with one equivalent of ligand **1** (Scheme 2.2). **5** in turn was prepared by refluxing 2,2'-dipyridyl with $RuCl_3$ in DMF in the presence of lithium chloride for 2h. Synthesis of **Ru-Ptz$_2$** and **Ru-Ptz$_3$** were done as shown in Scheme 2.2. The synthesis of all the *tris*-complexes were carried out in dioxan-ethanol-water medium by refluxing the starting materials at 80 ^{o}C for 36 hours. All the Ru-Ptz systems were thoroughly purified and characterized by spectroscopic methods such as NMR, IR, high- resolution mass and elemental analysis (see experimental section).

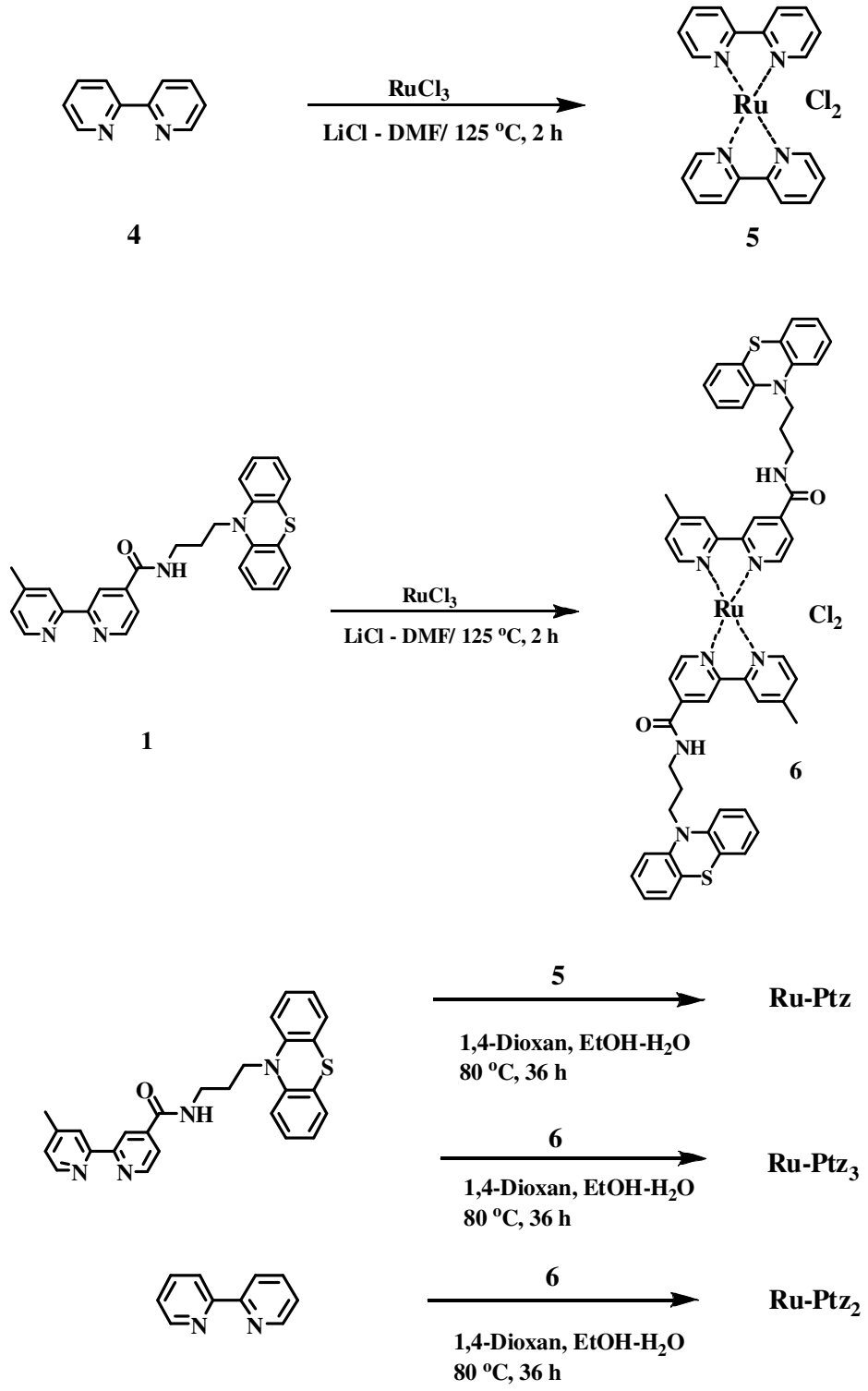

Scheme 2.2. Synthesis of $Ru(bpy)_3^{2+}$ - Ptz dyads

2.3.2. Absorption Studies

The absorption spectrum of $Ru(bpy)_3^{2+}$ consisted of intense bands in the UV and visible regions. The long wavelength absorption centered around 450 - 460 nm corresponds to the RuL_3^{2+} metal-to-ligand charge transfer (MLCT) transition and the band around 300 nm corresponds to the bipyridine π–π* transitions. Figure 2.3(a) shows the UV-Vis spectra of **Ru-Ptz**, **Ru-Ptz$_2$** and **Ru-Ptz$_3$** in acetonitrile (ACN). For the purpose of comparison, the absorption spectrum of $Ru(bpy)_3^{2+}$ also is shown in the figure. In Figure 2.3(b), the MLCT absorptions of the compounds are enlarged.

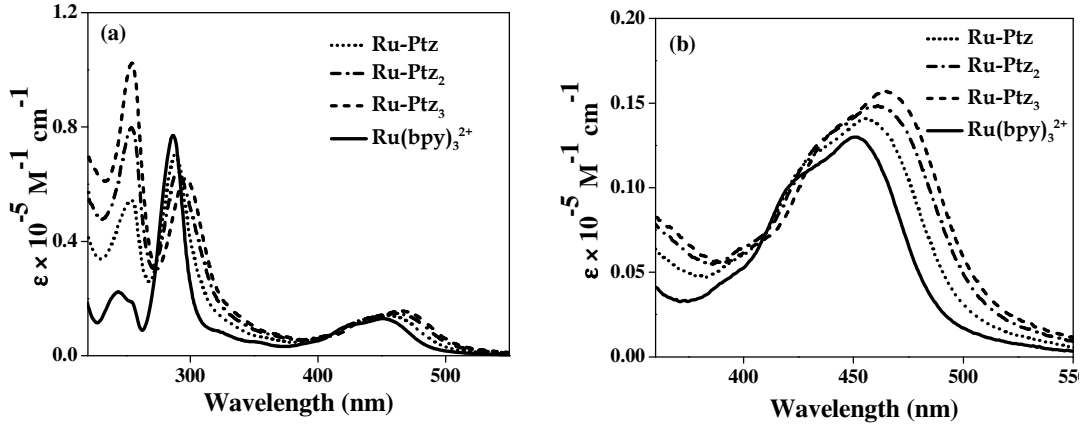

Figure 2.3. (a) Absorption Spectra of **Ru-Ptz**, **Ru-Ptz$_2$**, **Ru-Ptz$_3$** and **$Ru(bpy)_3^{2+}$** in ACN. (b) MLCT (π_M–π_L*) absorptions of the three systems are enlarged.

Depending on the number of bpy-Ptz ligands, the absorption spectra show slight red shifts for the MLCT and π–π* transitions. Upon going from **Ru-Ptz** to **Ru-Ptz$_3$** the MLCT band shifts from 456 to 465 nm with slight increase in the extinction coefficient. The bipyridine based π–π* transition shifts from 288 to 296 nm with

slight decrease in intensity. Absorptions corresponding to the coordinated Ptz units were observed around 255 nm and the intensity of this band increased considerably with increase in the number of Ptz units. Absorption maxima and extinction coefficients for the MLCT and π–π* transitions are given in Table 2.1. Absorption spectra of these compounds were very similar in dichloromethane (DCM) solution.

2.3.3. Emission Studies

Emission spectra of the Ru-Ptz dyads are shown in Figure 2.4(a). In Figure 2.4(b) the emission spectrum of **Ru-Ptz** is compared with that of $Ru(bpy)_3^{2+}$ standard. The emission maxima of the Ru-Ptz derivatives showed very little change, but the emission intensity exhibited considerable quenching compared to $Ru(bpy)_3^{2+}$.

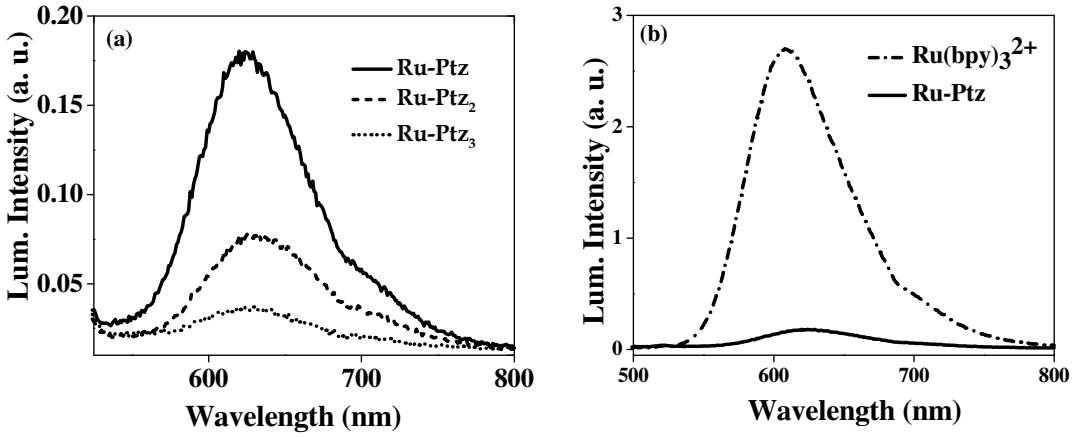

Figure 2.4. (a) Emission spectra of **Ru-Ptz**, **Ru-Ptz$_2$** and **Ru-Ptz$_3$** in ACN. (b) A comparison of the emission of **Ru-Ptz** with $Ru(bpy)_3^{2+}$ standard.

Based on literature reports we attribute the emission quenching to electron transfer. Excitation of the $Ru(bpy)_3^{2+}$ chromophore leads to formation of the MLCT

excited state, which is quenched by transfer of an electron from the Ptz moiety leading to the formation of $Ru(bpy)_3^+$ and phenothiazine radical cation ($Ptz^{\bullet+}$) as shown in equations (2.1) and (2.2).

$$\mathbf{Ru(bpy)_3^{2+}\text{—}Ptz \xrightarrow{h\nu} *Ru(bpy)_3^{2+}\text{—}Ptz} \qquad \mathbf{(2.1)}$$

$$\mathbf{*Ru(bpy)_3^{2+}\text{—}Ptz \longrightarrow Ru(bpy)_3^{+}\text{—}Ptz^{\bullet+}} \qquad \mathbf{(2.2)}$$

Figure 2.4 (a) shows that the emission quenching increases with increase in the number of Ptz groups. When the number of quencher groups increases, the probability of PET increases resulting in enhanced quenching. Observations similar to this were reported previously for Ru based systems containing different number of quencher units covalently connected to Ru chromophore.[3] The emission quantum yields for the systems were measured using the relative method. The emission maxima and quantum yields measured for these systems are given in Table 2.1. The extent of luminescence quenching with respect to the number of Ptz units are reflected in the decreasing values of emission quantum yields. Absorption and emission properties of the three systems were studied in DCM also. For all compounds, emission maxima were blue shifted by 20-30 nm in DCM solution (Table 2.2), but emission intensities were similar to those in ACN. For all these molecules the energy $E_{0,0}$ of the emitting state was calculated from the onset of the emission and these values are also given in Tables 2.1 and 2.2. These $E_{0,0}$ values were used for estimating the feasibility of the PET processes occurring in these systems (vide infra).

Table 2.1. Absorption and emission data for the Ru-Ptz complexes in ACN.

Complex	λ_{abs} (nm)	ε (M^{-1} cm^{-1})	λ_{em} (nm)	Φ_f	$E_{0,0}$ (eV)
Ru- Ptz	456 288 254	14,100 69,100 55,000	630	0.0035	2.14
Ru- Ptz_2	459 289 255	14,800 65,650 77,700	626	0.0014	2.11
Ru- Ptz_3	465 296 255	15,700 61,800 1,09,900	629	0.0003	2.1

Table 2.2. Absorption and emission data for the Ru-Ptz complexes in DCM.

Complex	λ_{abs} (nm)	ε (M^{-1} cm^{-1})	λ_{em} (nm)	Φ_f	$E_{0,0}$ (eV)
Ru- Ptz	457 288 254	15,847 78,260 57,326	608	0.0037	2.1
Ru- Ptz_2	459 292 255	15,020 67,020 76,257	611	0.0015	2.13
Ru- Ptz_3	463 297 255	14,602 61,204 91,225	598	0.00035	2.1

2.3.4. Electrochemical Studies

Redox potentials: Redox potentials of the Ru-Ptz derivatives were measured in ACN using square wave voltammetry. For all the compounds two oxidation peaks and three reduction peaks were observed. As an example, square wave voltammogram of **Ru-Ptz** is shown in Figure 2.5 and redox potentials of all the dyads are listed in Table

2.3. The oxidation peaks at 0.75 V and 1.34 V (vs SCE) were attributed to Ptz → $Ptz^{\bullet+}$ and Ru(II) → Ru(III) oxidations, respectively. The reductions are ligand based reductions[4] and hence substitution of electron withdrawing groups such as –CO–NH– on the bpy moiety is expected to facilitate the reduction of bpy and shift the reduction potential to less negative values. The fact that the first reduction of **Ru– Ptz_2** occurs at less negative potential compared to **Ru–Ptz** can be explained in this manner. In the case of **Ru–Ptz_3**, the first reduction potential shifts to more negative value and we attribute this to steric factors. In **Ru–Ptz_3**, three alkyl-Ptz units cover the $Ru(bpy)_3^{2+}$ core. Since the Ptz moieties are electron rich, the incoming electron would experience repulsive interactions from the Ptz electron cloud, and this could lead to a negative shift in the reduction potential. In the case of **Ru–Ptz** and **Ru–Ptz_2**, the bpy ligands are not fully covered by Ptz moieties and hence this effect may not operate.

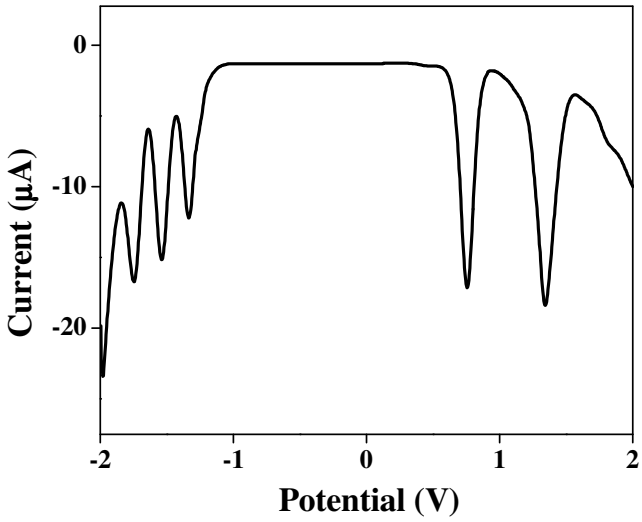

Figure 2.5. Sqaure wave voltammogram of **Ru-Ptz** in ACN using tetrabutyl- ammonium hexafluorophosphate as supporting electrolyte.

Using the redox potentials, we can calculate the free energy change (ΔG^0) for electron transfer (from Ptz to *$Ru(bpy)_3^{2+}$) using the Weller equation,

$$\Delta G^0 = E_{ox} - E_{red} - E_{0,0} - e^2/\varepsilon_S d \qquad (2.3)$$

where E_{ox} is the oxidation potential of the Ptz moiety and E_{red} is the first reduction potential of $Ru(bpy)_3^{2+}$ moiety in the dyad, $E_{0,0}$ is the energy of the MLCT state, ε_S is the dielectric constant of the solvent and d is the distance separating the D and A moieties. The dielectric constant is very high for ACN and hence the fourth term in equation (2.3) will be very small and can be neglected. ΔG^0 for the electron transfer reaction shown in equation (2.2) was calculated for all the three Ru-Ptz systems and these values are also given in Table 2.3. Notice that ΔG^0 are small but negative for all the systems, indicating that the electron transfer reactions are thermodynamically allowed.

Table 2.3. Redox potentials for the Ru-Ptz complexes in ACN at 298 K.

Complex	$E_{1/2}$ (V vs SCE)					ΔG^0 (eV)
	Oxidation		Reduction			
Ru- Ptz	1.302	0.712	-1.332	-1.492	-1.752	-0.056
Ru- Ptz_2	1.312	0.712	-1.242	-1.462	-1.712	-0.156
Ru- Ptz_3	1.322	0.712	-1.362	-1.462	-1.692	-0.026

2.3.5. Luminescence Lifetime Measurements

Emission decays of the Ru-Ptz systems were measured in ACN and DCM solutions using the single photon counting technique. Emission decays were bi-exponential for all the three Ru-Ptz dyads. Emission decay profiles of these derivatives in ACN are shown in Figure 2.6. These decays were fitted to the bi-exponential function,

$$I_t = a_1\exp(-t/\tau_1) + a_2\exp(-t/\tau_2) \qquad (2.4)$$

where I_t is the fluorescence intensity at time t, τ_1 and τ_2 represents the two lifetimes and a_1 and a_2 represent the contributions of these lifetimes. Goodness of the fits was examined using χ^2 values (between 1.0 and 1.2) and residual fits.

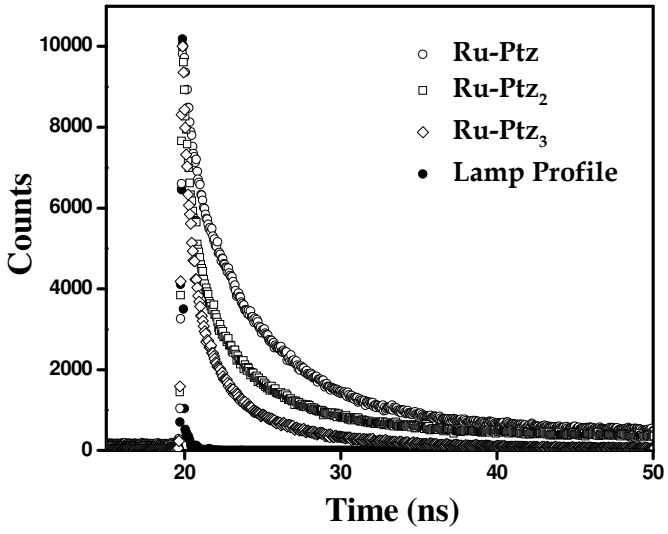

Figure 2.6. Emission decay profile of **Ru-Ptz**, **Ru-Ptz$_2$** and **Ru-Ptz$_3$** in ACN. Excitation was at 401 nm and emission was monitored at 630 nm. The lamp profile also is shown.

The lifetime values and their contributions in the two solvents are shown in Tables 2.4 and 2.5. For all the three derivatives in ACN the short lifetime (τ_1) was < 1 ns and its contribution was around 20% (Table 2.4). In DCM solution τ_1 was > 1 ns and its contribution also was high. In both the solvents τ_1 decreased with increase in the number of Ptz groups (Table 2.5). In ACN, the contribution due to the long component (τ_2) was larger and τ_2 decreased with the number of Ptz groups. For all these molecules an average lifetime $<\tau>$ was calculated using the following expression[6]

$$<\tau> = \sum a_i \tau_i^2 \,/\, \sum a_i \tau_i) \qquad (2.5)$$

$<\tau>$ values calculated using equation (2.5) are also given in Tables 2.4 and 2.5. It can be seen that $<\tau>$ value decreases with increase in the number of Ptz groups in ACN, but such a trend was not seen in DCM solution. Average lifetimes of Ru-Ptz systems were very small compared to the luminescence lifetime (τ_0 = 870 ns) of the parent $Ru(bpy)_3^{2+}$ chromophore. The reduction in the lifetime is attributed to electron transfer as shown in equation (2.2) and hence the average rate constant for electron transfer was calculated using equation (2.6).

$$k_{et} = (1/<\tau>) - (1/\tau_0) \qquad (2.6)$$

The k_{et} values thus calculated are also shown in Tables 2.4 and 2.5. Notice that k_{et} increases with number of Ptz groups in ACN, but no such correlation is observed in DCM. Using k_{et} values the quantum yield of electron transfer Φ_{et} can be calculated

($\Phi_{et} = k_{et}/[k_{et} + (1/\tau_0)]$). Since $k_{et} >> (1/\tau_0)$, Φ_{et} values are close to unity for all the three systems.

Table 2.4. Luminescence lifetimes and k_{et} values for the Ru-Ptz systems in ACN. Percentage contributions of the lifetimes are given in parenthesis.

	τ_1, ns	τ_2, ns	$<\tau>$, ns	k_{et}, 10^8 s^{-1}
Ru-Ptz	0.85 (17%)	4.16 (83%)	4.02	2.47
Ru-Ptz$_2$	0.75 (18%)	4.0 (82%)	3.91	2.54
Ru-Ptz$_3$	0.56 (22%)	2.93 (78%)	2.81	3.54

Table 2.5. Luminescence lifetimes and k_{et} values for the Ru-Ptz systems in DCM. Percentage contributions of the lifetimes are given in parenthesis.

	τ_1, ns	τ_2, ns	$<\tau>$, ns	k_{et}, 10^8 s^{-1}
Ru-Ptz	1.75 (48%)	6.08 (52%)	5.16	1.92
Ru-Ptz$_2$	1.72 (27%)	3.34 (73%)	3.08	3.23
Ru-Ptz$_3$	1.33 (33%)	5.08 (67%)	4.65	2.13

Emission lifetimes of several Ru-Ptz dyads were measured in the past by others.[4] In these systems the Ptz groups were attached to $Ru(bpy)_3^{2+}$ by flexible methylene chains (Ru-$(CH_2)_n$-Ptz) and the emission decays were single exponential with a small percentage of a long lifetime component. The contribution due to the long lifetime component varied with sample preparation. It was reported that the

samples were extremely sensitive to light and air and careful purification led to a decrease in the long-lived component. One can thus attribute the long-lived component to an impurity. In the case of the Ru-Ptz derivatives reported here, bi-exponential decays are not due to the presence of any impurity. The ^{1}H NMR, high-resolution mass spectrum and the elemental analysis (CHN) did not indicate the presence of impurities. The percentage contributions of the different components did not vary with sample preparation. If the two-component decay is due to the presence of an impurity, then the relative contributions of the two components should be similar in the two solvents. Tables 2.4 and 2.5 show that the contributions of the two components are highly solvent dependent. Our samples were not very sensitive to air or light. Absorption spectra and emission lifetime profiles of samples exposed to air and light were not different from those due to fresh samples. The bi-exponential decays might be most probably due to some different conformations of the Ptz group with respect to $Ru(bpy)_3^{2+}$ core or to different PET mechanisms (vide infra).

2.3.6. Nanosecond Laser flash photolysis

In order to further ascertain the PET between the photo-excited $Ru(bpy)_3^{2+}$ chromophore and the attached Ptz residues, nanosecond laser flash photolysis experiments were carried out using the 532 nm light from a Nd-YAG laser. For the $Ru(bpy)_3^{2+}$- D and $Ru(bpy)_3^{2+}$- A dyads reported earlier, no transients were observable in the nanosecond time scale. For all the Ru-Ptz systems reported here, transients assignable to Ru(I) and $Ptz^{\bullet+}$ could be observed in the nanosecond time scale. Figure

2.7(a) shows the transient absorption spectrum obtained for **Ru-Ptz** in ACN. The transient spectra exhibited absorptions around 370 nm and 510 nm regions. Figures 2.7(b) and (c) show the kinetic traces corresponding to the two absorption maxima. Similar spectra were obtained for ACN and DCM solutions. Based on literature reports we assign the 370 nm absorption to $Ru(bpy)_3^+$ and the 510 nm band to $Ru(bpy)_3^+$ and $Ptz^{\bullet+}$. Both the absorptions exhibited the same decay rate.

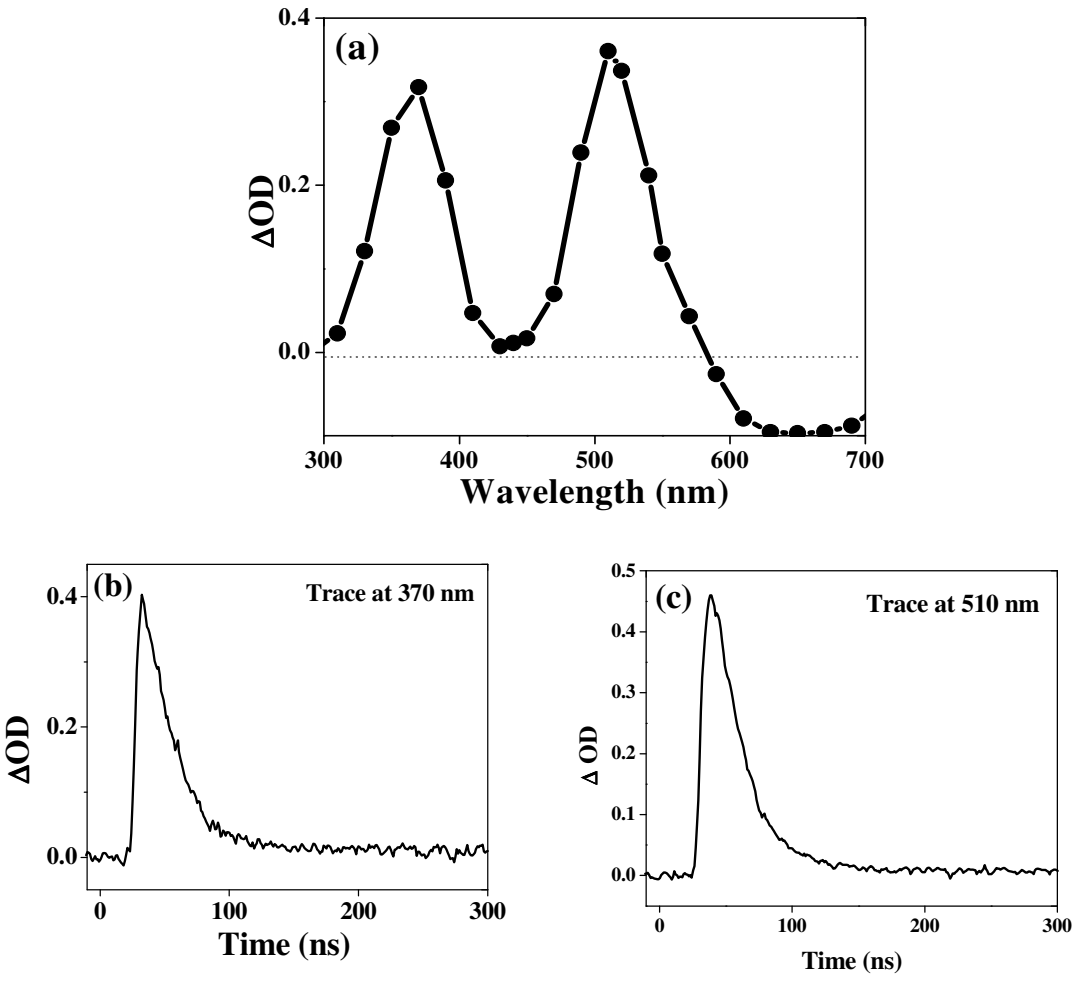

Figure 2.7.(a) Transient absorption spectrum of **Ru-Ptz** in deaerated ACN obtained immediately after the laser pulse. Kinetic profiles of the transient absorptions at (b) 370 nm and (c) 510 nm also are shown.

Similar transient absorption features were obtained for the **Ru-Ptz$_2$** and **Ru-Ptz$_3$** derivatives. Transient spectra and kinetic traces of the two derivatives are shown in Figures 2.8 and 2.9.

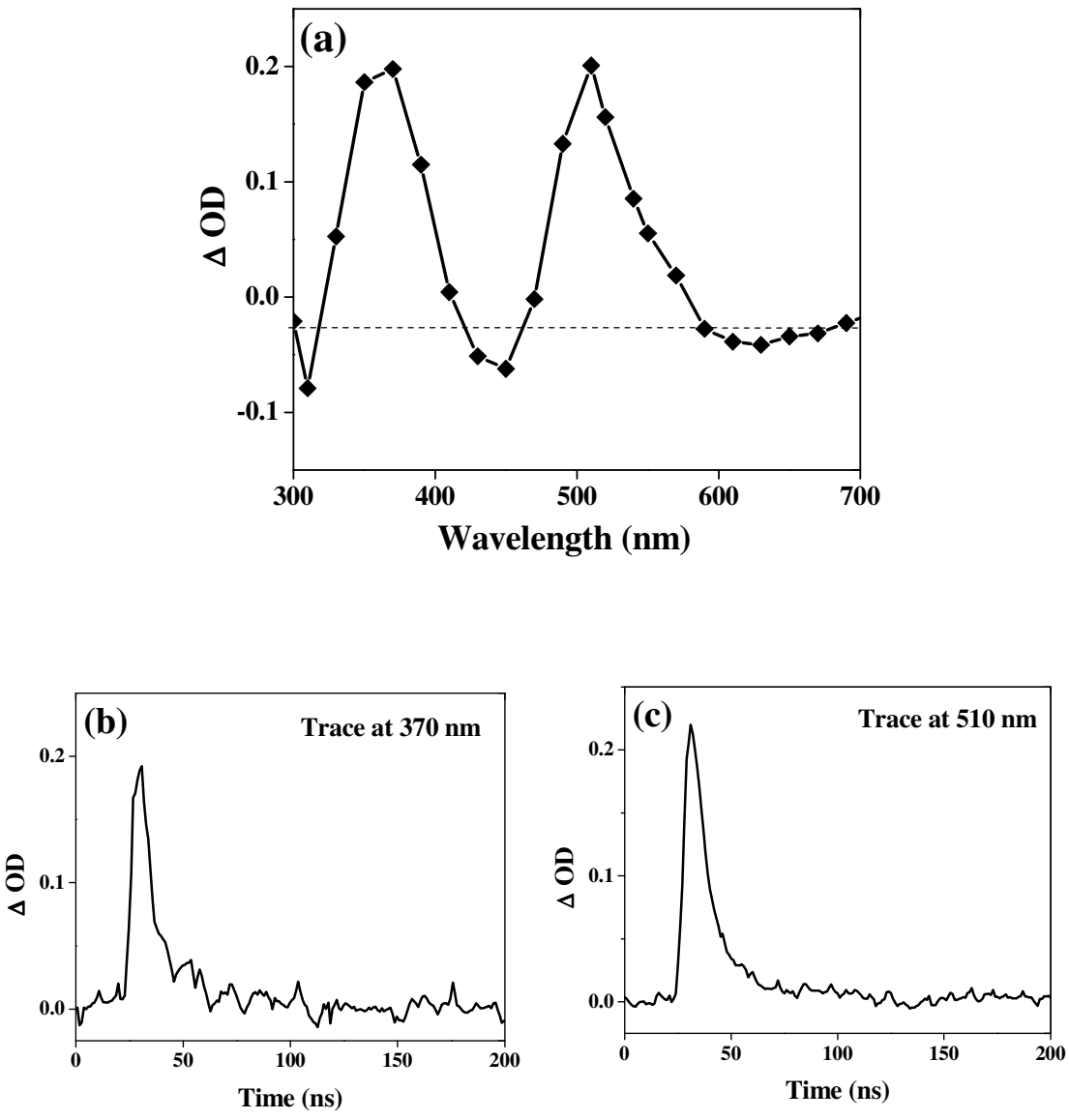

Figure 2.8.(a) Transient absorption spectrum of **Ru-Ptz$_2$** in deaerated ACN obtained immediately after the laser pulse. Kinetic profiles of the transient absorptions at (b) 370 nm and (c) 510 nm also are shown.

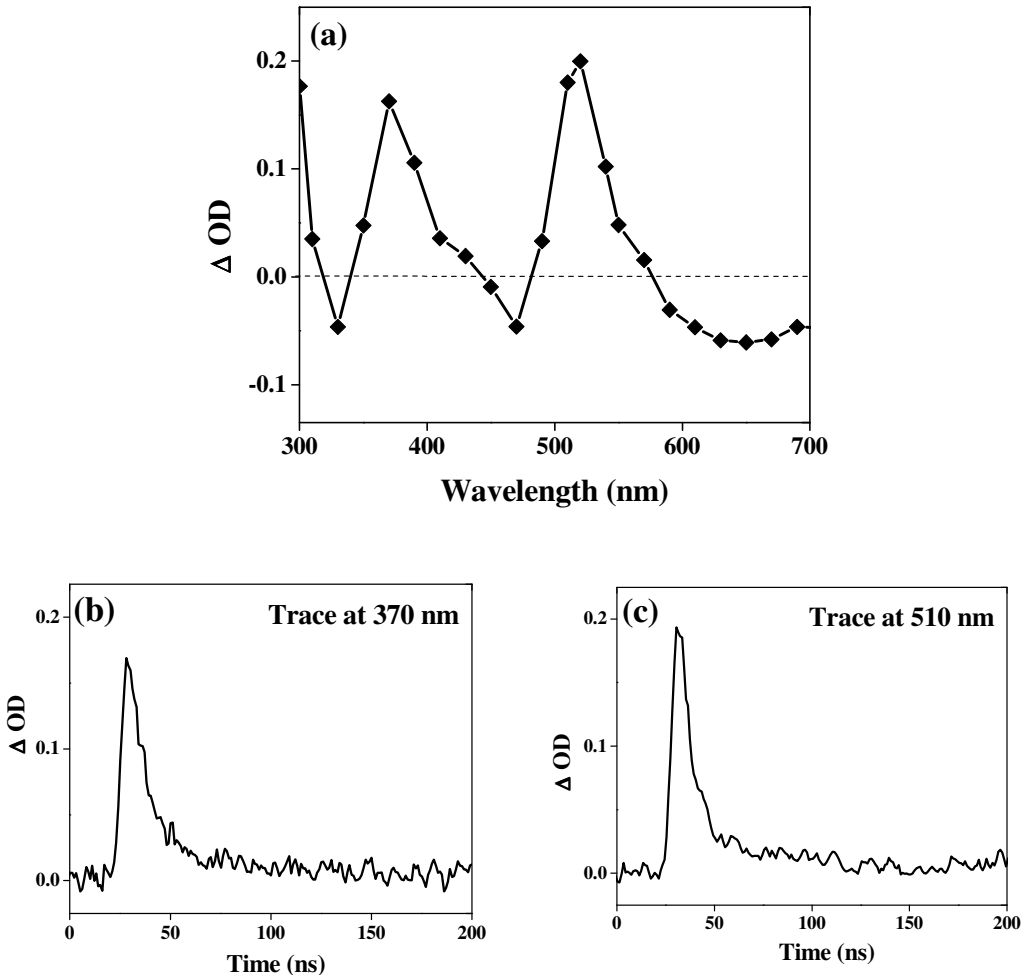

Figure 2.9. (a) Transient absorption spectrum of **Ru-Ptz$_3$** in deaerated ACN obtained immediately after the laser pulse. Kinetic profiles of the transient absorptions at (b) 370 nm and (c) 510 nm also are shown.

Reduction of $Ru(bpy)_3^{2+}$ to $Ru(bpy)_3^{+}$ has been accomplished previously by several methods.[7,8] In aqueous solution, $Ru(bpy)_3^{+}$ exhibits absorption bands at 360 nm ($\varepsilon = 2 \times 10^4$ M^{-1} cm^{-1}) and 500 nm ($\varepsilon = 1.5 \times 10^4$ M^{-1} cm^{-1}).[8b] In the present case, the flash photolysis experiments were carried out in ACN or DCM and the absorption maxima are shifted to the red by nearly 10 nm. For the $Ptz^{\bullet+}$, the absorption maximum is at 514 nm ($\varepsilon = 9.2 \times 10^3$ M^{-1} cm^{-1}) in ACN.[9] Thus, if PET occurs as per equation

(2.1), we would expect $Ru(bpy)_3^{+}$ and $Ptz^{\bullet+}$ to form in equal amounts and this would result in absorption at 360-370 nm (due to $Ru(bpy)_3^{+}$ alone, $\varepsilon = 2 \times 10^4$ $M^{-1}cm^{-1}$) and at 510 nm (due to $Ru(bpy)_3^{+}$ and $Ptz^{\bullet+}$ [1:1 ratio, total $\varepsilon = 2.42 \times 10^4$ M^{-1} cm^{-1}]). Transient absorption spectrum obtained for all the Ru-Ptz systems showed two peaks of nearly equal intensity confirming this assignment. In all cases, decays of the transients were exponential and independent of wavelength. Thus the decay is assigned to the back electron transfer (BET) process, which regenerates the starting dyads. No permanent product was formed in these laser irradiations. The absorption maxima and decay rates for the three systems in ACN are given in Table 2.6. Lifetimes of the transients are in the 10-30 ns range. For **Ru-Ptz**, decay of the transient was slightly faster in dichloromethane. For other systems the decays were similar in both solvents. By monitoring the absorption at 370 nm, the $\Phi_{CS(obsd)}$ values were determined (see experimental section) and these are also shown in Table 2.6. It may be noted that the $\Phi_{CS(obsd)}$ values also decreased with increase in the number of phenothiazine moieties present. It was mentioned previously that the quantum yield of electron transfer Φ_{et} is close to unity for all systems, but $\Phi_{CS(obsd)}$ obtained from the ΔOD values are much smaller. This is most probably due to the fast BET process. The time resolution of the nanosecond flash photolysis system is about 8 ns. Hence the 0-8 ns time window is not accessible and within this time window a fraction of the CS states would have undergone BET. Since BET rates are higher for **Ru-Ptz$_2$** and **Ru-Ptz$_3$**, $\Phi_{CS(obsd)}$ values are lower for these systems.

Table 2.6. Data obtained from transient absorption studies of Ru-Ptz systems in ACN.

Complex	λ_{max}, nm	τ, ns	k_{bet}, 10^7 s^{-1}	$\phi_{CS(obsd)}$
Ru- Ptz	370, 510	25.7	3.89	0.60
Ru- Ptz_2	370, 510	19.0	5.26	0.27
Ru- Ptz_3	370, 510	10.0	10.0	0.23

Phenothiazine is the most popular reductive quencher for metal polypyridyl systems. The pioneering studies of Meyer and co-workers[10] on Re(I)-Ptz systems showed rapid (< 10 ns) quenching of the MLCT excited state with formation of a CS state containing reduced Re(I) and $Ptz^{\bullet+}$. BET took place in several tens of nanoseconds in these systems. For the Ru-$(CH_2)_n$-Ptz systems,[3] quenching of the MLCT state was very slow (40-200 ns). Transient absorption data in the nanosecond time scale was not available for these systems and we believe that $k_{bet} >> k_{et}$ in these systems. In such cases absorptions due to the CS state will not be detected in nanosecond flash photolysis experiments. No transients were observed in the nanosecond time scales for the Ru-MV^{2+} systems also.[1a,b] An important aspect of the present work is that the charge separated state could be observed in the nanosecond time scales. In our systems, it was observed that $k_{et} > k_{bet}$, making it possible to observe the transients in the nanosecond time scales.

Compared to the Ru-$(CH_2)_n$-Ptz systems reported earlier, this report presents two new significant observations: (1) Charge separation in our systems is at least one order of magnitude faster and (2) BET occurs in the nanosecond time window which is about 100 time slower. The values of driving force for the PET reactions, we have calculated are very low, (Table 2.3) and do not support the fast k_{et} values observed. The Ru-Ptz systems reported here differ from the earlier systems only in the nature of the linkage. We have used a CO-NH-$(CH_2)_3$- group between the Ptz and bpy moieties instead of the alkyl chain. Photophysical and electrochemical properties of our Ru-Ptz systems are very much similar to those of Ru-$(CH_2)_n$-Ptz systems. We can thus safely attribute the observed differences to structural and geometrical factors arising due to substitution of the CO-NH group. The CO-NH group can affect the Ru-D system in two ways. The CO-NH fragment is very rigid and can cause turns or twists in the molecule. It is also an electron-withdrawing group and this could lead to changes in electronic effects. With the aid of these two aspects we try to explain our observations in the following way.

It is known that excitation of $Ru(bpy)_3^{2+}$ leads to population of the metal to ligand charge transfer state (MLCT) state. This involves transfer of an electron centered on the metal to one of the three bipyridine ligands. When all three ligands are the same, each ligand has 1/3 probability of having the transferred electron. When one of the ligands is having an electron-withdrawing CONH group, we expect the electron to be transferred preferably to that ligand due to the electron withdrawing property of the carbonyl group in the amide functionality, as shown in Scheme 2.3.

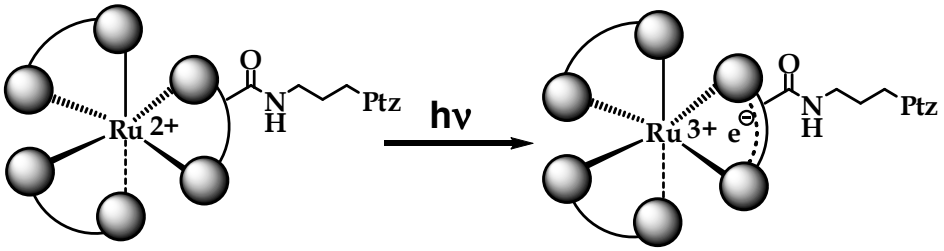

Scheme 2.3

The second step involves transfer of an electron from Ptz to the Ru^{3+} centre. If this electron transfer has to occur through the -NH-CO-bpy ligand, it would have to overcome a repulsive interaction from the electron already in the bpy ligand due to MLCT transition. This electron-electron repulsion would certainly reduce the PET rate and Φ_{CS}. The electron transfer actually occurs much faster compared to Ru-$(CH_2)_n$-Ptz systems. The fast electron transfer can be explained by invoking a closed conformation in which one of the bpy ligands or the Ru^{3+} metal center is spatially very close to the Ptz moiety. Electron transfer can then occur to the metal center either directly through space or through the bpy ligand orbitals as shown in Scheme 2.4.

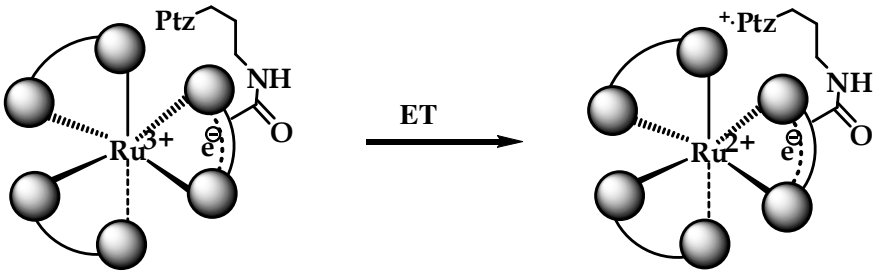

Scheme 2.4

Luminescence decays of Ru-Ptz were bi-exponential indicating two types of electron transfer processes. This could result from two different conformations of the Ptz group with respect to the bpy moiety or due to two different pathways of electron

transfer. For example, electron transfer can occur through the ligand or directly to the Ru centre through a Ptz-Ru interaction involving vacant *d* orbitals of Ru.

The slow BET occurring in the Ru-Ptz systems can also be explained on the basis of Scheme 2.4. In Scheme 2.4, an electron is transferred from Ptz to Ru^{3+} center to give Ru^{2+} and $Ptz^{\bullet+}$. BET from Ru^{2+} to $Ptz^{\bullet+}$ is thermodynamically uphill by about 0.5 eV. The excess electron now resides in the bpy-CONH- ligand and BET can occur in two ways; (1) transfer of the electron through the intervening –CO-NH-$(CH_2)_3$-linkage, (2) transfer of the electron to the Ru^{2+} center to give Ru^{+} followed by BET between Ru^{+} and $Ptz^{\bullet+}$. The former process is expected to be slow because of the six intervening bonds. The latter is a two step mechanism and is further slowed by the repulsion between the Ru^{2+} and $Ptz^{\bullet+}$ positive centers. Recently it has been pointed out that the coulombic repulsion between Ru^{2+} and $Ptz^{\bullet+}$ is about 80 kJ/mol.[11] As a result, immediately after electron transfer, the Ru^{2+} and $Ptz^{\bullet+}$ moieties would move away from each other at a rate somewhat greater than diffusion controlled rates.[11] All these factors can contribute to a lowering of the BET rate which enables us to observe absorptions due to the Ru^{+} and $Ptz^{\bullet+}$ moieties in the nanosecond time scale.

An important question which remains to be answered is whether the folded or closed conformation shown in Scheme 2.4 is formed from a pre-associated ground state or by bond reorganization in the excited state. In a recent report Elliot and co-workers suggested pre-association of bpy and Ptz moieties in DQ^{2+}-$Ru(bpy)_3^{2+}$-Ptz (DQ^{2+} = diquat) triads.[11] The pre-association is suggested to be driven by entropy and

van der Waals interactions and not by enthalpy. It was suggested that Ptz group in this triad folds back and associates with the bpy residue to which it is attached as shown in Scheme 2.5[11].

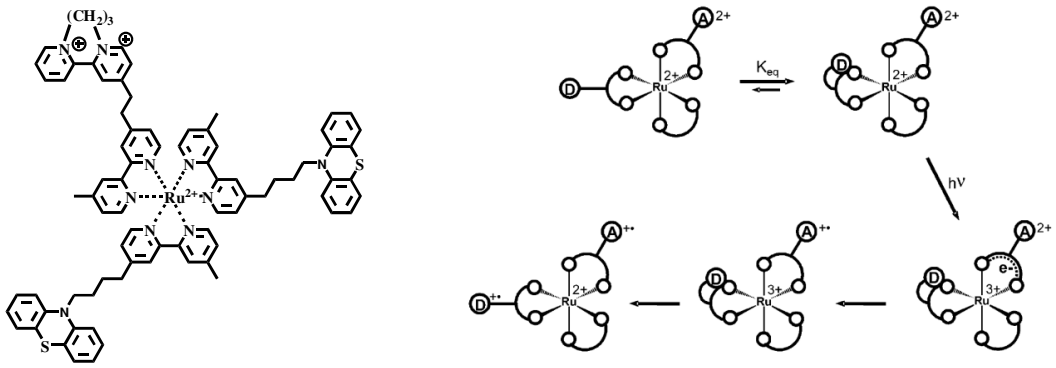

Scheme 2.5 (Taken from reference 11)

Based on the observation of fast PET and Scheme 2.4, we propose that in the Ru-Ptz systems studied here the Ptz moiety associates with a bpy moiety to which it is not attached, as shown in Scheme 2.4. The CO-NH group to which the Ptz moiety is attached may cause a twist in the spatial positioning of the linker and this could result in a geometry shown in Scheme 2.4. Molecular models show that such association is sterically possible without significant strain energy.

We have observed that both k_{et} and k_{bet} increases with increase in the number of Ptz moieties. This, however, is not a major effect and the rate increase was only by a factor of two, at most. Most probably this may arise due to geometric factors. When more Ptz groups are present, the average spatial separation between the bpy and Ptz and/or Ru^{+} and $Ptz^{\bullet+}$ decreases leading to the observed increase in the rates. Earlier

studies with Ru-$(CH_2)_n$-Ptz systems also showed increase in k_{et} rates with increase in the number of quencher groups,[3] but increase in the k_{bet} rates with increase in the number of quencher units was unexpected. The $\Phi_{CS(obsd)}$ also decreased with increase in the number of Ptz groups. For **Ru-Ptz$_2$** and **Ru-Ptz$_3$**, k_{bet} values are relatively high and this leads to a decrease in the optical density at 1 ns, which results in low $\Phi_{CS(obsd)}$ values.

2.4. Conclusions

In this chapter, we have investigated the charge separation and charge recombination in three covalently linked $Ru(bpy)_3^{2+}$ - Ptz systems. Charge separation in these molecules takes place about ten times faster compared to Ru-$(CH_2)_n$-Ptz systems studied earlier. The BET rates were slower by two orders of magnitude. We invoked the presence of a folded conformation where the Ptz moiety attached to a bpy ligand comes closer and pre-associates with another bpy group to explain the fast k_{et} and slow k_{bet}. Since the BET rates were slower than k_{et}, transient absorptions corresponding to $Ru(bpy)_3^{+}$ and $Ptz^{\bullet+}$ could be observed in the nanosecond time scales.

2.5. Experimental Section

2.5.1. Measurements

Melting points were determined on a Mel-Temp II melting point apparatus and are uncorrected. Proton NMR data were obtained from a JEOL EX-300 MHz Brucker

Avance DPX spectrometer. FT-IR spectra were recorded on a Shimadzu IR Prestige 21 spectrometer. Electronic absorption spectra were recorded on a Shimadzu UV-3101 PC NIR Scanning Spectrophotometer. Steady state emission studies were done on a SPEX Fluorolog F112X Spectrofluorimeter with right angle geometry. Emission quantum yields were determined in ACN by the relative method employing an optically matched solution of $Ru(bpy)_3^{2+}$ in ACN as reference (Φ_f = 0.059).[12] The following equation was used.[13]

$$\Phi_f = \Phi_R \frac{AOD_R n^2}{A_R OD n_R^2} \qquad (2.7)$$

In equation (2.7) the subscript R refers to the reference, *OD* is the optical density at the excitation wavelength ($OD < 0.1$), *n* is the refractive index of the solvent and *A* is the area under the emission spectrum. Emission lifetime measurements were performed using an IBH picosecond single photon counting system employing a 401 nm nano-LED excitation source and a Hamamatsu C4878-02 microchannel plate (MCP) detector. Electrochemical experiments were carried out with a BAS CV50W voltammetric analyzer in argon-purged ACN solutions with 0.1 M tetra-*n*-butylammonium hexafluorophosphate [(TBA)PF_6] as supporting electrolyte. Laser flash photolysis experiments were carried out with an Applied Photophysics Model LKS-20 laser kinetic spectrometer equipped with a Nd: YAG laser. The analyzing and laser beams were fixed at right angles to each other. The laser energy was 100 mJ at 532 nm. Optical densities of the argon purged solution samples for the experiments

were 0.3 at 532 nm in 1 cm cell. Observed quantum yields of the CS states ($\Phi_{CS(obsd)}$) for the Ru-Ptz systems were determined by relative actinometry employing an optically matched solution of $Ru(bpy)_3^{2+}$ in ACN as reference. The following equation was used.[14]

$$\Phi_{CS(obsd)} = \Phi_R \frac{\Delta OD_s \varepsilon_R}{\Delta OD_R \varepsilon_s} \quad \textbf{(2.8)}$$

Here, R refers to $Ru(bpy)_3^{2+}$ and S refers to $Ru(bpy)_3^{+}$; ΔOD = end-of-pulse optical densities of transients and ε = extinction coefficients of transients. For the reference compound $Ru(bpy)_3^{2+}$, values of Φ_R = 0.95 and ε_R = 13,500 M^{-1} cm^{-1} at 370 nm were used.[8a] For the transient absorptions of Ru-Ptz systems, ΔOD at 370 nm (ε = 20,000 M^{-1} cm^{-1})[8b] corresponding to $Ru(bpy)_3^{+}$ was used.

2.5.2. Chemicals and Solvents

4'-Methyl-2,2'-bipyridine-4-carboxylic acid,[5] $Ru(bpy)_2Cl_2$[15] and *N*-(3-aminopropyl)phenothiazine[16] were synthesized following reported procedures. Solvents used in the synthesis were dried before use by standard methods. Spectroscopic grade solvents were used for photophysical and electrochemical measurements.

Synthesis of ligand 1: 4'-methyl-2,2'-bipyridine-4-carboxylic acid (1.5 g, 6.14 mmol) was refluxed in thionyl chloride (10 mL) for 24 h in argon atmosphere. The excess thionyl chloride was thoroughly removed and the residue was used as such for

the next step assuming that all the acid was converted to the corresponding acid chloride. A solution of *N*-(3-aminopropyl)phenothiazine (1.88 g, 7.34 mmol) in DCM (10 mL) was added to a suspension of the acid chloride in DCM (15 mL) followed by triethylamine (0.5 mL). The reaction mixture was stirred at room temperature for 12 h. Solvent was removed and the residue was extracted with chloroform and water. The organic phase was washed with sodium bicarbonate solution and concentrated. The crude product was precipitated by the addition of hexane, which was further purified by chromatography over silica using chloroform as the eluent. Yield of **1**:- 1.20 g (43%); mp. 124-125 °C; IR ν_{max} cm^{-1} 3294, 3059, 2951, 2866, 1649, 1595, 1546, 1458, 1365, 1327, 1286, 1251, 831, 750; ^{1}H NMR ($CDCl_3$) δ 2.18 (m, 2 H), 2.46 (s, 3 H), 3.59 (q, 2 H), 4.02 (t, 2 H), 6.91 (m, 5 H), 7.05 (d, 2 H), 7.17 (m, 3 H), 7.49 (m, 1 H), 8.25 (s, 1 H), 8.47 (s, 1 H), 8.57 (d, 1 H), 8.69 (d, 1 H). HRMS (FAB); Observed 453.10 (Calculated 452.57).

Synthesis Ru-Ptz: $Ru(bpy)_2Cl_2$ (0.16 g, 0.33 mmol) was dissolved in 1,4-dioxane (7 mL) and it was diluted with 70% ethanol-water (15 mL). Ligand **1** (0.15 g, 0.33 mmol) was added to the above solution and the dark purple reaction mixture was refluxed for 16 h under Ar. The resultant red orange solution was cooled to room temperature; solvents were removed under vacuum, and the residue was dissolved in methanol and the complex was precipitated by the addition of saturated ammonium hexafluorophosphate solution. The orange solid obtained was filtered and dried. Further purification was done by column chromatography in silica using 1:1 acetonitrile/toluene

as the eluent. Yield 0.18 g (47%); mp > 300 °C; IR ν_{max} cm^{-1} 3657, 3425, 3078, 2935, 1664, 1541, 1460, 1305, 1242, 1035, 842, 761; ^{1}H NMR (CD_3CN) δ 2.08 (m, 2 H), 2.56 (s, 3 H), 3.50 (m, 2 H), 4.02 (t, 4 H), 6.86 (m, 4 H), 6.99 (d, 2 H), 7.18 (t, 2 H), 7.28 (d, 1 H), 7.44 (m, 5 H), 7.57 (d, 2 H), 7.79 (m, 4 H), 8.06 (m, 4 H), 8.41 (s, 1 H), 8.54 (m, 4 H). HRMS (FAB); Observed 866.22 (M - $2PF_6^-$); (Calculated 866.21).

Synthesis of Ru-Ptz$_2$: Ligand **1** (265 mg, 0.83 mmol) and LiCl (120 mg) were taken together in dry DMF (5 mL) in a two necked RB flask which was flushed with argon. $RuCl_3.3H_2O$ (109 mg, 0.42 mmol) was added and the reaction mixture was refluxed at 125 °C for 2 h to get a dark purple solution. After cooling to room temperature, water (50 mL) was added and repeatedly extracted with DCM. The dichloromethane fractions were combined and washed with water and dried with anhydrous sodium carbonate. It was then concentrated to 5 mL and the crude product was precipitated by addition of ether (50 mL) to yield the *bis* complex **6**. Yield: - 0.16 g (35%). mp > 300 °C. The product was used as such for the conversion to the *tris* complex. IR ν_{max} cm^{-1} 3456, 3061, 1963, 1695, 1591, 1514, 1338, 1259, 1012, 844. HRMS (FAB); Observed 1076.85 (Calculated 1077.12).

The *bis* complex obtained above (0.06 g, 0.05 mmol) was treated with 2,2'-bipyridine (0.015 g, 0.05 mmol) as given in the procedure for **Ru-Ptz**. Yield of **Ru-Ptz$_2$** was 0.031 g (48%); mp > 300 °C; IR ν_{max} cm^{-1} 3639, 3415, 3068, 2929, 2866, 1664, 1541, 1460, 1286, 1244, 1037, 842, 758; ^{1}H NMR (CD_3CN) δ 2.11 (m, 4 H), 2.60 (s, 6 H), 3.58 (m, 4 H), 4.08 (t, 4 H), 7.06 (m, 16 H), 7.57 (m, 2 H), 7.61 (m, 2

H), 7.77 (m, 2 H), 7.88 (m, 4 H), 8.13 (m, 7 H), 8.75 (d, 2 H), 8.84 (t, 2 H), 9.02 (s, 1 H). HRMS (FAB); Observed 1307.65 (M - PF_6^-) (Calculated 1307.36).

Synthesis of Ru-Ptz$_3$: The synthesis and purification was done following the procedure for **Ru-Ptz**. The *bis* complex (0.08 g, 0.07 mmol) and ligand **1** (0.035 g, 0.07 mmol) were used as starting materials. Yield 0.048 g (39%); mp > 300 °C; IRν_{max} cm^{-1} 3637, 3414, 3064, 2929, 2860, 1666, 1620, 1541, 1460, 1411, 1327, 1286, 1247, 1039, 842, 754; ^{1}H NMR (CD_3CN) δ 2.09 (m, 6 H), 2.61 (s, 9 H), 3.59 (m, 6 H), 4.07 (m, 6 H), 6.90 (t, 6 H), 7.04 (m, 12 H), 7.18 (m, 7 H), 7.45 (m, 3 H), 7.73 (m, 4 H), 7.90 (m, 3 H), 8.14 (m, 4 H), 8.76 (d, 3 H), 8.94 (s, 3 H). HRMS (FAB); Observed 1604.49 (M - PF_6^-) (Calculated 1603.75).

2.6. References

(1) (a) Cooley, L. F.; Headford, C. E. L.; Elliott, C. M.; Kelley, D. F. *J. Am. Chem. Soc.* **1988**, *110*, 6673-6682. (b) Kelly, L. A.; Rodgers, M. A. J. *J. Phys. Chem.* **1995**, *99*, 13132- 13140. (c) Elliott, C. M.; Freitag, R. A.; Blaney, D. D. *J. Am. Chem. Soc*. **1985**, *107*, 4647-4655. (d) Opperman, K. A.; Mecklenburg, S. L.; Meyer, T. J. *Inorg. Chem.* **1994**, *33*, 5295-5301. (e) Dixon, D. W.; Thornton, N. B.; Steullet, V.; Netzel, T. *Inorg. Chem.* **1999**, *38*, 5526-5534. (f) Johansson, O.; Borgstrom, M.; Lomoth, R.; Palmblad, M.; Bergquist, J.; Hammarstrom, L.; Sun, L.; Akermark, B. *Inorg. Chem.* **2003**, *42*, 2908-2918. (g) Immoos, C. E.; Bilio, A. J. D.; Cohen, M. S.; Veer, W. V.; Gray. H. B.; Farmer, P. J. *Inorg.*

Chem. **2004**, *43*, 3593-3596. (h) Cabello, A. G.; Vazquez, P.; Torres, T.; Guldi, D. M. *J. Org. Chem.* **2003**, *68*, 8635-8642.

(2) Yonemoto, E. H.; Riley, R. L.; Kim, Y.; Atherton, S. J.; Schmehl, R. H.; Mallouk, T. E. *J. Am. Chem. Soc*. **1992**, *114*, 8081-8087.

(3) Larson, S. L.; Elliott, C.M.; Kelley, D.F. *Inorg. Chem.* **1996**, *35*, 2070–2076.

(4) Borgstrom, M.; Johansson, O.; Lomoth, R.; Baudin, H. B.; Wallin, S.; Sun, L.; Akermark, B.; Hammarstrom, L. *Inorg. Chem.* **2003**, *42*, 5173-5184.

(5) Khairoutdinov, R. F.; Daubova, L. V.; Haddon, R. C.; Sraf, L. *J. Phys. Chem. B* **2004**, *108*, 19976–19981.

(6) James, D. R.; Liu, Y.-S.; De Mayo, P.; Ware, W. R. *Chem. Phys. Lett.* **1985**, *120*, 460–465.

(7) (a) Anderson, C. P.; Salmon. D. J.; Meyer, T. J.; Young, R. C. *J. Am. Chem. Soc.* **1977**, *99*, 1980–1982. (b) Pramod, P.; Sudeep, P. K.; Thomas, K. G.; Kamat, P. V. *J. Phys. Chem. B* **2006**, *110*, 20737–20741.

(8) (a) Lomoth, R.; Häupl, T.; Johansson, O.; Hammarström, L. *Chem. Eur. J.* **2002**, *8*, 102–110. (b) Mulazzani, Q. G.; Emmi, S.; Fuochi, F. G.; Hoffman, M. Z.; Venturi, M. *J. Am. Chem. Soc.* **1978**, *100*, 981–983.

(9) Moroi, Y.; Braun, A. M.; Grätzel, M. *J. Am. Chem. Soc.* **1979**, *101*, 567–572.

(10) (a) Chen, P.; Westmoreland, T. D.; Danielson, E.; Schanze, K. S.; Anthon, D.; Neveux, P. E.; Meyer, T. J. *Inorg. Chem.* **1987**, *26*, 1116–1126. (b) Chen, P.; Duesing, R.; Tapolsky, G.; Meyer, T. J. *J. Am. Chem. Soc.* **1989**, *111*, 8305–8306.

(11) Weber, J. M.; Rawls, M. T.; MacKenzie, V. J.; Limoges, B. R.; Elliott, C. M. *J. Am. Chem. Soc.* **2007**, *129*, 313–320.

(12) Nakamura, K. *Bull. Chem. Soc. Jpn.* **1982**, *55*, 1639–1640.

(13) Eaton, D. F. in *Handbook of Organic Photochemistry*; Scaiano, J. C., Ed.; CRC Press, Boca Raton, FL, **2000**; Vol. 1, p. 234.

(14) Lutz, H.; Breheret, E.; Lindqvist, L. *J. Phys. Chem.* **1973**, *77*, 1758–1762.

(15) Sullivan, B. P.; Salmon, D. J.; Meyer, T. J. *Inorg. Chem.* **1978**, *17*, 3334–3341.

(16) Godefroi, E. F.; Wittle, E. L. *J. Org. Chem.* **1956**, *21*, 1163–1168.

CHAPTER 3

Synthesis, Photophysical and Electron Transfer Studies of Some $Ru(bpy)_3^{2+}$ Based Higher Order Donor-Acceptor Systems

3.1. Abstract

As a continuation of the Ru-Ptz systems with one, two or three Ptz units studied in Chapter 2, we have investigated $Ru(bpy)_3^{2+}$ systems with two, four and six Ptz moieties and the results are presented in this chapter. These systems are designated as ***Ru-Ptz*** $_{2(S)}$, ***Ru-Ptz*** $_4$ *and* ***Ru-Ptz*** $_6$, *respectively. In these systems forward electron transfer rates increased with increase in the number of Ptz donors. Among these systems,* ***Ru-Ptz*** $_{2(S)}$ *exhibited the highest CS state lifetime of 47 ns. BET rates were also found to increase with increase in the number of Ptz units. Secondary electron transfers from / to the CS state of* ***Ru-Ptz*** $_{2(S)}$ *were also attempted. Acceptors such as dodecylviologen and pyromellitic diimide and the donor trimethoxytriphenylamine were employed in these studies. Products of secondary electron transfers were very long-lived and these were characterized by laser flash photolysis studies. A donor-chromophore-acceptor type triad,* ***Ptz-Ru-NT*** *(NT = 4-nitrotoluene), was also synthesized and studied. Although efficient charge separation occurred in the triad, the CS state lifetime did not show any improvement over the corresponding dyad.*

3.2. Introduction

In the second chapter of this thesis, we have discussed the PET properties of a class of $Ru(bpy)_3^{2+}$-Phenothiazine dyads possessing higher forward electron transfer rates and low back electron transfer rates. This study outlined a novel strategy in designing $Ru(bpy)_3^{2+}$ based systems with long lived charge separation. As a continuation we have investigated the effect of introducing more phenothiazine donor units in the PET reactions of Ru-Ptz systems. Ru-Ptz systems studied in the second chapter had only one Ptz unit attached to the bipyridine ligand. In this chapter we employ bipyridine ligands containing two Ptz moieties and attaching these ligands to $Ru(bpy)_3^{2+}$ resulted in Ru-Ptz systems with two, four and six Ptz units as shown in Figure 3.1 (Ru-Ptz system containing two Ptz units is designated as **Ru-Ptz$_{2(S)}$** to distinguish it from **Ru-Ptz$_2$** reported in the previous chapter. Subscript 'S' is used to indicate that both Ptz units are on the 'same' ligand). Synthesis, characterization and photophysical studies of **Ru-Ptz$_{2(S)}$**, **Ru-Ptz$_4$** and **Ru-Ptz$_6$** are reported in this chapter. Emission quantum yields are very low in these systems indicating rapid electron transfer occurring from the donor Ptz groups to the $Ru(bpy)_3^{2+}$ core.

In the Ru-Ptz dyads we have studied, PET reactions generated dyads observable in the nanosecond time window. Our experiments showed that the CS state of these systems can participate in secondary electron transfer reactions. Taking **Ru-Ptz$_{2(S)}$** as an example we have studied the secondary electron transfer reactions with acceptors such as dodecyl viologen (DV^{2+})[1] and pyromellitic-*N*-(*n*-butyl)-*N'*-(*N*-pyridium)ethyl

diimide (PMDI)[2] and the good electron donor trimethoxytriphenylamine (TMTPA).[3] Structures of these molecules are shown in Figure 3.2.

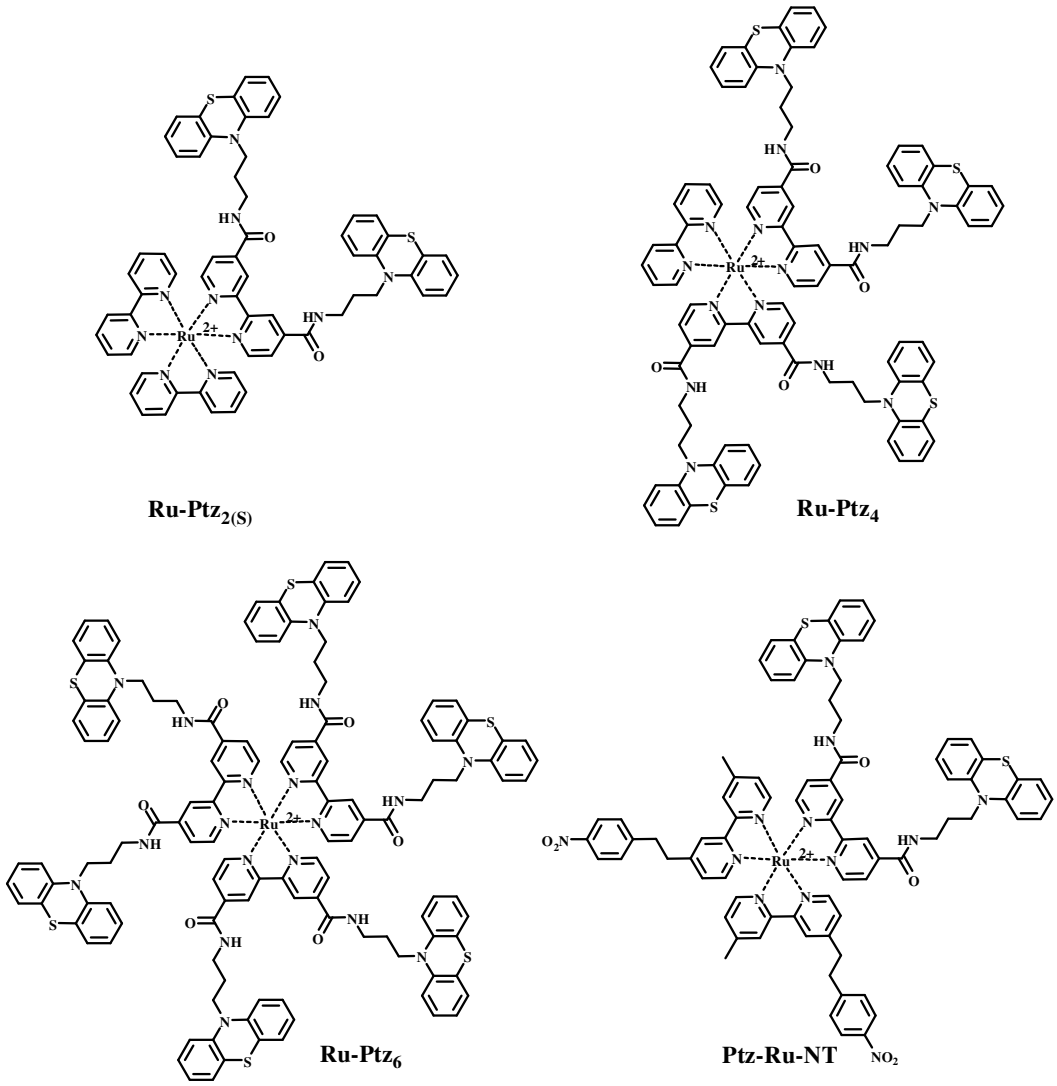

Figure 3.1. Structures of the dyads and triad studied in this chapter

Secondary acceptors / donors shown in Figure 3.2 were selected because of the high extinction coefficients of the transient absorptions of the radical ion products from these

acceptors and donors. We observed that secondary electron transfer resulted in the generation of extremely long-lived products.

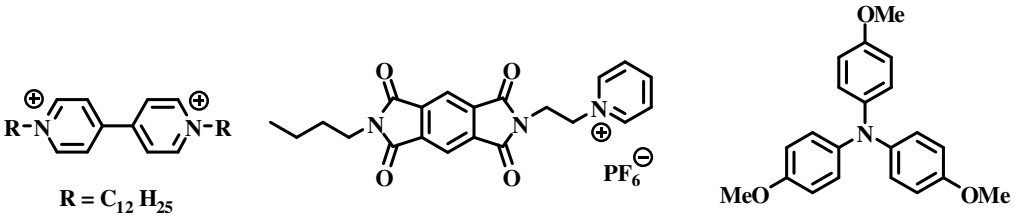

Figure 3.2. Structures of the secondary acceptors/donors employed in this study

Lifetimes of the CS states in general show enhancements upon going from dyads to triads. In order to see if the Ru-Ptz systems can give rise to triads with long CS state lifetimes we have designed the triad **Ptz-Ru-NT** (Figure 3.1), where two of the bipyridine ligands carried the relatively weak electron acceptor, 4-nitrotoluene moiety and the third ligand carried two Ptz donor groups. Synthesis, characterization and photophysical studies of this triad also are described in this chapter.

3. 3. Results and Discussion

3.3.1. Ru-Ptz$_{2(S)}$, Ru-Ptz$_4$ and Ru-Ptz$_6$ dyads

3.3.1.1. Synthesis

Synthesis of the **Ru-Ptz$_{2(S)}$**, **Ru-Ptz$_4$** and **Ru-Ptz$_6$** systems were carried out by following standard synthetic procedures. The bipyridine ligand containing two Ptz units **3**, was synthesized from 2,2'-bipyridine-4,4'-dicarboxylic acid[4] **1** as shown in Scheme

3.1. **1** was converted to the acid chloride **2** by treatment with $SOCl_2$ followed by reaction with *N*-(3-aminopropyl)phenothiazine[5] in dichloromethane (DCM) at room temperature to give **3**.

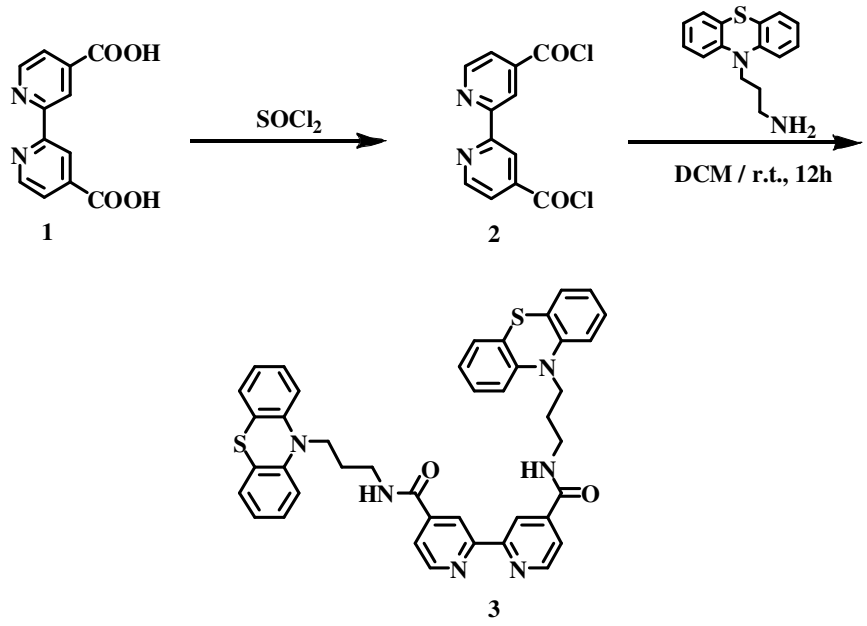

Scheme 3.1

The Ru-Ptz dyads **Ru-Ptz$_{2(S)}$**, **Ru-Ptz$_4$** and **Ru-Ptz$_6$** were synthesized as shown in Scheme 3.2. For the synthesis of **Ru-Ptz$_{2(S)}$** the *bis* bipyridine complex **4** was refluxed with ligand **3** in a mixture of dioxane, ethanol and water for 36 h as shown in Scheme 3.2. For the synthesis of **Ru-Ptz$_4$** and **Ru-Ptz$_6$** the *bis* complex **5** was required. This was synthesized by heating the ligand **3** with $RuCl_3$ in dimethylformamide (DMF) at 125 °C in the presence of lithium chloride. The *bis* complex **5** upon reaction with bipyridine gave **Ru-Ptz$_4$**. Similarly, reaction of **5** with the ligand **3** gave **Ru-Ptz$_6$** (Scheme 3.2).

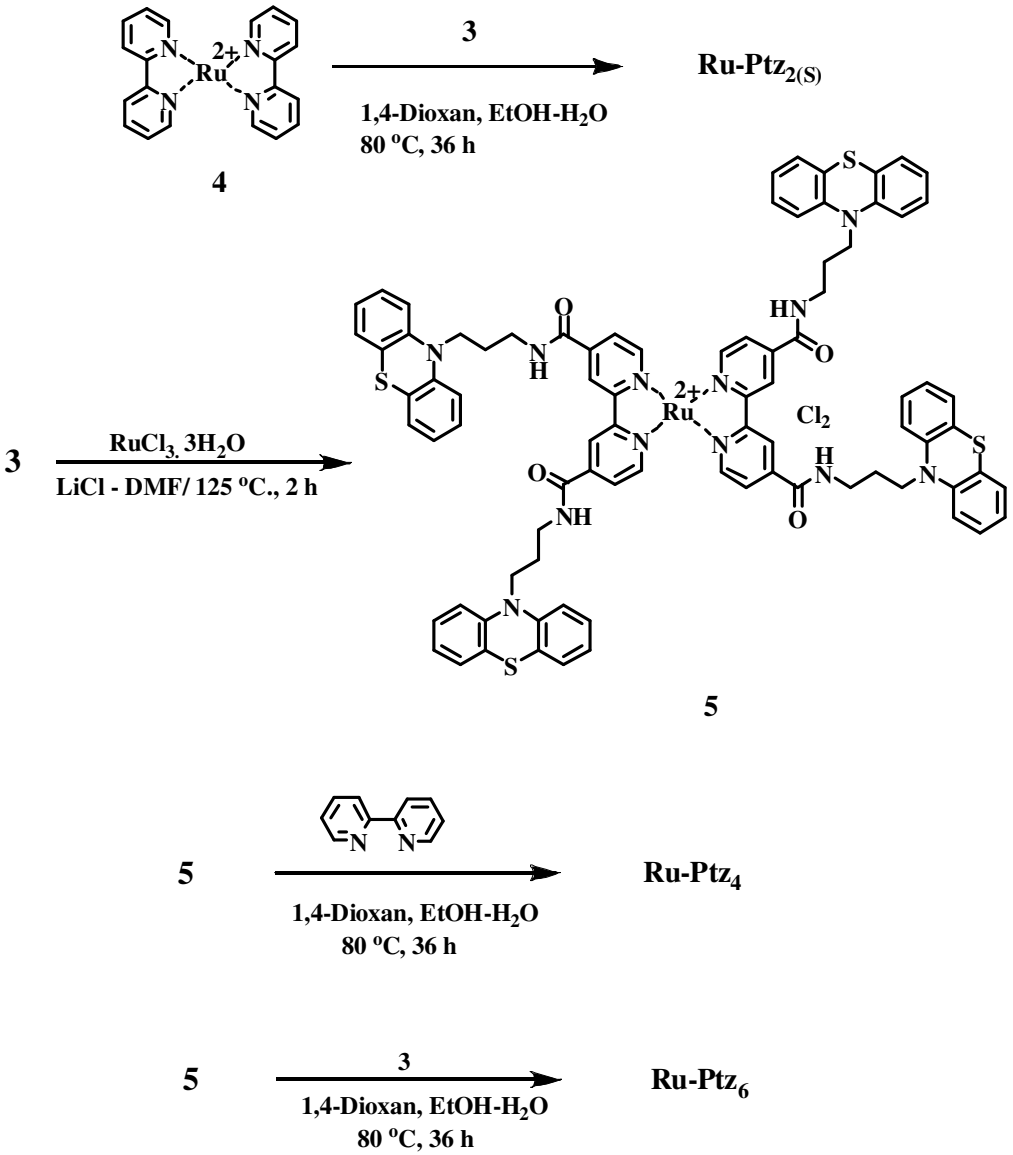

Scheme 3.2

All the three dyads were purified using column chromatography over silica gel using acetonitrile : toluene (1:1) as eluent and characterized thoroughly by various spectroscopic techniques.

3.3.1.2. Absorption Studies

Absorption spectra of **Ru-Ptz$_{2(S)}$**, **Ru-Ptz$_4$** and **Ru-Ptz$_6$** exhibited characteristic bands corresponding to the MLCT absorption in the 400 – 450 nm region and bipyridine based π–π* transitions near 260-320 nm (Figure 3.3).

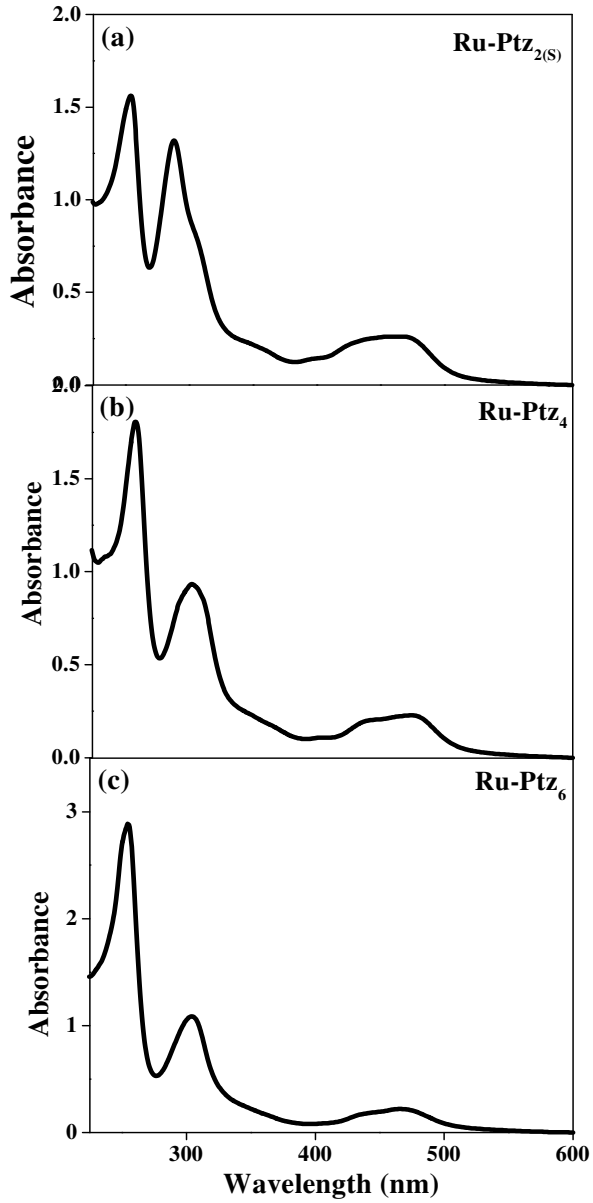

Figure 3.3. Absorption spectra of (a) **Ru-Ptz$_{(2)S}$** (b) **Ru-Ptz$_4$** and (c) **Ru-Ptz$_6$** in ACN.

The contribution from the phenothiazine moiety appeared around 220-260 nm. Although the intensity of the Ptz bands increased with number of Ptz units, the increase in the extinction coefficient was not linear. The absorption corresponding to the bipyridine ligands was found to be slightly red shifted and broadened with the number of substituents in the bpy ligand. Absorption maxima and extinction coefficients of the various transitions are given in Table 3.1. Absorption spectra of these compounds were very similar in other solvents like DCM and toluene.

3.3.1.3. Emission Studies

In Figure 3.4(a) emission spectra of **Ru-Ptz$_{2(S)}$**, **Ru-Ptz$_4$** and **Ru-Ptz$_6$** are compared with that of $Ru(bpy)_3^{2+}$, which showed that emission exhibited by these compounds are extremely weak. The spectra due to **Ru-Ptz$_4$** and **Ru-Ptz$_6$** are barely seen in Figure 3.4(a) and hence these are enlarged in Figure 3.4(b). An examination of the figures clearly suggested that the Ptz groups quenched the $Ru(bpy)_3^{2+}$ emission and that the extent of quenching increased with the number of donor Ptz groups as observed in Chapter 2 of this thesis. The quenching of luminescence could be attributed to the electron transfer from Ptz donor to the $*Ru(bpy)_3^{2+}$. The emission quantum yields for the systems were measured using the relative method employing optically dilute solutions. More efficient quenching of the luminescence was observed here compared to the previous class of dyad systems. The emission maxima and quantum yields measured for these systems also are given in Table 3.1. The emission profiles of these systems

were similar in DCM solution, except a small blue shift observed in the emission maximum.

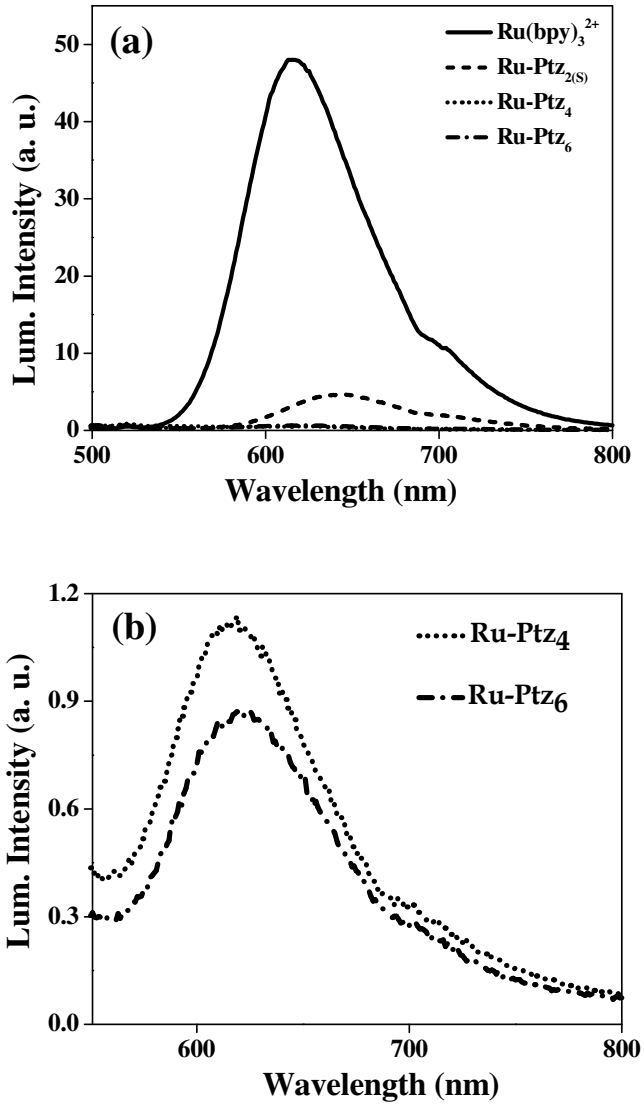

Figure 3.4. (a) Luminescence spectra of **Ru-Ptz$_{2(S)}$**, **Ru-Ptz$_4$** and **Ru-Ptz$_6$** are compared with Ru(bpy)$_3^{2+}$ in ACN. (b) Luminescence spectra of **Ru-Ptz$_4$** and **Ru-Ptz$_6$** are enlarged 45 times.

For the Ru-Ptz systems, energy of the MLCT excited state, $E_{0,0}$ can be

obtained from the onset of the emission spectrum. $E_{0,0}$ values for the three systems are also given in Table 3.1.

Table 3.1. Absorption and emission data of the three Ru-Ptz complexes in ACN.

Complex	λ_{abs} (nm)	ε (M^{-1} cm^{-1})	λ_{em} (nm)	Φ_f	$E_{0,0}$ (eV)
Ru- Ptz$_{2(S)}$	466 288 254	14,890 65,300 78,613	625	0.0018	2.15
Ru- Ptz$_4$	470 297 254	15,200 59,600 1,22,400	621	0.0004	2.13
Ru- Ptz$_6$	474 304 254	15,800 61.600 1,65,300	623	0.00025	2.12

3.3.1.4. Electrochemical Studies

Redox potentials of the three systems were measured by square wave voltammetry in ACN. Square wave voltammogram of **Ru-Ptz$_{2(S)}$** is shown in Figure 3.5, as an example. The voltammogram exhibited two oxidation peaks and three reduction peaks. The first oxidation peak observed in the 0.71 – 0.72 V (vs SCE) region corresponds to the conversion of Ptz to $Ptz^{\bullet+}$ and the second oxidation peak at 1.32 – 1.34 V originated from the Ru (II) → Ru(III) conversion. The oxidation peaks observed here are similar to those obtained for the Ru-Ptz dyads reported in the previous chapter. The three peaks observed in the reduction side are attributed to the bipyridine based reductions and these peaks are shifted to more negative values compared to the systems

described in the second chapter. Upon going from **Ru-Ptz$_{2(S)}$** to **Ru-Ptz$_4$**, values of all the three reduction potentials exhibited shifts to less negative values, indicating that all the three reduction processes become facilitated (Table 3.2). This is due to the substitution of more number of electron withdrawing CO-NH groups to the bpy ligands. Compared to **Ru-Ptz$_4$**, reduction potentials of **Ru-Ptz$_6$** are shifted to more negative values indicating that reduction has become more difficult in this system and this can be attributed to steric factors. Ptz is an electron rich molecule and when more and more Ptz groups surround the $Ru(bpy)_3^{2+}$ core, electrons approaching the bpy ligands would experience a repulsive interaction from the electron cloud of Ptz, making the reduction more difficult. This steric effect would be expected to be maximum for the **Ru-Ptz$_6$** system which has a complete shell of Ptz units surrounding the $Ru(bpy)_3^{2+}$ core.

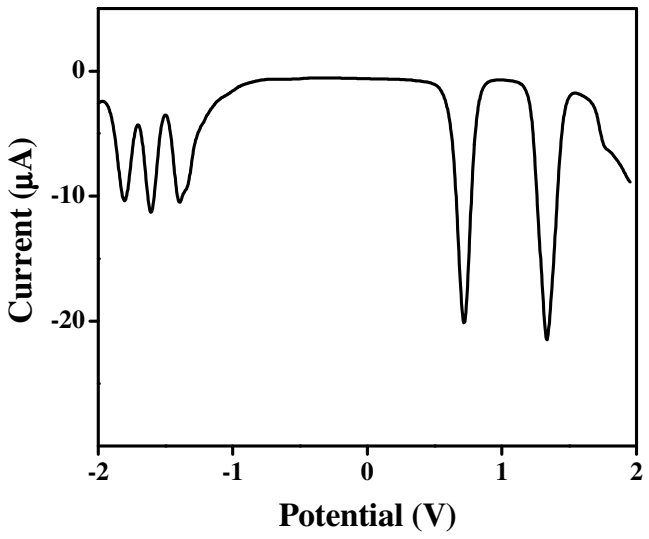

Figure 3.5. Square wave voltammogram of **Ru-Ptz$_{2(S)}$** in ACN using tetrabutylammonium hexafluorophosphate as supporting electrolyte.

The values of redox potentials obtained for **Ru-Ptz$_{2(S)}$**, **Ru-Ptz$_4$** and **Ru-Ptz$_6$** are summarized in Table 3.2. Using the redox potentials and $E_{0,0}$ values (Table 3.1), one can calculate the free energy change (ΔG^0) for electron transfer (from Ptz to *Ru(bpy)$_3^{2+}$) in these systems using the Weller equation,

$$\Delta G^0 = E_{ox} - E_{red} - E_{0,0} - e^2/\varepsilon_S d \qquad (3.1)$$

where E_{ox} is the oxidation potential of the Ptz moiety and E_{red} is the first reduction potential of Ru(bpy)$_3^{2+}$ in the dyad systems, ε_S is the dielectric constant of the solvent and d is the distance separating the two moieties. In ACN solution, the fourth term of the equation will be very small and can be neglected. ΔG^0 for the electron transfer reaction from Ptz to *Ru(bpy)$_3^{2+}$ were calculated for all the three Ru-Ptz dyads studied here and these values are also given in Table 3.2. Notice that ΔG^0 are small but negative for all the systems, indicating that the electron transfer reactions are thermodynamically allowed.

Table 3.2. Redox potentials for the Ru-Ptz complexes in ACN at 298 K

Complex	$E_{1/2}$ (V vs SCE)					ΔG^0
	Oxidation		Reduction			(eV)
Ru- Ptz$_{2(S)}$	1.335	0.719	-1.396	-1.612	-1.808	-0.038
Ru- Ptz$_4$	1.342	0.721	-1.311	-1.599	-1.797	-0.089
Ru- Ptz$_6$	1.319	0.718	-1.362	-1.462	-1.812	-0.044

3.3.1.5. Emission Lifetime Measurements

Emission decays of **Ru-Ptz$_{2(S)}$**, **Ru-Ptz$_4$** and **Ru-Ptz$_6$** were measured in ACN using the single photon counting technique. Decay profiles in ACN for the three systems are shown in Figure 3.6.

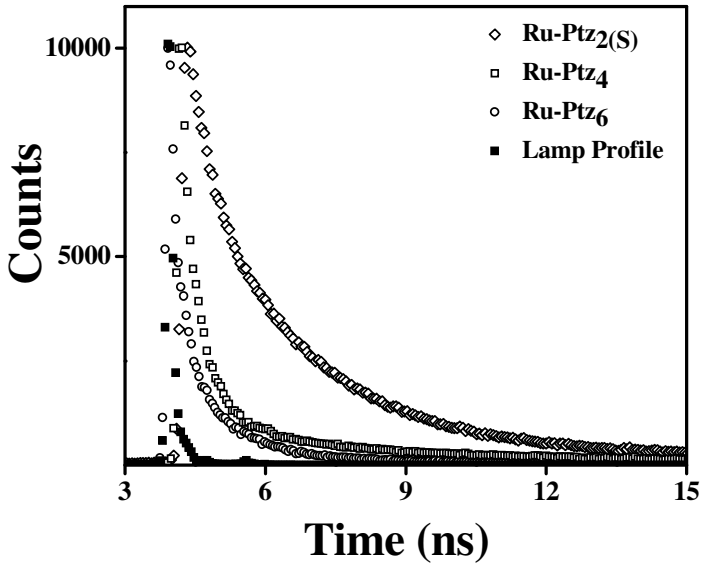

Figure 3.6. Emission decay profiles of **Ru-Ptz$_{2(S)}$**, **Ru-Ptz$_4$** and **Ru-Ptz$_6$** in ACN. Excitation was at 401 nm and emission was monitored at 630 nm. The lamp profile also is shown.

The decays were found to be tri-exponential and were fitted with the following function,

$$I_t = a_1\exp(-t/\tau_1) + a_2\exp(-t/\tau_2) + a_3\exp(-t/\tau_3) \qquad (3.2)$$

where I_t is the fluorescence intensity at time t, τ_1, τ_2 and τ_3 represent the three lifetimes and a_1, a_2 and a_3 represent the contributions of these lifetimes. Fits to the equation were judged using χ^2 values (between 1.0 and 1.2) and fits to the residuals. We have ascertained that the tri-exponential decays are not due to the presence of any impurity in

the sample. The percentage contributions of the different components did not vary with sample preparation. We attribute the tri-exponential decays to different conformations of Ptz groups with respect to the $Ru(bpy)_3^{2+}$ core or to different PET mechanisms.

Lifetime values and their contributions in ACN for the three systems are shown in Table 3.3. The shortest lifetime τ_1 was less than a nanosecond for all the compounds. τ_1 and τ_2 decreased with increase in the number of Ptz groups. For these systems an average lifetime $<\tau>$ was calculated using equation (3.3).

$$<\tau> = \sum a_i \tau_i^2 / \sum a_i \tau_i) \qquad (3.3)$$

$<\tau>$ values calculated using equation (3.3) are also given in Table 3.3. It can be seen that $<\tau>$ value decreases with increase in the number of Ptz groups. Also, $<\tau>$ value for the Ru-Ptz systems were very small compared to the emission lifetime of $Ru(bpy)_3^{2+}$ (τ_0 = 870 ns) in ACN. Lowering of the emission lifetime is due to quenching of $*Ru(bpy)_3^{2+}$ by electron transfer from the attached Ptz moiety and hence the average rate constant for electron transfer can be calculated using equation (3.4).

$$k_{et} = <\tau>^{-1} - \tau_0^{-1} \qquad (3.4)$$

k_{et} values thus calculated are also given in Table 3.3. Notice that k_{et} values are in the 10^8 – 10^9 s^{-1} range and increased with number of Ptz groups. As described in Chapter 1, PET in several $Ru(bpy)_3^{2+}$-Ptz dyads were examined in detail in the past. Rate constants for electron transfer from Ptz to $*Ru(bpy)_3^{2+}$ in these systems were < 10^8 s^{-1}. The k_{et}

values reported in this chapter for the Ru-Ptz systems are the highest ever for intramolecular PET in $Ru(bpy)_3^{2+}$-Ptz dyads.

Table 3.3. Luminescence lifetimes and k_{et} values for the Ru-Ptz systems in ACN. Percentage contributions of the lifetimes are given in parenthesis

	τ_1 (ns)	τ_2 (ns)	τ_3 (ns)	$<\tau>$ (ns)	k_{et} (s^{-1})
Ru-Ptz$_{2(S)}$	0.279 (10.7%)	2.06 (69.6%)	6.06 (19.6%)	2.66	3.7×10^8
Ru-Ptz$_4$	0.196 (63.9%)	0.95 (26.7%)	4.03 (9.4%)	0.75	1.33×10^9
Ru-Ptz$_6$	0.029 (40.6%)	0.463 (28.1%)	4.61 (31.3%)	0.52	1.92×10^9

3.3.1.6. Laser Flash Photolysis Experiments

Laser flash photolysis experiments were carried out in ACN using a 532 nm laser source. **Ru-Ptz$_{2(S)}$**, **Ru-Ptz$_4$** and **Ru-Ptz$_6$** exhibited similar transient absorptions with absorption maxima at 370 and 510 nm. As example, transient absorption spectrum and kinetic traces obtained for **Ru-Ptz$_{2(S)}$** are given in Figure 3.7. Following the assignments made in Chapter 2, we assign the 370 nm absorption to $Ru(bpy)_3^+$ and the 510 nm absorption to $Ru(bpy)_3^+$ and $Ptz^{\bullet+}$. These species are generated as a result of electron transfer from phenothiazine to the ruthenium chromophore. Both absorptions exhibited the same decay kinetics.

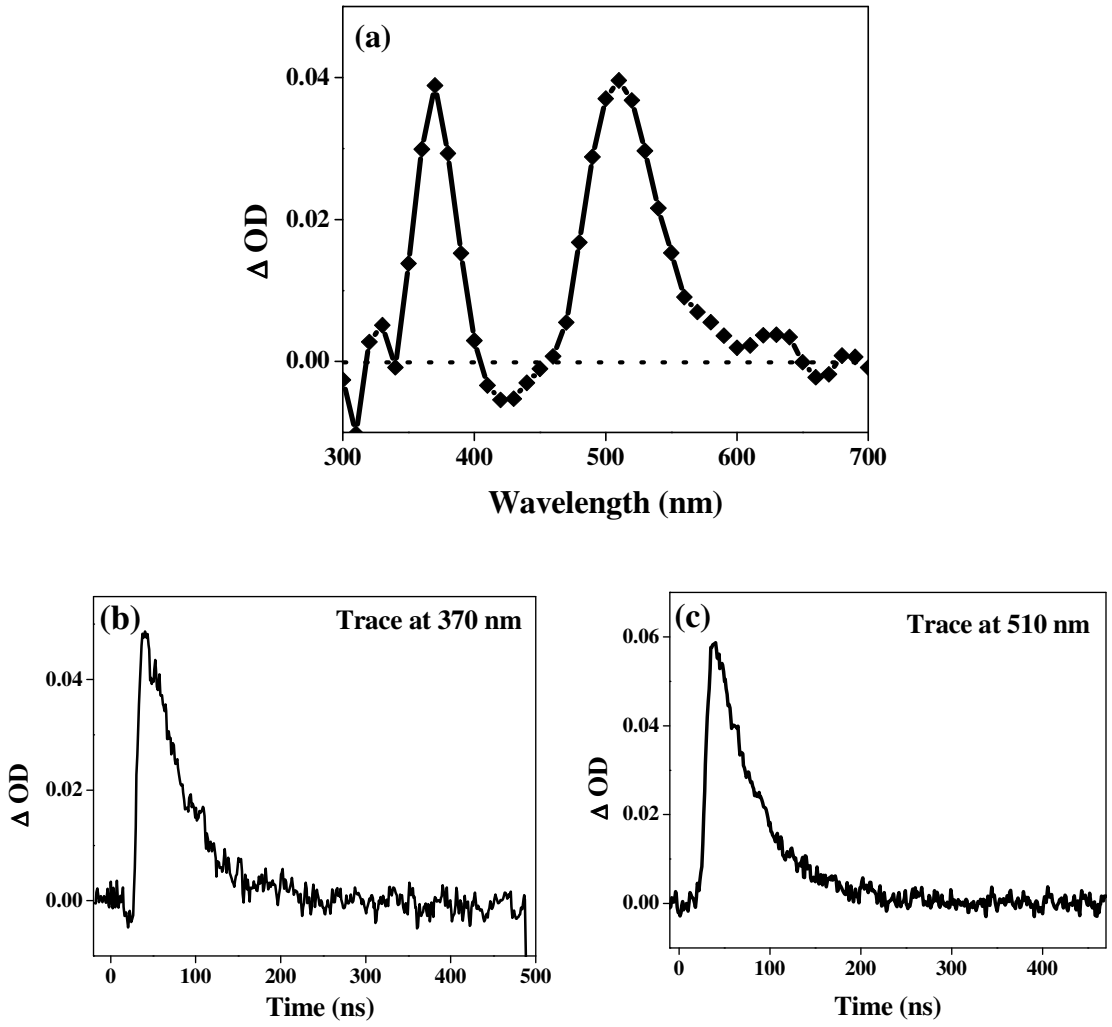

Figure 3.7.(a)Transient absorption spectrum of **Ru-Ptz$_{2(S)}$** in deaerated ACN obtained immediately after the laser pulse. Insets show the decay traces at (b) 370 nm and (c) 510 nm**.**

Lifetimes and the yields of CS states were found to decrease with increase in the number of Ptz groups. Similar trend was observed for the **Ru-Ptz**, **Ru-Ptz$_2$** and **Ru-Ptz$_3$** derivatives described in the second chapter of this thesis. Data pertaining to the lifetimes and yields of the CS state are given in Table 3.4. The 47 ns lifetime we obtained here for **Ru-Ptz$_{2(S)}$** is the highest value reported for any $Ru(bpy)_3^{2+}$ based dyad.

Table 3.4. The lifetime and quantum yield of charge separation in the three Ru-Ptz derivatives

Solvent: ACN	λ_{max}	Lifetime (τ), ns	Φ_{CS}
Ru- Ptz$_{2(S)}$	370, 510	47	0.79
Ru- Ptz$_4$	370, 510	12	0.23
Ru- Ptz$_6$	370, 510	7	0.15

Notice that the ΔG^0 for PET from Ptz to $Ru(bpy)_3^{2+}$ in the Ru-Ptz dyads is very small (Table 3.2) and the large k_{et} values obtained cannot be explained in terms of the ΔG^0 value. The extremely rapid electron transfer rates obtained for the Ru-Ptz systems can only be explained by invoking a closed conformation in which one of the bpy ligands or the Ru metal centre is spatially very close to the Ptz moiety. Electron transfer can then occur to the metal centre either directly through space or through the bpy ligand orbitals as described in detail in Chapter 2. For all the Ru-Ptz systems studied, k_{bet} also increased with increase in the number of Ptz groups. When more Ptz groups are present, the average spatial separation between the bpy and Ptz and/or Ru^+ and $Ptz^{\bullet+}$ decreases, leading to the observed increase in BET rates. Another probability is the fast exchange of electron between $Ptz^{\bullet+}$ and Ptz. Such self-exchange reactions can lead to formation of $Ptz^{\bullet+}$ very close to the Ru^+ centre which can facilitate rapid BET.

3.3.2. Intermolecular electron transfer studies of Ru-Ptz$_{2(S)}$

We have carried out laser flash photolysis of six Ru-Ptz systems and in all cases we obtained transient spectra with absorption bands at 370 and 510 nm. Based on literature reports we assigned the 370 nm band to $Ru(bpy)_3^{+}$ and the 510 nm band to $Ru(bpy)_3^{+}$ and $Ptz^{\bullet+}$. These assignments can be confirmed using secondary electron transfer experiments. If the CS state $Ru(bpy)_3^{+}$- $Ptz^{\bullet+}$ exhibits lifetime in the nanosecond range, then it would be possible for it to react with donors or acceptors as shown in Scheme 3.3. If a donor D, which is a better donor compared to Ptz is present in the solution, then D can donate an electron to the $Ptz^{\bullet+}$ terminal of the CS state to generate $D^{\bullet+}$ and $Ru(bpy)_3^{+}$-Ptz. Similarly if an acceptor A, which is a better acceptor than $Ru(bpy)_3^{2+}$ is present in the medium, then A can accept an electron from the $Ru(bpy)_3^{+}$ terminal of the CS state to generate $A^{\bullet-}$ and $Ru(bpy)_3^{2+}$-$Ptz^{\bullet+}$.

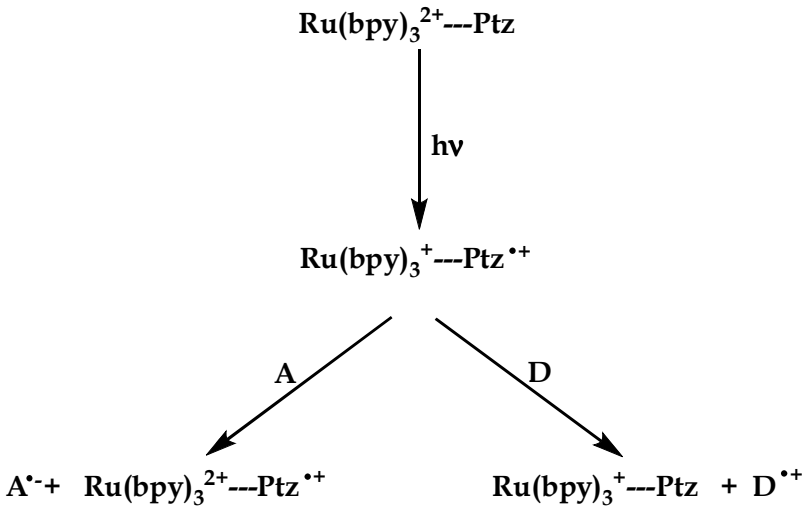

Scheme 3.3

Formation of $D^{\bullet+}$ or $A^{\bullet-}$ in the secondary electron transfer reactions implied the existence of the CS state. Also, the secondary electron transfer serves the role of a sequential electron transfer leading to spatial separation of the charge centers, thereby enhancing the lifetime of the CS state. Here we show that the CS state of **Ru-Ptz$_{2(S)}$** is capable of secondary electron transfer reactions with donors such as TMTPA and acceptors such as DV^{2+} or PMDI.

3.3.2.1. Secondary electron transfer involving acceptors

We have observed that the CS state of **Ru-Ptz$_{2(S)}$** can participate in secondary electron transfer reactions with acceptors such as DV^{2+} and PMDI. While attempting the secondary electron transfer process, care should be taken to see that the primary event is the intramolecular charge separation within **Ru-Ptz**. This is the case in the present systems because the intramolecular reactions are very fast. We also used low concentrations of the secondary acceptor. As control experiments we also measured the emission lifetime of **Ru-Ptz$_{2(S)}$** in the presence of secondary acceptors and donors. We observed that emission lifetime of **Ru-Ptz$_{2(S)}$** is unaffected by milli molar concentrations of these molecules.

Figure 3.8 shows the transient absorption spectra obtained in the flash photolysis of **Ru-Ptz$_{2(S)}$** (2×10^{-5} M) in the presence of DV^{2+} (3×10^{-4} M) in ACN. The transient spectrum exhibited absorption at 390, 520 and 610 nm. The 390 and 610 nm bands are the well-known absorptions due to reduced viologen[6] $DV^{\bullet+}$ and the 520 nm peak is due to $Ptz^{\bullet+}$. Observation of absorptions due to $DV^{\bullet+}$ suggests that secondary electron

transfer as shown in Scheme 3.3 and equation (3.5) are taking place in the photolysis. Reduction potential of dialkyl viologen is -0.45 V (vs SCE)[7] and hence ΔG^0 for reaction 3.5 is estimated as -0.9 eV.

$$DV^{2+} + Ru(bpy)_3^{+}\text{----}Ptz^{\bullet +} \longrightarrow DV^{\bullet +} + Ru(bpy)_3^{2+}\text{----}Ptz^{\bullet +} \qquad (3.5)$$

Absorption due to $Ru(bpy)_3^{+}$ at 370 nm is absent in Figure 3.8, while absorption due to $Ptz^{\bullet +}$ at 520 nm is present. This indicates that $Ru(bpy)_3^{+}$ is consumed in the secondary electron transfer without affecting $Ptz^{\bullet +}$. Insets in Figure 3.8 show the decays of the transient absorptions at 390 and 510 nm. An inspection of these profiles shows that the products of secondary electron transfer are very long lived.

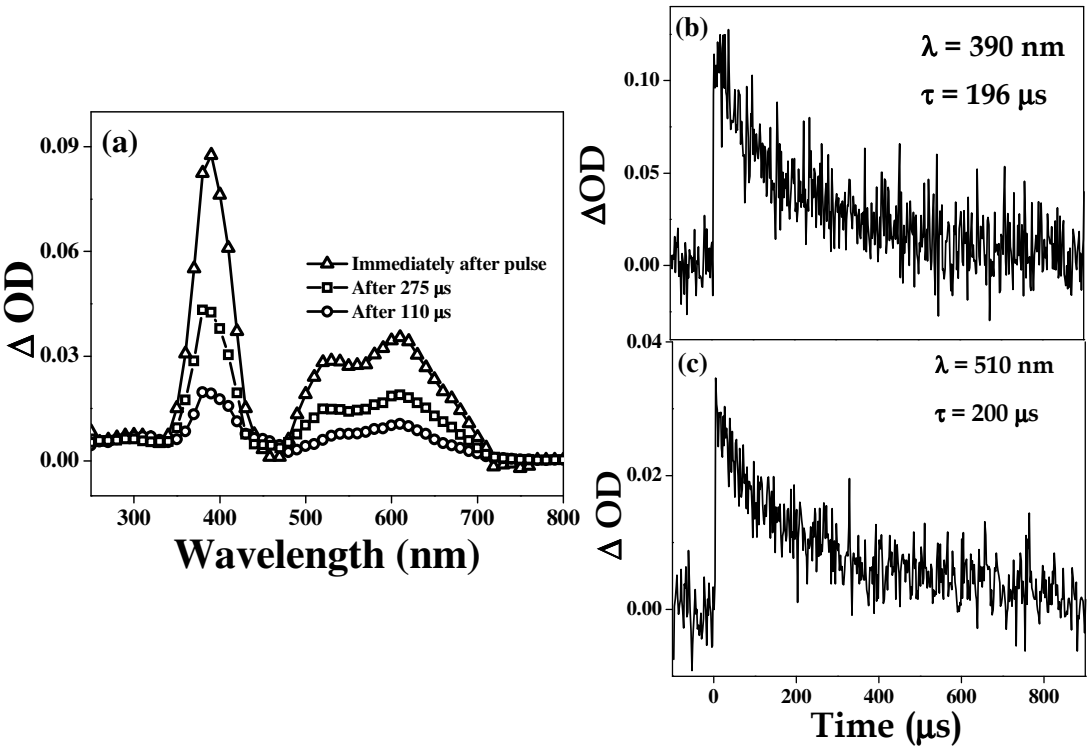

Figure 3.8.(a) Transient absorption spectra of **Ru-Ptz$_{2(S)}$**/DV^{2+} system (2×10^{-5} M / 3×10^{-4} M). Kinetic traces (b) at 390 nm and (c) at 510 nm also are shown.

Figure 3.9 shows the transient absorption spectra obtained in the flash photolysis of **Ru-Ptz$_{2(S)}$** in the presence of PMDI in ACN. The transient absorption consists of the bands corresponding to $PMDI^{\bullet-}$ (700-720 nm)[8] and $Ptz^{\bullet+}$ (500-520 nm). $PMDI^{\bullet-}$ is formed by the secondary ET between the CS state and PMDI as shown in equation (3.6). Reduction potential of PMDI is -0.58 V (vs SCE)[9] and hence ΔG^0 for reaction 3.6 is estimated as -0.79 eV.

$$PMDI + Ru(bpy)_3^{+}\text{-----}Ptz^{\bullet+} \longrightarrow PMDI^{\bullet-} + Ru(bpy)_3^{2+}\text{----}Ptz^{\bullet+} \quad (3.6)$$

Figure 3.9(b) and (c) show the decay of the radical ions, which suggested that secondary electron transfer has efficiently separated the product ion radicals.

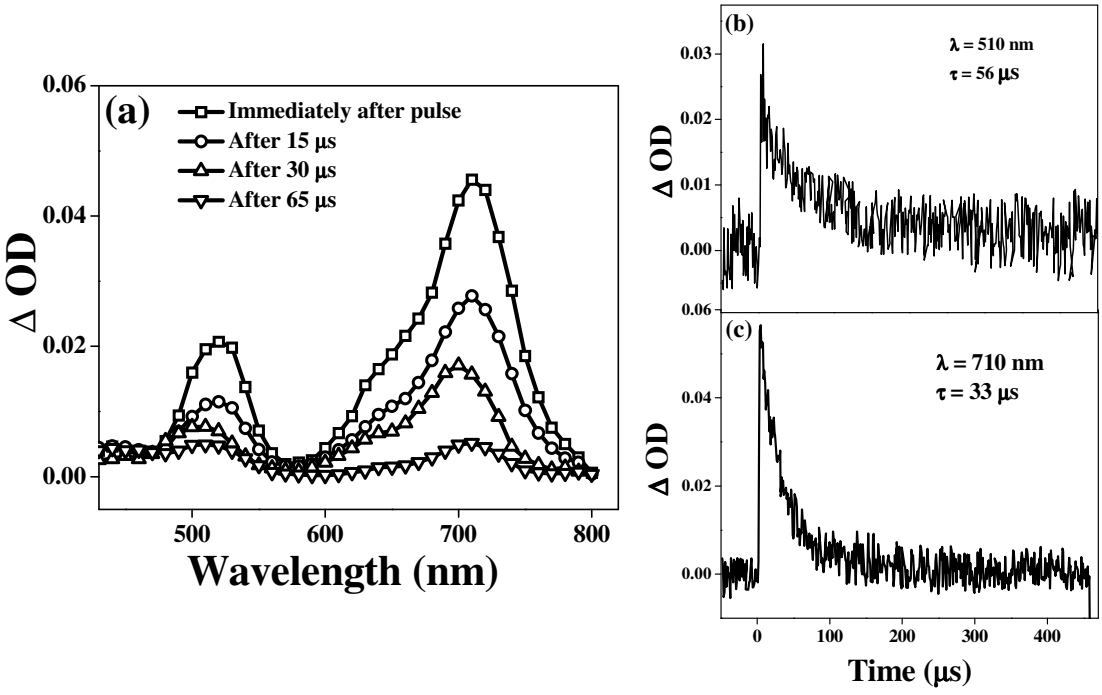

Figure 3.9.(a) Transient absorption spectrum of **Ru-Ptz$_{2(S)}$**/PMDI system (2×10^{-5} M / 3×10^{-4} M). Kinetic traces (b) at 510 nm and (c) at 710 nm also are shown.

3.3.2.2. Secondary electron transfer involving a Donor

The oxidation potential of TMTPA is +0.51 V (vs SCE)[10] and hence ΔG^0 for electron transfer from TMTPA to $Ptz^{\bullet+}$ is about -0.2 eV. Hence we expect facile secondary electron transfer in the **Ru-Ptz$_{2(S)}$**/TMTPA system. Figure 3.10 shows the transient absorption spectra obtained in the flash photolysis of **Ru-Ptz$_{2(S)}$** (2×10^{-5} M) in the presence of TMTPA (3×10^{-4} M) in ACN. The transient absorption spectrum exhibited absorption at 510 nm corresponding to $Ru(bpy)_3^+$ and in the 690-720 nm corresponding to $TMTPA^{\bullet+}$.[3] The absorption corresponding to the $Ptz^{\bullet+}$ observed normally at 510 nm could be assumed to be disappeared here by the intermolecular electron transfer. The absorption corresponding to the Ru^+ in the 370-390 nm region could not be monitored since the optical density of the sample solution was very high due to the TMTPA absorption in that region. These factors suggest that secondary electron transfer as per equation (3.7) is taking place in the **Ru-Ptz$_{2(S)}$**/TMTPA system.

$$\mathbf{TMTPA + Ru(bpy)_3^{+}\text{----}Ptz^{\bullet+} \longrightarrow TMTPA^{\bullet+} + Ru(bpy)_3^{+}\text{----}Ptz} \qquad \mathbf{(3.7)}$$

Kinetic traces obtained for the system are shown in the insets of Figure 3.10. The Ru^+ decay was observed in a time span of 15 μs, while $TMTPA^{\bullet+}$ absorption decayed within 33 μs time span. Compared to the transients observed for **Ru-Ptz$_{2(S)}$** in ACN, transients in the **Ru-Ptz$_{2(S)}$**/TMTPA system are long-lived, which again suggest that secondary electron transfer is an excellent tool to enhance the lifetime of the CS state.

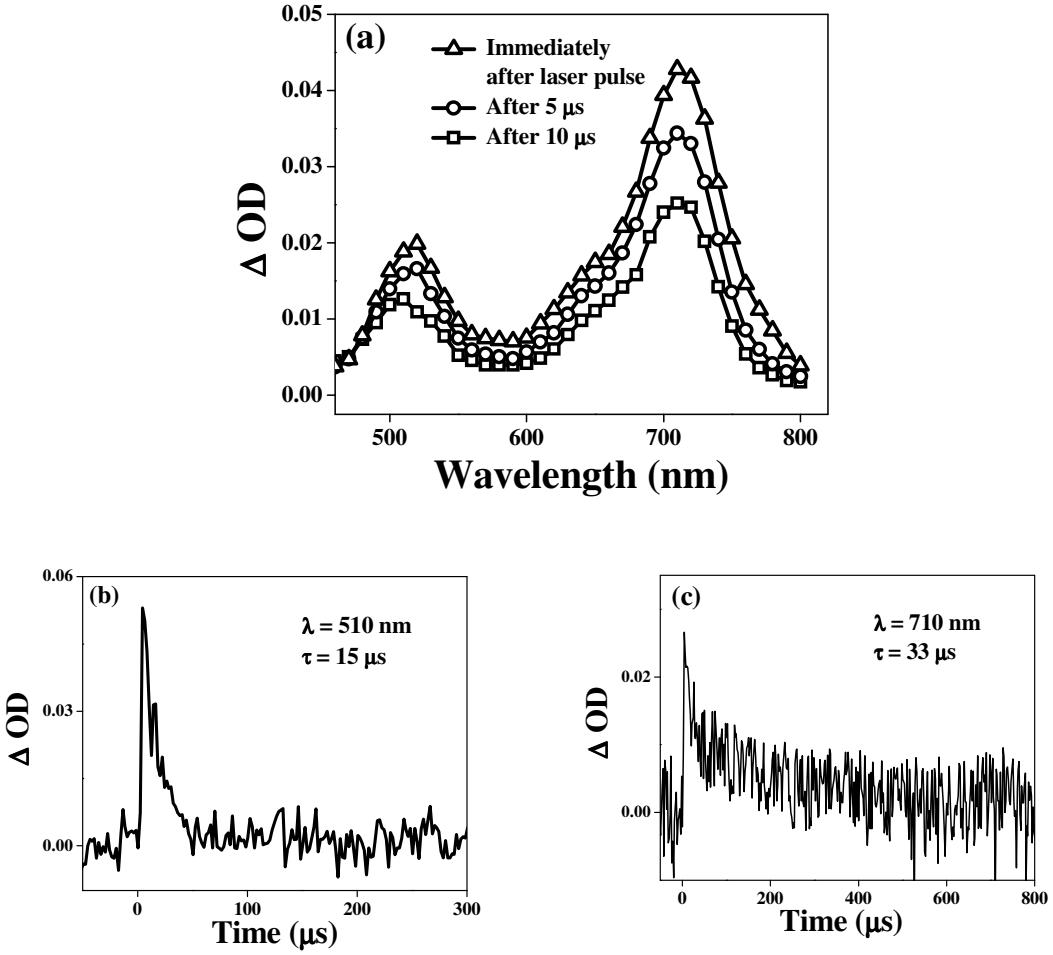

Figure 3.10.(a) Transient absorption spectra obtained in the flash photolysis of of **Ru-Ptz$_{2(S)}$** (2×10^{-5} M) in the presence of TMTPA (3×10^{-4} M). Kinetic traces at (b) 510 nm and (c) at 710 nm also are shown.

3.3.3. Design and Study of a Acceptor-Ru-Ptz triad system

This section describes our attempts to design a triad based on the Ru-Ptz systems investigated in this thesis. Compared to dyads, triads exhibit higher CS state lifetimes and quantum yields. A few triads based on $Ru(bpy)_3^{2+}$ systems are described in the literature.[11-13] These are A-$Ru(bpy)_3^{2+}$-D type systems, where a viologen

derivative,[11] diquat[12] or anthaquinone[13] acts as the acceptor and phenothiazine acts as the donor. In these systems, the first step is the oxidative quenching of the $Ru(bpy)_3^{2+}$ chromophore by the acceptor, which is followed by a second electron transfer from Ptz to the oxidized metal centre. What is attempted here is a reversal of the above electron transfer sequence. The first electron transfer in the triad we designed is the reductive quenching of the $Ru(bpy)_3^{2+}$ chromophore by Ptz. The acceptor moiety was selected in such a way that it could engage in the electron transfer process only in the second step.

The above strategy requires the use of a very weak acceptor. When a donor and acceptor are linked to the $Ru(bpy)_3^{2+}$ chromophore, the sequence of the electron transfer reactions is decided by the ΔG^0 for the PET reactions. When MV^{2+} is the acceptor and Ptz is the donor, ΔG^0 = -0.5 eV for the oxidative electron transfer and $\Delta G^0 \approx 0$ eV for the reductive electron transfer. Hence the oxidative electron transfer is the preferred first step. If Ptz is the donor, oxidative electron transfer can be the second step only if ΔG^0 for this process is moderately positive. Calculations using the Weller equation show that an acceptor having reduction potential in the range -0.8 to -1.4 V (vs SCE) may serve the purpose. We have selected a nitrobenzene derivative as the acceptor moiety. The triad designed this way is designated as **Ptz-Ru-NT** (see Scheme 3.1 for structure)

3.3.3.1. Synthesis

Synthesis of **Ptz-Ru-NT** was accomplished using Scheme 3.4. 4,4'-dimethyl-2,2'-dipyridyl (**6)** was reacted with 4-nitrobenzylbromide (**7)** in the presence of butyllithium and diisopropylamine in THF to get the nitrophenyl-substituted bipyridine

ligand **8**. This was refluxed with $RuCl_3$ in DMF in the presence of lithium chloride to get the *bis* complex **9**, which was treated with ligand **3** to yield triad **Ptz-Ru-NT**, as shown in Scheme 3.4. **Ptz-Ru-NT** was purified by column chromatography and characterized by spectroscopic techniques.

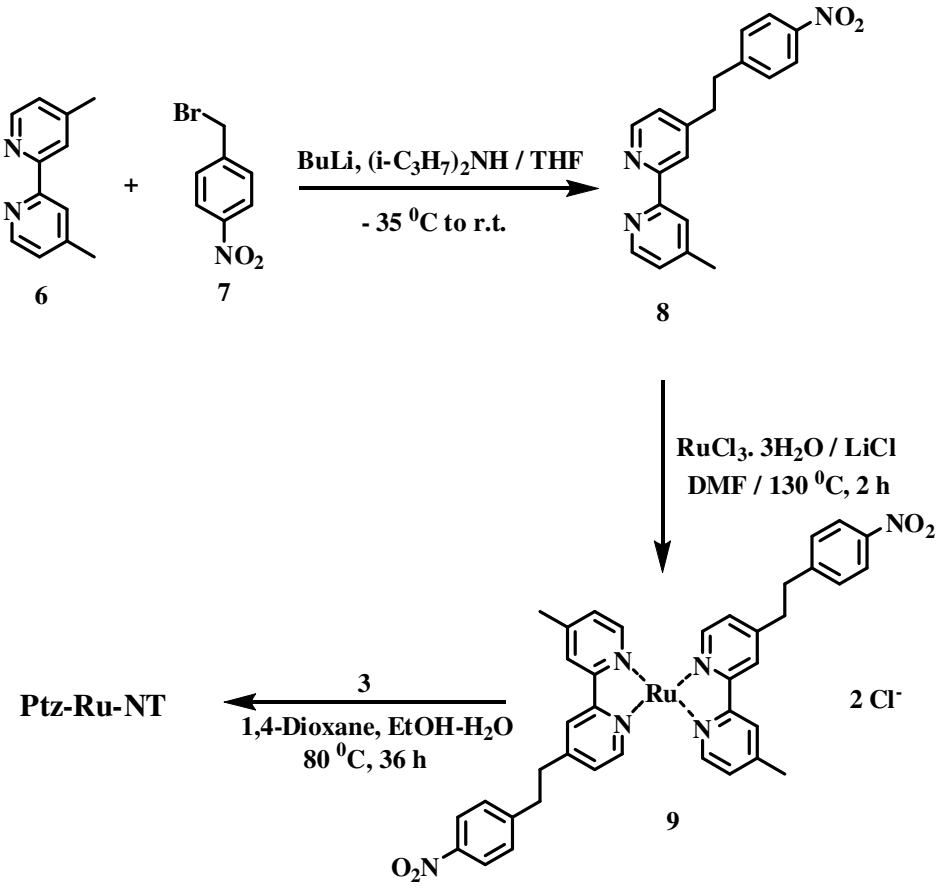

Scheme 3.4

3.3.3.2. Absorption and Emission Spectra

The absorption spectrum of **Ptz-Ru-NT** in ACN is shown in Figure 3.11(a). The characteristic MLCT band of the $Ru(bpy)_3^{2+}$ chromophore is prominent in the spectrum

and is centered around 480 nm. The absorption bands corresponding to the ligand centered π–π* transition is present around 290 nm and is slightly broadened by the substitution in the bpy ligand. Absorption corresponding to Ptz moiety is seen around 250 nm and the nitrotoluene absorption is seen as the shoulder around 350 nm.

The emission spectrum of **Ptz-Ru-NT** in ACN is shown in Figure 3.11(b). Emission maximum of **Ptz-Ru-NT** is red shifted by about 20 nm when compared to that of **Ru-Ptz$_{2(S)}$**. The emission quantum yield (Φ_f = 0.0006) was also somewhat lower for the triad. The low fluorescence quantum yield suggested very facile electron transfer quenching of the $Ru(bpy)_3^{2+}$ moiety in this system.

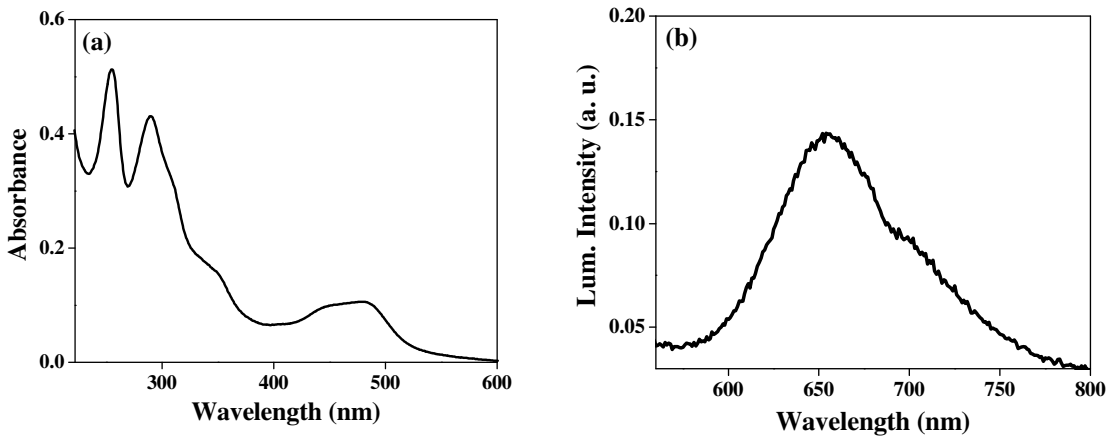

Figure 3.11. (a) Absorption and (b) emission spectra of **Ptz-Ru-NT** in ACN.

3.3.3.3. Electrochemical studies

Redox potentials of **Ptz-Ru-NT** were determined using square wave voltammetry. Figure 3.12 shows the square wave voltammogram of **Ptz-Ru-NT** in ACN.

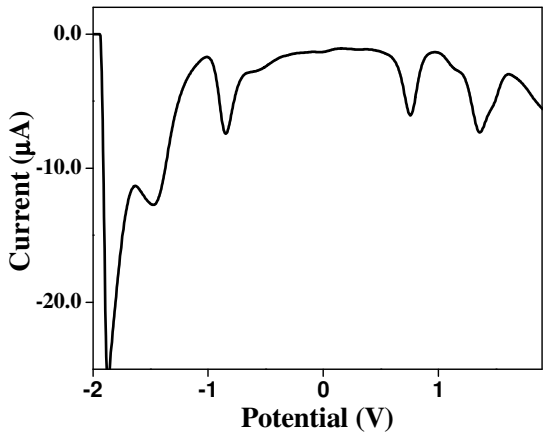

Figure 3.12. Square wave voltammogram of **Ptz-Ru-NT** in ACN. Tetrabutylammonium hexafluorophosphate was used as the supporting electrolyte

The peak at 0.76 V is assigned to Ptz → $Ptz^{\bullet+}$ oxidation and the peak at 1.37 is assigned to Ru(II) to Ru(III) oxidation. For the Ru-Ptz dyads studied in this thesis the first reduction peak appeared around -1.3 to -1.4 V (vs SCE). For **Ptz-Ru-NT**, the first reduction peak appeared at -0.845 V (vs SCE) and we attribute this to the reduction of the NT moiety to $NT^{\bullet-}$. The peak corresponding to this process was expected at -1.15 V,[14] and the reason for the shift to -0.845 is not understood. The first $Ru(bpy)_3^{2+}$ centered reduction appeared at -1.47 V which is about 0.075 V more negative than that observed for **Ru-Ptz$_{2(S)}$**. For all the Ru-Ptz derivatives studied in this thesis, we observed three reduction peaks of nearly equal intensity. In the case of triad **Ptz-Ru-NT** we observe only two $Ru(bpy)_3^{2+}$ centered reduction peaks. The intensity of the second peak at -1.87 V is nearly twice as that of the first peak at -1.47 V. Most probably the second and third $Ru(bpy)_3^{2+}$ based reduction peaks got merged in to one for this system. Using E_{ox} for the Ptz moiety and the first reduction potential of the $Ru(bpy)_3^{2+}$ core, ΔG^0 for PET was calculated. ΔG^0 thus obtained was +0.07 eV. Although ΔG^0 is positive

electron transfer to *$Ru(bpy)_3^{2+}$ from the Ptz moiety is very facile in this system as indicated by the very low Φ_f value. Calculations would also show that ΔG^0 for oxidative PET is similar in this system. In Chapter 2 of this thesis, we proposed that the large k_{et} values observed in our Ru-Ptz systems is due to the folding back of the Ptz moiety which brings it very close to the metal centre. We believe that the conformations of Ptz with respect to the metal centre is preserved in the triad also and hence we propose that the first electron transfer in **Ptz-Ru-NT** is from the Ptz moiety to the $Ru(bpy)_3^{2+}$ core. Direct electron transfer from Ptz to the NT moiety is ruled out because the excitation is localized in the $Ru(bpy)_3^{2+}$ moiety.

3.3.3.4. Laser Flash Photolysis

In order to understand the details of the electron transfer processes taking place in **Ptz-Ru-NT**, the molecule was subjected to laser flash photolysis experiments using the 532 nm laser out put from a Nd-YAG laser. The transient absorption spectrum obtained along with a kinetic trace is shown in Figure 3.13. The transient exhibited absorption maxima at 510 and 620 nm. The 510 nm peak can be assigned to $Ptz^{\bullet+}$ and we assign the 620 nm absorption to $NT^{\bullet-}$. It is to be noted that for several NT derivatives the radical anions exhibited absorption at 470-480 nm with a shoulder around 600 nm in non polar solvents.[15] It is not clear as to why the $NT^{\bullet-}$ absorption shifts to longer wavelengths in the case of **Ptz-Ru-NT**. It is to be noted that the NT moiety exhibits a difference in the reduction potential also. E_{red} for NT was expected at -1.15 V, but the observed value in the triad was -0.845 V, indicating that the NT moiety

is placed in a highly polar environment or is in a partially charge transferred state. This perhaps may have shifted the absorption maxima to longer wavelengths. It is to be noted that the absorption due to $Ru(bpy)_3^+$ at 370 nm observed in the transient spectra of all Ru-Ptz dyads, is absent in Figure 3.13. This indicates that the $Ru(bpy)_3^+$ formed as a result of electron transfer from Ptz has transferred that electron to the NT group.

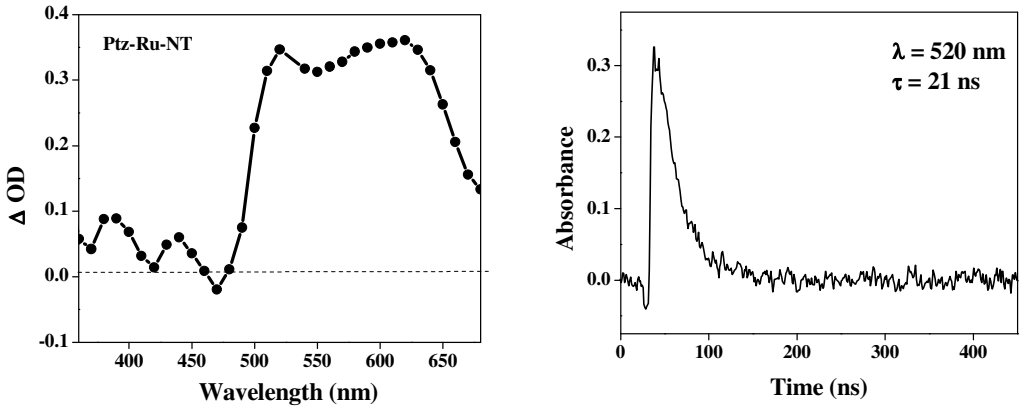

Figure 3.13. Transient absorption spectrum obtained in the flash photolysis of **Ptz-Ru-NT** immediately following the laser pulse. Kinetic profile at 520 nm is also shown.

Decays of the transients were exponential and we obtained a lifetime of 21 ns for the CS state. This showed that upon going from the **Ru-Ptz** dyad to the **Ptz-Ru-NT** triad, the CS state lifetime had decreased. Because of this we have not explored triad systems in detail. Most probably the Ptz and NT moieties are spatially very close in the triad, which resulted in lowering the CS state lifetime.

3.4. Conclusions

We have synthesized Ru-Ptz dyads having two, four or six Ptz donors covalently linked to the $Ru(bpy)_3^{2+}$ chromophore. Very good PET properties were observed in all

the three systems. Among the Ru-Ptz systems investigated, **Ru-Ptz$_{2(S)}$** exhibited the longest CS state lifetime. Both forward and back electron transfer rates increased with increase in the number of Ptz units. We also studied intermolecular electron transfer reactions of the CS state of **Ru-Ptz$_{2(S)}$** with two acceptors and one donor. Extremely long-lived charge separation, of the order of hundreds of microseconds, could be achieved by these intermolecular electron transfer processes. We have also synthesized the triad **Ptz-Ru-NT** and studied the PET processes taking place in this system. Lifetime of the CS state in the triad was comparable to that in the dyad. Since the expected enhancement in lifetime was not observed, triad systems were not explored in detail.

3.5. Experimental Section

3.5.1. Measurements

Proton NMR data were recorded on a JEOL EX-300 MHz Brucker Avance DPX spectrometer. GC-MS analyses were performed on a Shimadzu QP 2010 Gas Chromatograph-Mass Spectrometer. IR spectra were recorded on a Shimadzu IR Prestige 21 spectrometer. Melting points were determined on a Mel-Temp II melting point apparatus. Fluorescence spectra were recorded on a SPEX Fluorolog F112X spectrofluorimeter with right angle geometry. Electrochemical experiments were carried out by using BAS CV50W voltammetric analyser. Laser flash photolysis experiments were carried out with an Applied Photophysics Model LKS-20 laser kinetic spectrometer equipped with a Nd:YAG laser. The analysing and laser beams were fixed

at right angles to each other. The laser energy was 100 mJ at 532 nm. Optical densities of solution for flash photolysis were 0.5 at 532 nm in 1 cm cell.

3.5.2. Chemicals and Solvents.

Dodecyl viologen (DV^{2+}),[6] pyromellitic diimide (PMDI)[2d] and trimethoxy triphenylamine[16] were synthesized following reported procedures. Solvents used in the synthesis were dried before use by standard methods. Spectroscopic grade solvents were used for photophysical and electrochemical measurements.

Synthesis of bpy-Ptz$_2$ (3): The diacid **1**[4] (1.5 g, 6.14 mmol) was refluxed in thionyl chloride (10 mL) for 24 h in argon atmosphere. Excess thionyl chloride was distilled out and the pale yellow product was dried in a desiccator under vacuum. This was used as such for the next step assuming that all the acid was converted to the acid chloride. The acid chloride thus obtained was dissolved in DCM (30 mL) and *N*-(propylamine)phenothiazine[5] (3.76 g, 14.69 mmol) and triethyl amine (0.5 mL) were added and the reaction mixture stirred at room temperature for 2 h and then refluxed for 10 h. At the end of the reaction, the precipitated mass was filtered and washed with dichloromethane and dilute ammonia solution to obtain the ligand **3**. Yield: 1.8 g (40.7%); mp 232-236 ^{o}C; IR ν_{max} cm^{-1} 1292, 1323, 1357, 1456, 1544, 1593, 1639, 2328, 2355, 2582, 2864, 2927, 2953, 3062, 3155, 3275; HRMS (FAB); Observed 720 (Calculated 720.91). ^{1}H NMR ($CDCl_3$) δ 2.17 (m, 4 H) 3.6 (t, 4 H), 4.0 (t, 4 H), 6.8 (m, 10 H), 7.2 (m, 4 H), 7.4 (m, 4 H), 7.5 (d, 2 H), 8.4 (s, 2 H), 8.7 (d, 2 H). ^{13}C NMR

($CDCl_3$) δ 26.3, 37.4, 44.4, 115.7, 118.2, 121.9, 122.5, 123.7, 127.1, 127.5, 142.9, 144.7, 149.9, 155.4, 164.7.

Synthesis of Ru[bpy-Ptz$_2$]$_2$ (5): $RuCl_3.3H_2O$ (29 mg, 0.14 mmol), the ligand **3** (150 mg, 0.3 mmol) and LiCl (200 mg) were heated at reflux in dry DMF (2.5 mL) for 2 h. It was then cooled to room temperature and diluted with acetone (5 mL). The solvent was removed and the residue extracted with chloroform and chromatographed over neutral alumina using chloroform as the eluent to yield the *bis* complex **5**. Yield- 0.143 g (64%) mp: > 350 ^oC.

Synthesis of Ru-Ptz$_{2(S)}$: The ligand **3** (435 mg, 0.6033 mmol) was dissolved in dioxane (15 mL) and EtOH-Water (70%, 20 mL) was added. Solid $Ru(bpy)_2Cl_2$ (**4,** 250 mg, 0.5175 mmol) was added and the dark purple reaction mixture was refluxed for 36 h under argon atmosphere. Solvent was removed and the resultant solid was dissolved in methanol and then precipitated with saturated ammonium hexafluorophosphate solution. It was than filtered and dried. Final purification was done by column chromatography in silica using 1:1 ACN / toluene mixture. Yield - 0.23 g (34.8%) mp > 350 ^oC; IR ν_{max} cm^{-1} 759, 842, 1274, 1313, 1406, 1539, 1668, 3064, 3450, 3668; HRMS Observed; 1133.8 (M - $2PF_6^-$) (calculated 1134.8); ^1H NMR (DMSO-d_6) δ 2.06 (m, 4 H), 3.5 (4 H, alongwith DMSO signal), 4.0 (t, 4 H), 6.9 (t, 4 H), 7.1 (m, 8 H), 7.2 (m, 4 H), 7.5 (m, 4 H), 7.6 (m, 8H), 8.16 (m, 4 H), 8.8 (d, 4 H), 9.0 (d, 4 H).

Synthesis of Ru-Ptz$_4$: *Bis* complex **5** (0.235 g, 0.15 mmol) was dissolved in dioxane (5 mL) and EtOH-Water (70%, 5 mL) was added. 2,2'-bypyridine (0.025 mg,

0.14 mmol) was added and the mixture was refluxed for 36 h under argon atmosphere. The solvent was removed and the resultant solid was dissolved in methanol and then precipitated with saturated ammonium hexafluorophosphate solution. Final purification was done by column chromatography on silica gel using 30-50% Acetonitrile in toluene as the eluent. Yield - 0.143 g (35%) mp > 350 ^{o}C; IR ν_{max} cm^{-1} 754, 842, 1249, 1284, 1352, 1458, 1529, 1666, 2931, 3062, 3414, 3641; ^{1}H NMR (Acetone-d_6) δ 2.07 (8 H, along with acetone signal), 3.5 (t, 8 H), 4.0 (t, 8 H), 6.8 (t, 4 H), 7.1 (m, 9 H), 6.9 (m, 14 H), 7.0 (m, 9 H), 7.6 (t, 2H), 7.8 (d, 4 H), 8.0 (d, 2 H), 8.1-8.3 (m, 6 H), 8.8 (d, 2 H), 8.9 (s, 4 H).

Synthesis of Ru-Ptz$_6$: Procedure for the synthesis of **Ru-Ptz$_4$** was exactly followed with the ligand **3** instead of 2,2'-bypyridine. Yield - 0.143g (35%) mp > 350 ^{o}C; IR ν_{max} cm^{-1} 752, 842, 1128, 1251, 1284, 1327, 1458, 1533, 1668, 2666, 2935, 3061, 3309, 3410, 3650; NMR (Acetone-d_6) δ 2.09 (m, 12 H), 3.5 (12 H, along with the DMSO signal), 4.0 (t, 12 H), 6.9 (m, 12 H), 7.1 (m, 12 H), 7.2 (m, 24 H), 7.8 (d, 3 H), 7.9 (d, 6 H), 8.05 (s, 3 H), 9.1 (m, 12 H) .

Synthesis of 8: Diisopropylamine (2 mL) and dry THF (5 mL) were added to a two-necked RB flask which was previously cooled to -10 $^{\circ}$C under argon atmosphere. A solution of *n*-BuLi (1.6 M in hexane, 4 mL) was added and the temperature was reduced to -15 $^{\circ}$C. The mixture was stirred for 20 minutes and compound **6** (1.0 g, 5.43 mmol) in dry THF (10 mL) was slowly added to it over a period of 30 minutes. A deep red colour characteristic of the monoanion of **6** was observed. The temperature was then lowered

to -35 °C and stirring was continued for 1 h. Compound **7** (11.74 g, 54.27 mmol) in dry THF (10 mL) was then added to the reaction mixture. Stirring was continued for 10 minutes at -35 °C and then brought into room temperature gradually and stirred overnight. The excess reagent was quenched by the addition of water .The mixture was extracted first with ether and then with DCM repeatedly. Combined organic extracts were concentrated by rotary evaporation .The crude mixture was purified by column chromatography over neutral alumina using 30% chloroform – petroleum ether as the eluent. Yield - 0.4 g (23%); mp 102-106 °C; GC MS- 318 (M^+).

Synthesis of 9: Compound **8** (0.2 g, 0.63 mmol) and LiCl (0.09 g) were taken together in dry DMF (5 mL) in a two-necked RB flask, which was flushed with argon. $RuCl_3.3H_2O$ (0.08 g, 0.31 mmol) was added and reaction mixture refluxed at 130 °C for 2 h. It was then poured into water and extracted with dichloromethane. The extract was concentrated and product was precipitated by adding ether. Yield - 0.095 g (35.5%); mp > 250 °C (charring). The product was used as such for the conversion to the *tris* complex. IR ν_{max} cm^{-1}: 829, 856, 1342, 1425, 1446, 1473, 1514, 1595, 1614, 1687, 1969, 2959, 3062.

Synthesis of Ptz-Ru-NT: 3 (0. 09 g, 0.14 mmol) was dissolved in 1,4-dioxane (5 mL) and 10 mL of ethanol (70%) was added to it. The *bis* complex **9** (0.1 g, 0.14 mmol) was added to the above solution and the dark purple reaction mixture was refluxed for 16 h under Ar atmosphere. The resultant red orange solution was cooled to room temperature; solvents were removed by rotary evaporation under vacuum, and the

resultant orange solid obtained was dissolved in methanol and then precipitated with saturated ammonium hexafluorophosphate solution. It was then filtered and dried. The purification was done by column chromatography over silica gel using 30% acetonitrile in toluene as the eluent. Yield of **Ptz-Ru-NT** was 0.04 g (23%); mp > 300 ^{o}C; IR ν_{max} cm^{-1} 754, 842, 1342, 1458, 1516, 1598, 1664, 1971, 3034, 3115; ^{1}H NMR (CD_3CN): δ 2.09 (m, 4 H with H_2O peak), 2.53 (m, 6 H), 3.27 (m, 8 H), 3.52 (m, 4 H), 4.01 (m, 4 H), 6.79 (m, 8 H), 6.97 (m, 4 H), 7.17-7.2 (m, 14 H), 7.35 (m, 8 H), 7.5 (m, 4 H), 7.77 (m, 3 H), 8.3 (m, 4 H), 8.68 (m, 3 H).

3.6. References

(1) (a) Thompson, D. H. P.; Barrette, Jr., W. C.; Hurst, J. K. *J. Am. Chem. Soc.* **1987**, *109*, 2003-2009. (b) Colaneri, M. J.; Kevan, L.; Thompson, D. H. P.; Hurst, J. K. *J. Phys. Chem.* **1987**, *91*, 4072-4077. (c) Patterson, B. C.; Thompson, D. H.; Hurst, J. K. *J. Am. Chem. Soc.* **1988**, *110*, 3656-3657. (d) Colaneri, M. J.; Kevan, L.; Schmehl, R. *J. Phys. Chem.* **1989**, *93*, 397-401. (e) Sakaguchi, M.; Kevan, L. *J. Phys. Chem.* **1989**, *93*, 6039-6043. (f) McManus, H. J. D.; Kevan, L. *J. Phys. Chem.* **1991**, *95*, 10172-10178.

(2) (a) Wiederrecht, G. P.; Niemczyk, M. P.; Svec, W. A.; Wasielewski, M. R. *J. Am. Chem. Soc.* **1996**, *118,* 81-88. (b) Debreczeny, M. P.; Walter, A.; Svec, W. A.; Marsh, E. M.; Wasielewski, M. R. *J. Am. Chem. Soc.* **1996**, *118*, 8174-8175. (c) Lukas, A. S.; Miller, S. E.; Wasielewski, M. R. *J. Phys. Chem. B* **2000**, *104,* 931-940.

(3) Gould, I. R.; Ege, D.; Moser, J. E.; Farid, S. *J. Am. Chem. Soc.* **1990**, *112*, 4290-4301.

(4) Garelli, N.; Vierling, P. *J. Org. Chem.* **1992**, *57*, 3046-3051.

(5) Godefroi, E. F.; Wittle, E. L. *J. Org. Chem.* **1956**, *21*, 1163-1168.

(6) Monk, P. M. S., *The viologens: Physicochemical properties, synthesis and applications of the salts of 4,4'-bipyridine*, Wiley, Chichester, 1998.

(7) Kavarnos, G. J.; Turro, N. J. *Chem. Rev*. **1986**, *86*, 401-449.

(8) Hayes, R. T.; Walsh, C. J.; Wasielewski, M. R. *J. Phys. Chem. A* **2004**, *108*, 2375-2381.

(9) Balan, B.; Gopidas, K. R. *Chem. Eur. J*. **2007**, *13*, 5173-5185.

(10) Mann, C. K.; Barnes, K. K. *Electrochemical Reactions in Nonaqueous Systems*; Marcel Dekker, Inc., New York, 1970, p. 278.

(11) (a) Treadway, J. A.; Chen, P.; Rutherford, T. J.; Keene, F. R.; Meyer, T. J. *J. Phys. Chem. A* **1997**, *101*, 6824-6826. (b) Rutherford, T. J.; Keene, F. R. *Inorg. Chem.* **1997**, *36*, 2872-2878. (c) Anderson, P. A.; Deacon, G. B.; Haarmann, K. H.; Keene, F. R.; Meyer, T. J.; Reitsma, D. A.; Skelton, B. W.; Strouse, G. F.; Thomas, N. C.; Treadway, J. A.; White, A. H. *Inorg. Chem.* **1995**, *34*, 6145-6157. (d) Strouse, G. F.; Anderson, P. A.; Schoonover, J. R.; Meyer, T. J.; Keene, F. R. *Inorg. Chem.* **1992**, *31*, 3004-3006. (e) Anderson, P. A.; Strouse, G. F.; Treadway, J. A.; Keene, F. R.; Meyer, T. J. *Inorg. Chem.* **1994**, *33*, 3863-3864.

(12) (a) Cooley, L. F.; Larson, S. L.; Elliott, C. M.; Kelley, D. F. *J. Phys. Chem.* **1991**, *95*, 10694-10700. (b) Danielson, K.; Elliott, C. M.; Merkert, J. W.; Meyer, T. J. *J. Am. Chem. Soc.* **1987**, *109*, 2519-2520. (c) Larson, S. L.; Elliott, C. M.; Kelley, D. F. *J. Phys. Chem.* **1995**, *99,* 6530-6539.

(13) Opperman, K. A.; Mecklenburg, S. L.; Meyer, T. J. *Inorg. Chem.* **1994**, *33*, 5295-5301.

(14) Ref 10, p. 363.

(15) Shida, T. *Electronic Absorption Spectra of Radical Ions*; Elsevier Science Publishers B. V., Amsterdam, Netherlands, 1998, p. 329.

(16) Goodbrand, H. B.; Hu, N.-X. *J. Org. Chem.* **1999**, *64*, 670-674.

CHAPTER 4

Phenothiazine Substituted $Ru(bpy)_3^{2+}$ Derivatives as Highly Selective Luminescence "Turn-ON" Chemodosimeters for Cu^{2+}

4.1. Abstract

*Potential applications of phenothiazine substituted $Ru(bpy)_3^{2+}$ systems such as **Ru-Ptz**, **Ru-Ptz$_2$**, **Ru-Ptz$_3$** and **Ru-Ptz$_{2(S)}$** as selective "turn-ON" luminescence chemodosimeters for metal ions are examined. We observed that these systems can act as good dosimeters for Cu^{2+} in acetonitrile solution. The ability of Cu^{2+} ions to oxidize aromatic amines in acetonitrile forms the basis for this study. The aromatic amine present in these systems is a phenothiazine moiety which is covalently linked to one of the bipyridine units. Excitation of the $Ru(bpy)_3^{2+}$ moiety leads to electron transfer from the phenothiazine unit which resulted in efficient quenching of the luminescence. In the presence of excess Cu^{2+}, phenothiazine moiety is oxidized to a stable entity which is incapable of electron donation to the MLCT state of $Ru(bpy)_3^{2+}$. The emission of the $Ru(bpy)_3^{2+}$ moiety would be restored in this way. Metal ions such as Li^+, Na^+, K^+, Ag^+, Mg^{2+}, Ca^{2+}, Ba^{2+}, Mn^{2+}, Fe^{2+}, Ni^{2+}, Zn^{2+}, Cd^{2+}, Hg^{2+}, Pb^{2+}, Cr^{3+}, Fe^{3+} and Co^{3+} did not interact with these systems. Thus phenothiazine substituted $Ru(bpy)_3^{2+}$ systems can be used as very selective chemodosimeters for Cu^{2+}. We also show that **Ru-Ptz** could act as a chemodosimeter for Fe^{3+} in methanol medium.*

4.2. Introduction

The development of highly selective and sensitive luminescence sensors for metal ions has gained considerable interest in recent years.[1] Among the essential heavy metal ions in human body, Cu^{2+} is third in abundance after Fe^{3+} and Zn^{2+} and it plays very important roles in several biological processes.[2] Cu^{2+} however becomes toxic if the concentration exceeds cellular needs. Exposure to high levels of Cu^{2+} for short periods of time can cause gastrointestinal disorders and long term exposures can cause kidney and liver damage.[3] Copper is also considered as a significant environmental pollutant.[4] Design and development of luminescence based sensors and chemodosimeters capable of detecting trace amounts of Cu^{2+}, therefore, is a very active research area.[5] Cu^{2+}, being paramagnetic, presents an inherent problem for luminescence based sensing because of the effective quenching of luminescence.[5c,6a-f] Hence, most of the luminescence sensors for Cu^{2+} are based on the luminescence quenching strategies.[5c,6] Sensors based on luminescence "turn-ON" or luminescence 'enhancement' upon metal binding are more desirable because of the high sensitivity of the luminescence technique. A commonly employed design in this context is the 'Fluorophore-Spacer-Receptor' architecture. The components of these sensors are chosen such that the luminescence is quenched by the receptor unit in the absence of the metal ion. In most of these systems the fluorophore is an electron acceptor (A) and the receptor is an electron donor (D). Excitation of the fluorophore induces transfer of an electron from the receptor leading to luminescence quenching. When a metal ion binds to the receptor module, the donor electrons in the

receptor unit are engaged in metal binding and are not available for transfer to the fluorophore. Thus the quenching interaction is cut off and excitation leads to observation of luminescence. This is illustrated in Scheme 4.1.

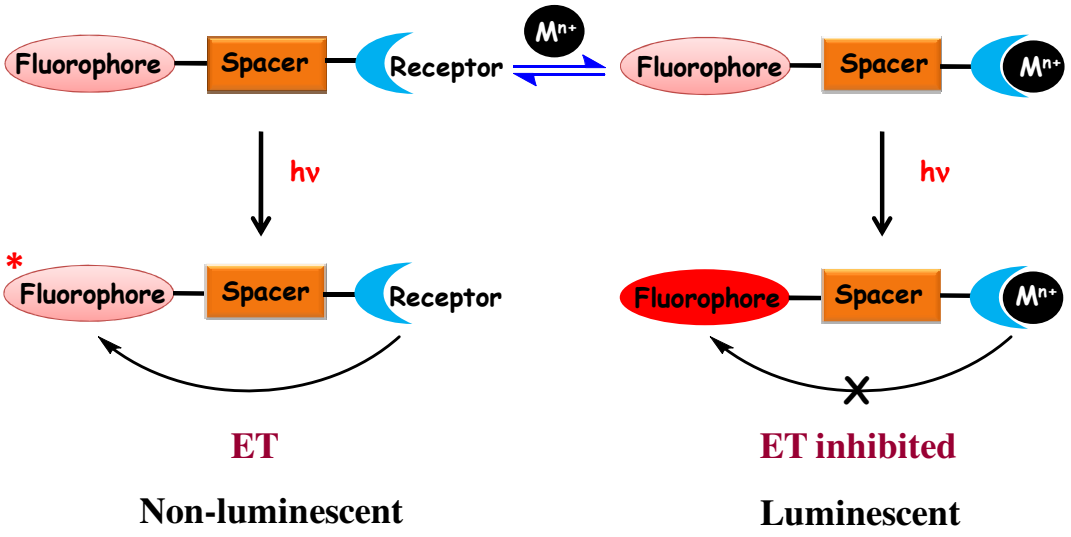

Scheme 4.1

The "turn-ON" luminescence signaling shown in Scheme 4.1 allows the detection of sub-micromolar amounts of metal ions. The very first system for the sensing of Cu^{2+} based on this principle was designed by Bharadwaj and co-workers.[7] Their system (**1**, Figure 4.1) consisted of a cryptand receptor containing three anthracene residues.

Cryptand **1**, however, is not highly selective for Cu^{2+}. It shows luminescence enhancement in the presence of Cu^{2+}, Ni^{2+}, Zn^{2+} and H^{+} ions. Several other sensor systems for Cu^{2+} ions were designed based on the fluorophore-spacer-receptor architecture and some of these are shown in Figure 4.2 (a) and (b).[8]

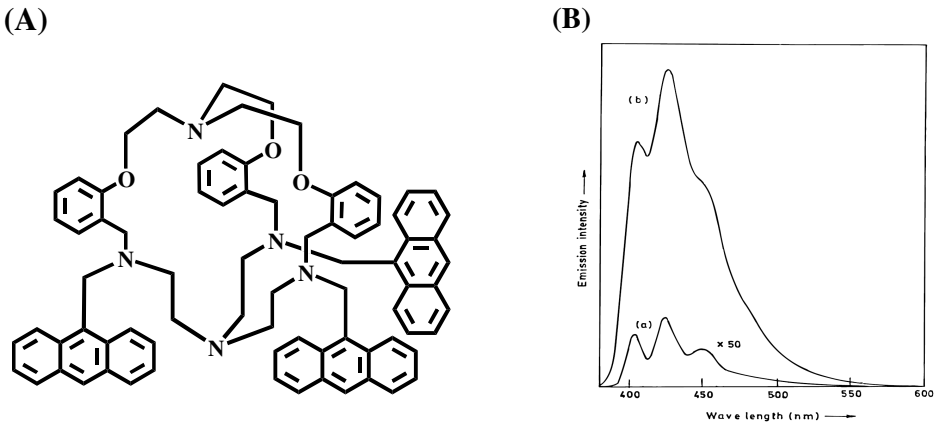

1

Figure 4.1. (A) Structure of cryptand **1** capable of sensing Cu^{2+}. (**B**) Emission spectrum of **1** in the absence (a) and presence (b) of Cu^{2+}.[7]

All the sensors shown in Figure 4.2(a) and 4.2 (b) are based on the Fluorophore-Spacer-Receptor principle and showed enhancement of luminescence in the presence of Cu^{2+}. The selectivity of the sensors would actually depend on the Cu^{2+} binding ability of the receptor unit. In general, most of the binding units exhibit low to moderate affinity for other metal ions also, and hence sensors of this type are not highly selective for Cu^{2+}.

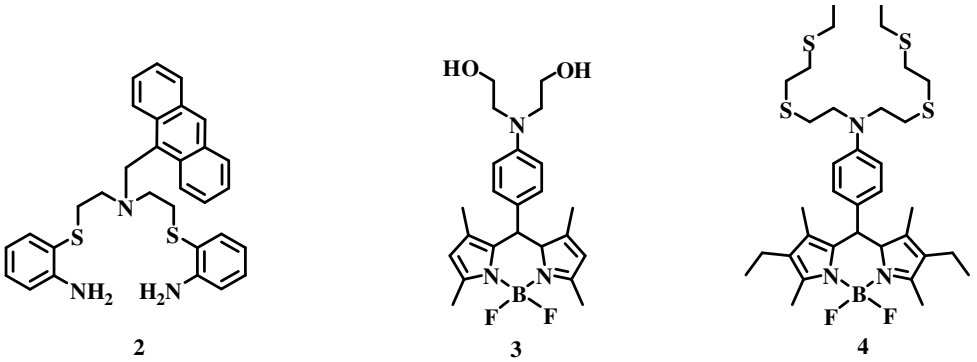

2 **3** **4**

Figure 4.2(a)

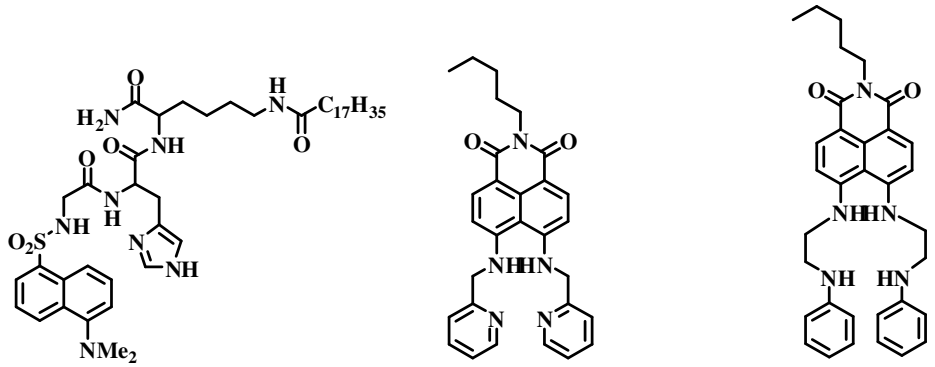

5 **6** **7**

Figure 4.2(b)

Czarnik and co-workers have designed a luminescence "turn-ON" dosimeter for Cu^{2+}, which is based on the propensity of Cu^{2+} to hydrolyze α-amino acid esters.[9] The hydrolysis actually proceeds as shown in Scheme 4.2.

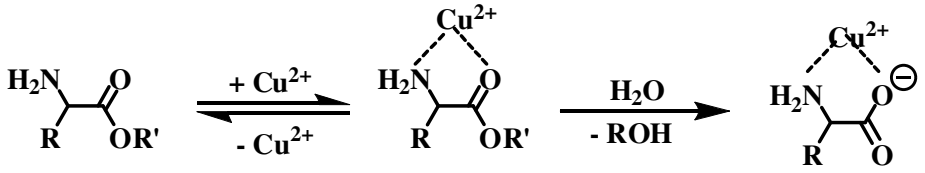

8 **9** **10**

Scheme 4.2

Other metal ions also catalyze this reaction, but Cu^{2+} reacts much faster. For most of the α-amino acid esters, hydrolysis is complete within seconds at room temperature and in neutral pH under reasonable reactant concentrations, yielding the Cu^{2+}-α-amino acid chelate **10** (Scheme 4.2) as product. Czarnik *et al*. incorporated the α-amino acid

molecular recognition motif into a Rhodamine derivative and designed the dosimeter **11**. The "turn-ON" luminescence sensing mechanism of **11** is shown in Scheme 4.3.

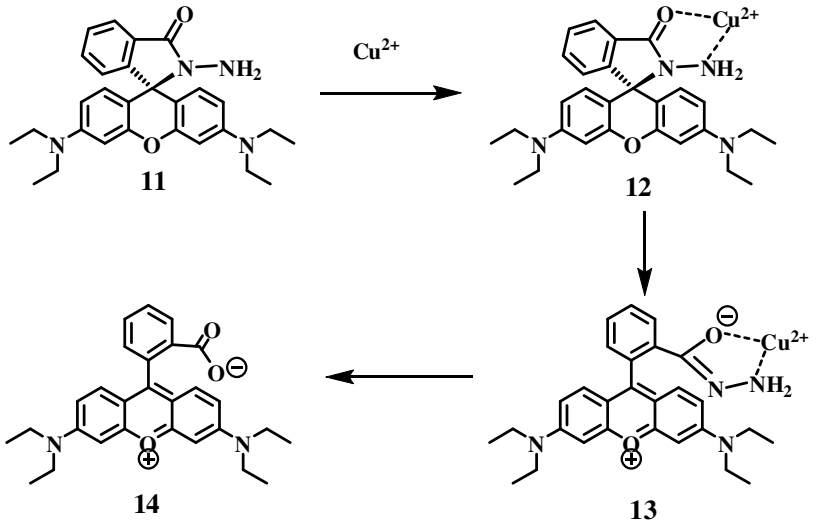

Scheme 4.3

11 is the lactam form of Rhodamine which is non-luminescent. Complexation with Cu^{2+} leads to hydrolysis of the lactam ring and generation of the fluorescent form **14**. Reactions of **11** with other metal ions are extremely slow and hence this molecule can act as a dosimeter for Cu^{2+}. Following this work, several other similar systems have been proposed as Cu^{2+} sensors.[10] Structures of some of these molecules are shown in Figure 4.3.

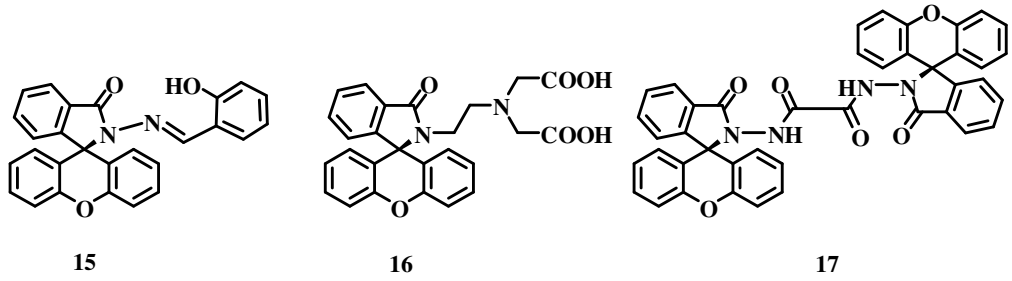

Figure 4.3

Several other "turn-ON" luminescence sensors for Cu^{2+} are known. For example, **18** and **19** (Figure 4.4) are proposed as Cu^{2+} "turn-ON" luminescence sensors.[11] In these molecules, the azadiene moiety is proposed as the site for Cu^{2+} binding. In addition to these, few other luminescence "turn-ON" sensors are also known for Cu^{2+} detection.[12]

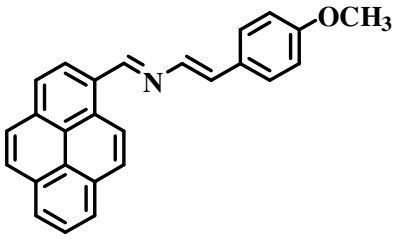

18

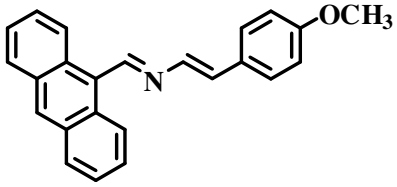

19

Figure 4.4

In Chapters 2 and 3 of this thesis we have studied the photophysics and PET properties of phenothiazine-linked $Ru(bpy)_3^{2+}$ systems such as **Ru-Ptz**, **Ru-Ptz$_2$**, **Ru-Ptz$_3$**, **Ru-Ptz$_{2(S)}$** etc. In these systems excitation of the $Ru(bpy)_3^{2+}$ chromophore resulted in electron transfer from the attached phenothiazine moieties leading to quenching of $Ru(bpy)_3^{2+}$ emission. We could characterize the charge separated states for all the Ru-Ptz systems. In this chapter we propose that the same Ru-Ptz dyads could be used as "turn-ON" luminescence dosimeters for Cu^{2+}. The principle behind this proposal is the propensity of aromatic amines such as Ptz to react with Cu^{2+} in acetonitrile (ACN).[13-15] Previous studies from our group showed that *N*-methylphenothiazine (NMPtz) reacted with Cu^{2+} in ACN to generate NMPtz radical cation ($NMPtz^{\bullet+}$) as shown in Scheme 4.4.

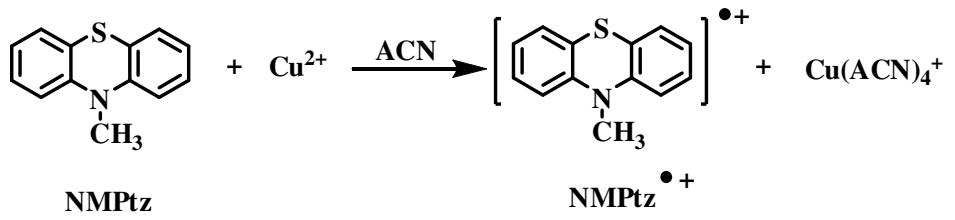

Scheme 4.4

In this chapter we show that in the presence of excess Cu^{2+} (2-5 equivalents), NMPtz is oxidized to its dication $[NMPtz]^{2+}$, which reacts with traces of water giving *N*-methylphenothiazine-5-oxide (abbreviated as NMPtzO), as shown in Scheme 4.5.

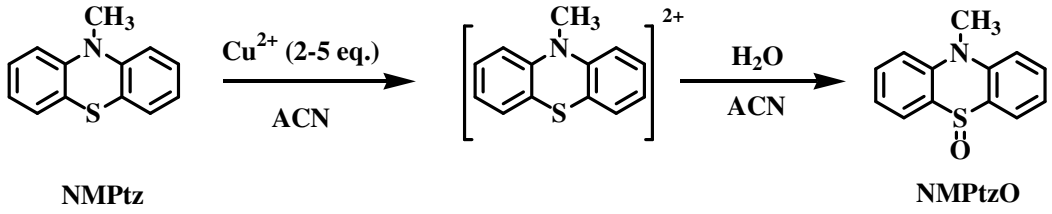

Scheme 4.5

Thus, NMPtz, which is a very good electron donor, upon reaction with Cu^{2+} forms NMPtzO, which is neither a donor nor an acceptor. This result suggested that in the presence of Cu^{2+}, the non luminescent **Ru-Ptz** would be converted to luminescent Ru-PtzO. In order to see if this strategy works, we have studied the photophysical properties of the Ru-Ptz systems shown in Figure 4.5 in presence of Cu^{2+} and the results are presented in this chapter. The luminescent derivative **Ru-Ph** (Figure 4.5) which did not contain the Ptz moiety, was used as a model system in this study for comparing the results.

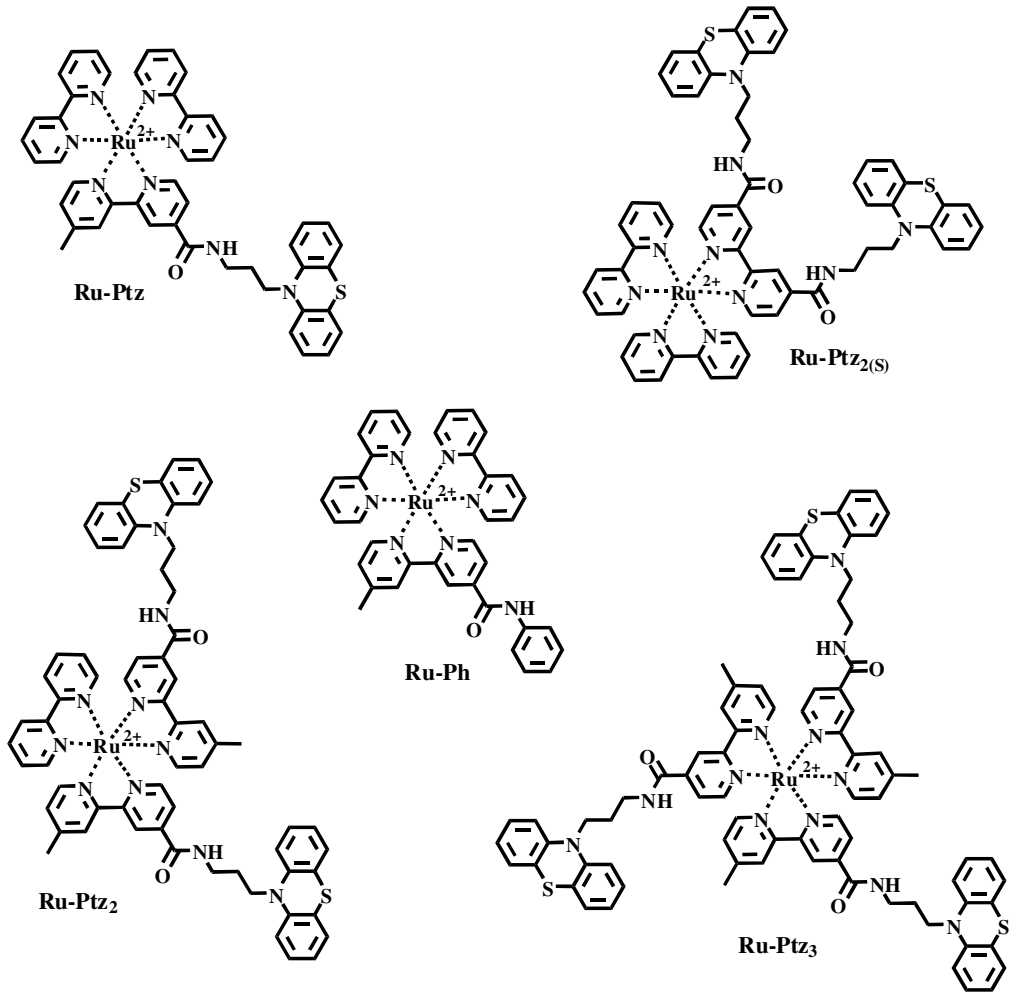

Figure 4.5. Structures of $Ru(bpy)_3^{2+}$-phenothiazine systems and model compound used in this study.

4.3 Results and Discussion

4.3.1 Metal ion sensing studies

Upon excitation of the $Ru(bpy)_3^{2+}$ chromophore in **Ru-Ptz**, very rapid electron transfer occurs from the Ptz moiety to the $Ru(bpy)_3^{2+}$ core with a rate constant $k_{et} = 2.47 \times 10^8$ s^{-1}, leading to the formation of $Ptz^{\bullet+}$ and $Ru(bpy)_3^{+}$ (details are presented in Chapter 2). Because of the fast PET process, emission of the $Ru(bpy)_3^{2+}$ moiety is

highly quenched and as a result the emission quantum yield of **Ru-Ptz** is only 0.0035 in ACN solution. The charge separated state undergoes rapid back electron transfer (k_{bet} = 3.89×10^7 s^{-1}) leading to the regeneration of **Ru-Ptz** in the ground state. Hence no permanent products are formed upon irradiation of **Ru-Ptz** and this molecule is stable to visible light irradiation. A solution of **Ru-Ptz** (7×10^{-6} M) in ACN upon excitation in a dark chamber did not show visible luminescence, although its emission spectrum can be recorded using a fluorimeter.

We have observed that the emission of **Ru-Ptz** solution is enhanced more than 15 times upon addition of micromolar amounts of Cu^{2+} as shown in Figures 4.6 and 4.7. Concentration of Cu^{2+} ions were increased from 0 to 60 μM in these experiments.

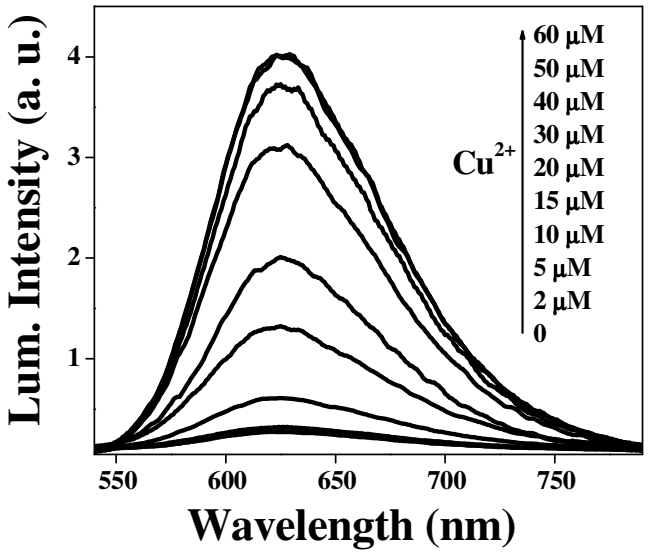

Figure 4.6. Emission spectra of **Ru-Ptz** in ACN in the absence and presence of Cu^{2+}. All spectra were recorded 30 minutes after adding Cu^{2+}.

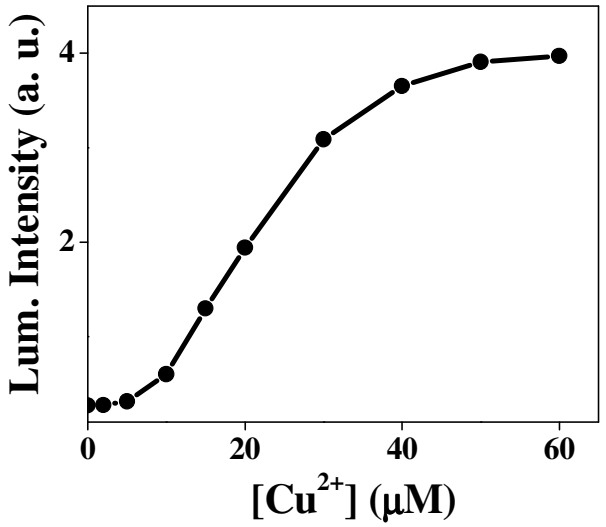

Figure 4.7. Plot of emission intensity at 620 nm vs [Cu^{2+}].

Luminescence behavior of **Ru-Ptz** in presence of several other metal ions (Li^{+}, Na^{+}, K^{+}, Ag^{+}, Mg^{2+}, Ca^{2+}, Ba^{2+}, Mn^{2+}, Fe^{2+}, Ni^{2+}, Zn^{2+}, Cd^{2+}, Hg^{2+}, Pb^{2+}, Cr^{3+}, Fe^{3+} and Co^{3+}) were examined. Emission enhancement was not observed in the presence of any of these ions in ACN. It is to be noted that metal ions like Zn^{2+}, Cd^{2+}, Hg^{2+}, Pb^{2+} etc., which are normally interfering with Cu^{2+} in the sensing studies are not making any effect here. Results of these studies are presented in Figure 4.8, which shows that **Ru-Ptz** can be used as a highly selective and sensitive "turn-ON" luminescence chemodosimeter for Cu^{2+}. This aspect is further illustrated in Figure 4.9 which shows the photograph of solutions of **Ru-Ptz** (7×10^{-6} M) in the presence of various metal ions (5×10^{-5} M) under illumination. Only the solution containing Cu^{2+} is luminescent under illumination, which is a confirmatory proof that **Ru-Ptz** in ACN can be used as a "turn-ON" luminescence chemodosimeter for Cu^{2+}.

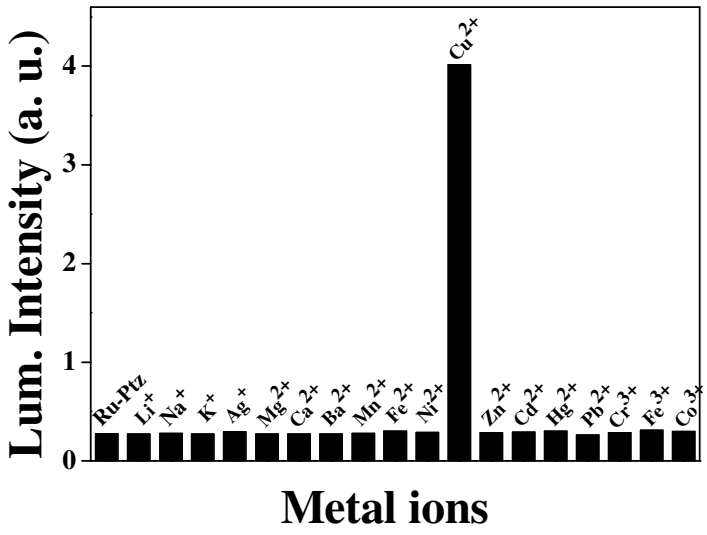

Figure 4.8. Bar graph showing the emission intensity of **Ru-Ptz** in the presence of various metal ions. [**Ru-Ptz**] = 7×10^{-6} M, [Metal salts] = 5×10^{-5} M.

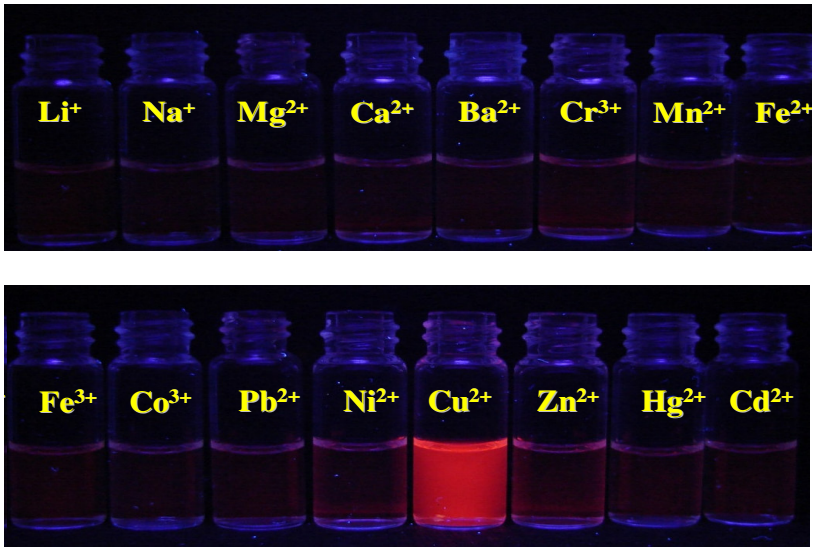

Figure 4.9. Photograph of solutions of **Ru-Ptz** (7×10^{-6} M) in the presence of various metal ions (5×10^{-5} M) under illumination.

We confirmed that none of the metal ions shown in Figure 4.8 and 4.9 interfered with the detection of Cu^{2+} using **Ru-Ptz**. Spectrum 'a' in Figure 4.10 is the emission of **Ru-Ptz** in ACN in the presence of 50 μM each of K^+, Ag^+, Mg^{2+}, Mn^{2+}, Fe^{3+}, Cr^{3+}, Pb^{2+}, Co^{2+} and Cr^{3+}. The emission intensity was same as that of **Ru-Ptz**. Upon addition of 50 μM Cu^{2+} to the same solution, emission intensity increased as shown in Figure 4.10 'b', indicating that only Cu^{2+} can cause emission enhancement.

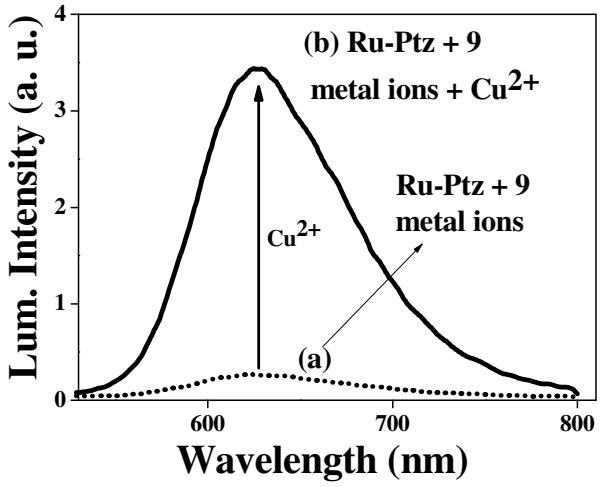

Figure 4.10. (a) Emission spectrum of **Ru-Ptz** in the presence of 50 μM each of K^+, Ag^+, Mg^{2+}, Mn^{2+}, Fe^{3+}, Cr^{3+}, Pb^{2+}, Co^{2+} and Cr^{3+}. (b) Emission spectrum of above solution after addition of 50 μM Cu^{2+}.

The fact that other metal ions do not interfere with Cu^{2+} sensing is further confirmed by Figure 4.11. Spectrum 'a' in Figure 4.11 is the emission due to **Ru-Ptz** in the presence of 50 μM Cu^{2+}. The emission intensity did not change when K^+, Ag^+, Mg^{2+}, Mn^{2+}, Fe^{3+}, Cr^{3+}, Pb^{2+}, Co^{2+} and Cr^{3+} (each 50 μM) were added. The small decrease of luminescence intensity observed in Figure 4.11 'b' is attributed to dilution

effects. These results indicated that other metal ions do not interfere with the detection of Cu^{2+} in the concentration range studied. It may be noted that several of these ions including Cu^{2+} will quench the emission of **Ru-Ptz** at concentrations greater than 2 mM.

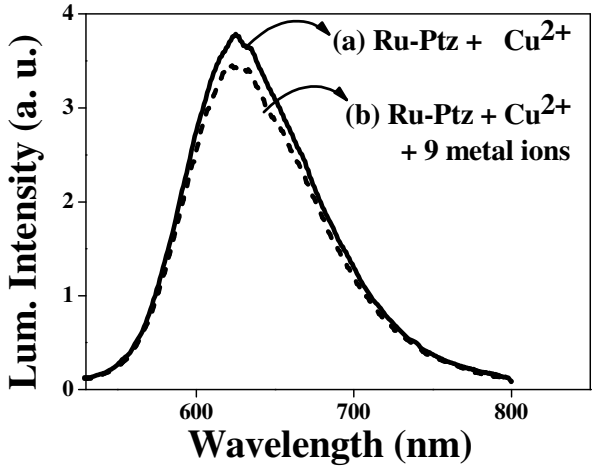

Figure 4.11. (a) Emission spectrum of **Ru-Ptz** in the presence of 50 μM Cu^{2+}. (b) Emission spectrum of solution in (a) after addition of 50 μM each of K^+, Ag^+, Mg^{2+}, Mn^{2+}, Fe^{3+}, Cr^{3+}, Pb^{2+}, Co^{2+} and Cr^{3+}.

The $Ru(bpy)_3^{2+}$ chromophore in **Ru-Ptz** is very similar to that in the model compound **Ru-Ph** (Figure 4.5) and we have attempted a comparison of the luminescence properties of **Ru-Ph** with those of **Ru-Ptz** containing Cu^{2+}. For this comparison we used optically matched solutions (at 440 nm) of **Ru-Ph** and **Ru-Ptz** (≈ 7 × 10^{-6} M). To the latter we added $Cu(ClO_4)_2$.$6H_2O$ (5 × 10^{-5} M) and this solution was designated as **Ru-Ptz**/Cu^{2+}. In Figure 4.12, emission spectra of **Ru-Ph** and **Ru-Ptz**/Cu^{2+} are compared. It can be seen that emission intensity is slightly higher for **Ru-Ptz**/Cu^{2+}.

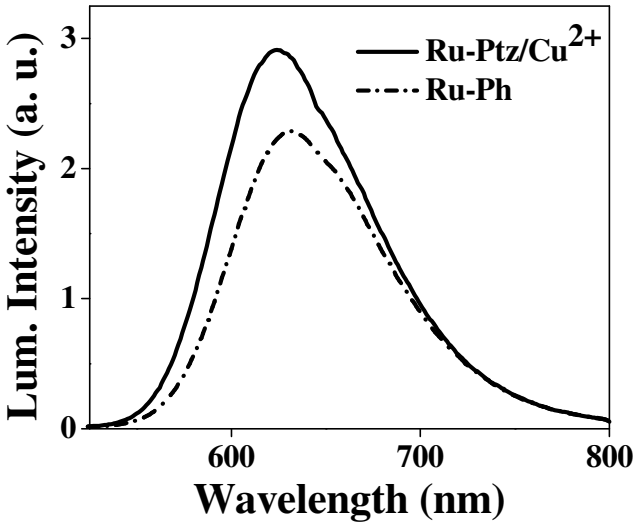

Figure 4.12. Emission spectra of optically matched solutions of **Ru-Ph** and **Ru-Ptz**/Cu^{2+}.

We also recorded the emission lifetimes of **Ru-Ph** and **Ru-Ptz**/Cu^{2+} by the TC-SPC technique. The emission decay profiles obtained for the **Ru-Ptz** dyad after the addition of five equivalents of Cu^{2+} is compared with that of the **Ru-Ph** model derivative in Figure 4.13. Both the emission decays were mono-exponential and the lifetime values obtained were 1.2 μs and 1.4 μs, respectively, for **Ru-Ph** and **Ru-Ptz**/Cu^{2+}. This observation is in contrast to the extremely small, bi-exponential decay behavior exhibited by Ru-Ptz derivatives due to the efficient PET occurring in those systems (see Chapter 2). The very high emission intensity and large emission lifetime of **Ru-Ptz**/Cu^{2+} suggested that the Ptz moiety of **Ru-Ptz** got converted into a form which cannot quench the emission of $Ru(bpy)_3^{2+}$ core in the presence of excess (2 - 5 eq) Cu^{2+}. Lifetime studies of other Ru-Ptz systems in presence of 2-5 equivalents of Cu^{2+} also resulted in similar observations.

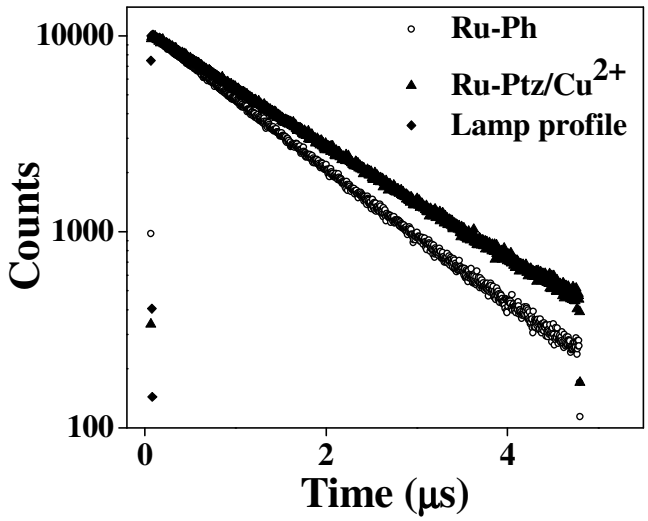

Figure 4.13. Emission decay profiles of **Ru-Ph** and **Ru-Ptz**/Cu^{2+} in ACN.

The proposal to use **Ru-Ptz** as a Cu^{2+} chemodosimeter in this study was based on the premise that Cu^{2+} would react with the Ptz moiety. Based on results from our research group,[13-15] we anticipated that addition of one equivalent of Cu^{2+} would convert **Ru-Ptz** to Ru-$Ptz^{\bullet+}$. We observed that Ru-$Ptz^{\bullet+}$ is relatively stable, but in the presence of excess Cu^{2+} it reacts further, presumably to generate a stable product (vide infra). In order to get a detailed understanding of this reaction, spectroscopic and product isolation studies were carried out and the results are described in the following section.

Figure 4.14 shows the absorption spectrum of **Ru-Ptz** in ACN (solid line). The 400-500 nm band is due to the MLCT absorption of $Ru(bpy)_3^{2+}$. The bipyridine based $\pi-\pi^*$ absorption is seen in the 300 nm region and the absorption at 255 nm is due to the Ptz moiety (see Chapter 2 for details). Figure 4.14 also shows the absorption spectrum

of **Ru-Ptz** in the presence of two equivalents of Cu^{2+} immediately after mixing (dotted line), which showed an increase in absorption in the 260-300 and 400-600 nm regions. The difference spectrum is shown in Figure 4.15.

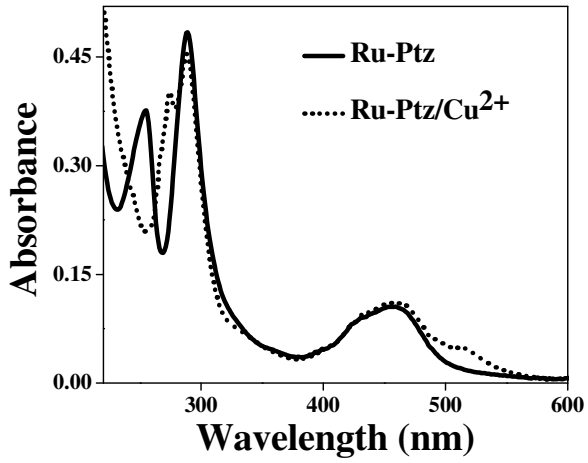

Figure 4.14. Absorption spectra of **Ru-Ptz** (7×10^{-6} M) and **Ru-Ptz/**Cu^{2+} (7×10^{-6} / 1.4×10^{-5} M) in ACN.

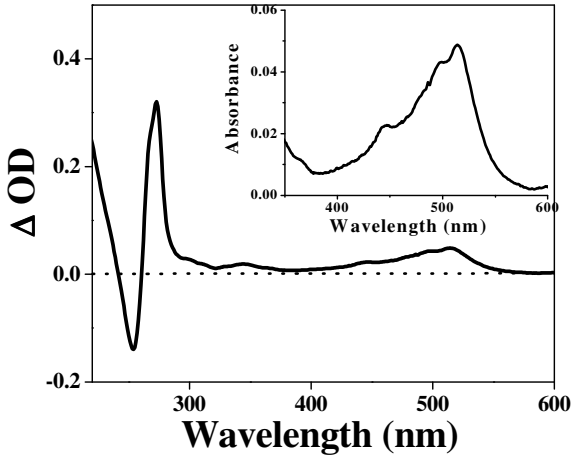

Figure 4.15. The difference spectrum between **Ru-Ptz** (7×10^{-6} M) and **Ru-Ptz /** Cu^{2+} (7×10^{-6} / 1.4×10^{-5} M) in ACN. In the inset absorption in the 350-600 nm region is enlarged.

The difference spectrum showed bleaching at 255 nm corresponding to loss of absorption due to Ptz and positive bands at 272 and 514 nm corresponding to the formation of $Ptz^{\bullet+}$. Inset of Figure 4.15 shows an enlarged version of the absorption in the 350-600 nm region and this spectrum is identical to the well-known $Ptz^{\bullet+}$ absorption spectrum[13] and based on this we identified the dotted line spectrum in Figure 4.14 as that of Ru-$Ptz^{\bullet+}$.

The absorptions due to $Ptz^{\bullet+}$ at 272 and 514 nm in Figure 4.14 disappeared with time and the actual band structure due to $Ru(bpy)_3^{2+}$ in the 400-500 nm was restored in a few hours. This indicated that the final product formed from $Ptz^{\bullet+}$ exhibited no absorption above 400 nm. **Ru-Ptz** has strong absorption at wavelengths below 350 nm and it was difficult to follow this reaction. Hence we used NMPtz (Scheme 4.4) as a model compound to study the time dependent absorption changes. Figure 4.16 shows the absorption spectrum of NMPtz (5×10^{-5} M) in ACN with 2 equivalents of Cu^{2+} immediately after mixing. The absorption band in the 400-600 nm region was assigned to $NMPtz^{\bullet+}$ and was identical to the inset figure in Figure 4.15. Spectra 'a-k' in Figure 4.16 show the time dependent variation of this absorption. It can be seen that the absorption due to $NMPtz^{\bullet+}$ gradually decreased with a concomitant increase in a new absorption with maxima near 300 and 345 nm. Isosbestic point at 392 nm suggested that only two absorbing specie are present in solution. This stable absorption in the 320-400 nm region gave the impression of a new compound and from a literature survey, we could assign the absorption to *N*-methylphenothiazine-5-oxide (NMPtzO).[16]

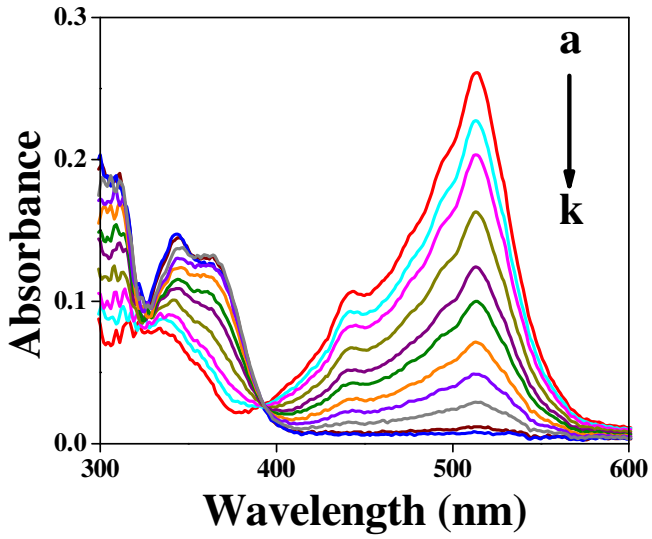

Figure 4.16. Time dependence of the decay of **NMPtz**$^{\bullet+}$ in the presence of Cu^{2+} (2 eq.).

In order to unequivocally identify the product of the reaction of NMPtz with excess Cu^{2+}, we have carried out the reaction using 100 mg of NMPtz and 5 equivalents of $Cu(ClO_4)_2$. The product was isolated and characterized as NMPtzO using spectroscopic and analytical techniques (see experimental section).

We have carried out the reaction of NMPtz with Cu^{2+} at different concentrations of Cu^{2+} and in all cases the formation of NMPtzO was monitored by absorption spectroscopy. We observed that the rate of formation of NMPtzO depended on Cu^{2+} concentration. In Figure 4.17, the change of absorbance at 514 nm (corresponds to depletion of NMPtz$^{\bullet+}$) is plotted as a function of time for different Cu^{2+} concentrations. When NMPtz and Cu^{2+} are present in equal concentrations, absorption due to NMPtz$^{\bullet+}$ exhibited only marginal decrease in 2 h. Decay of NMPtz$^{\bullet+}$ was accelerated in the presence of 2 equivalents of Cu^{2+} and when 5 equivalents of Cu^{2+} were present, decay was nearly complete within 40 minutes. The results suggested that 2 or more

equivalents of Cu^{2+} are required for the conversion of NMPtz to NMPtzO. As shown in Figure 4.6, maximum luminescence enhancement for **Ru-Ptz** was observed in the presence of 5×10^{-5} M Cu^{2+}, indicating that all the Ptz groups are converted to PtzO at this concentration. At very high concentrations of Cu^{2+} (> 2 mM), the paramagnetic nature of Cu^{2+} becomes operational leading to quenching of the emission. Control experiments showed that luminescence of the model compound **Ru-Ph** is unaffected by low concentration of Cu^{2+}, but at higher concentrations, emission quenching occurs.

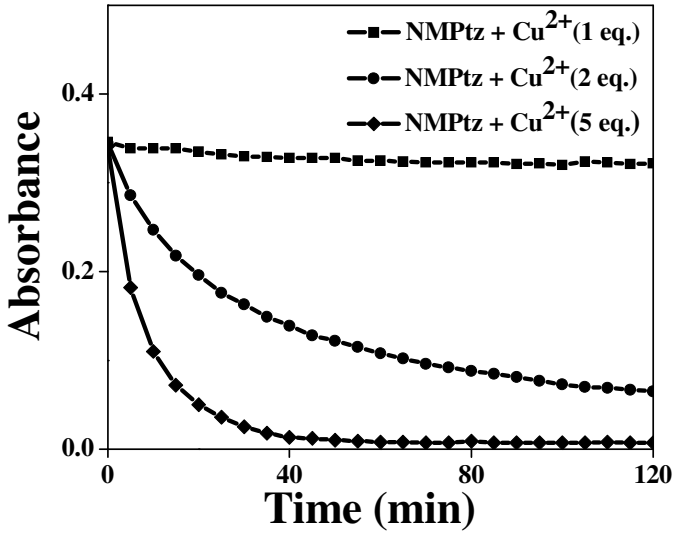

Figure 4.17. The change of absorbance at 514 nm in NMPtz/Cu^{2+} reaction with time at different Cu^{2+} concentrations.

Figure 4.16 and 4.17, however, do not suggest a possible mechanism for the conversion of $NMPtz^{\bullet+}$ to NMPtzO. It was reported previously that $NMPtz^{\bullet+}$ can be oxidized electrochemically to the $[NMPtz]^{2+}$, which immediately reacts with water to

form NMPtzO.[16b] Based on these reports, Scheme 4.5, which involve oxidation of $NMPtz^{\bullet+}$ to $[NMPtz]^{2+}$ by Cu^{2+}, is suggested for the conversion of NMPtz to NMPtzO.

Figures 4.14 – 4.17 suggested that upon reaction with excess Cu^{2+}, **Ru-Ptz** would be converted to Ru-PtzO. Since PtzO is not a good electron donor it cannot quench the luminescence of the $Ru(bpy)_3^{2+}$ core. This would result in the restoration of the emission due to $Ru(bpy)_3^{2+}$. Based on these observations a probable mechanism for the "turn-ON" luminescence is suggested in Scheme 4.6.

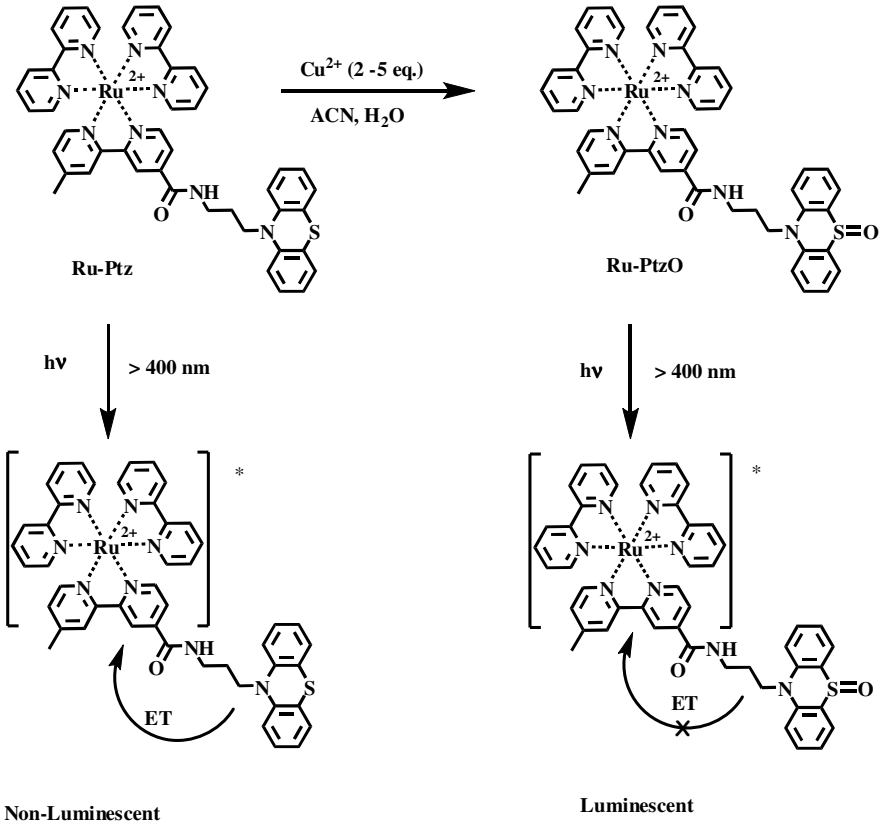

Scheme 4.6. Probable mechanism for the "turn-ON" luminescence of **Ru-Ptz** in the presence of Cu^{2+} (Cu^{2+} concentration is 2-5 eq).

Figure 4.17 suggests that reaction of **Ru-Ptz** with Cu^{2+} is relatively slow and even in the presence of five equivalents of Cu^{2+} the reaction requires 40 minutes for completion. Thus restoration of full emission intensity would require nearly 30 minutes. Because of this, successive emission spectra in Figure 4.6 were recorded 30 minutes after mixing **Ru-Ptz** with Cu^{2+} solution.

Thermodynamics of the reactions described in Schemes 4.4 - 4.6 also are worked out. For the ground state ET reactions described in Schemes 4.4 and 4.5, ΔG^0 can be obtained using equation 4.1,

$$\Delta G^0 = E_{ox} - E_{red} - e^2/d\varepsilon \qquad (4.1)$$

where E_{ox} is the oxidation potential of the donor (NMPtz or $NMPtz^{\bullet+}$) and E_{red} is the reduction potential of the acceptor (Cu^{2+}), d is the center-center distance between the donor and acceptor and ε is the solvent dielectric constant. These reactions take place only in ACN. E_{red} of Cu^{2+} in ACN is + 0.952 V vs SCE. In fact this value is approximately 1 V more positive than E_{red} in water and the gain in energy by changing the solvent to ACN is attributed to the formation of the stable tetrakis(acetonitrile)Copper(I) complex immediately following the reduction of Cu^{2+} to Cu^{+} as shown in Scheme 4.4.[17] Under these conditions it is advisable to replace E_{red} in equation 4.1 with the reduction peak potential (E_p) obtained by linear sweep voltammetry. For the reduction of Cu^{2+} in ACN we obtained E_p as +1.082 V. For NMPtz, the first and second oxidation potentials were at 0.7 and 1.27 V (vs SCE).[18] Assuming d = 7 Å, we obtained ΔG^0 for the electron transfer reactions in Schemes 4.4

and 4.5 as -0.437 and + 0.133 eV, respectively. These calculations show that oxidation of NMPtz to $NMPtz^{\bullet+}$ by Cu^{2+} in ACN is spontaneous, whereas oxidation to $[NMPtz]^{2+}$ is endergonic. Although ΔG^0 is slightly positive, dication formation still takes place, albeit slowly, in the presence of two or more equivalents of Cu^{2+}.

For the PET reactions shown in Scheme 4.6, ΔG^0 values are calculated using the Weller equation 4.2,

$$\Delta G^0 = E_{ox} - E_{red} - e^2/d\varepsilon - E_{0,0} \qquad (4.2)$$

where $E_{0,0}$ is the excitation energy of $Ru(bpy)_3^{2+}$ core (= 2.12 eV). For **Ru-Ptz**, excitation leads to electron transfer from Ptz to the $Ru(bpy)_3^{2+}$ core and hence E_{ox} of Ptz and E_{red} of $Ru(bpy)_3^{2+}$ are relevant. Assuming d = 7 Å, we calculated ΔG^0 = -0.13 eV for this electron transfer. Rate constant for this PET reaction was measured as 2.47×10^8 s^{-1} (see Chapter 2).

For emission quenching in Ru-PtzO, we have to consider both oxidative and reductive quenching mechanisms shown in Scheme 4.7.

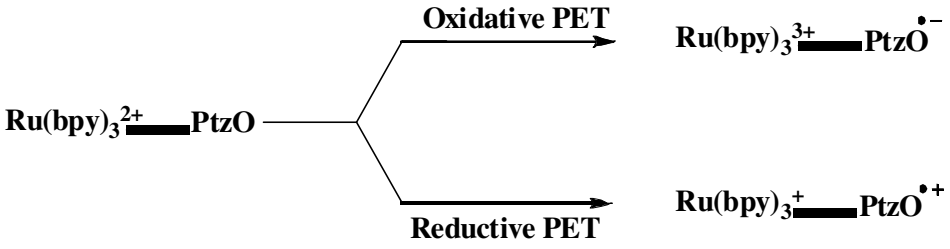

Scheme 4.7. Probable quenching mechanisms in Ru-PtzO.

In order to calculate ΔG^0 values for these reactions, redox potentials of NMPtzO are required. Cyclic voltammogram of NMPtzO was recorded in ACN using tetrabutyl-ammonium hexafluorophosphate as the supporting electrolyte and this is shown in Figure 4.18.

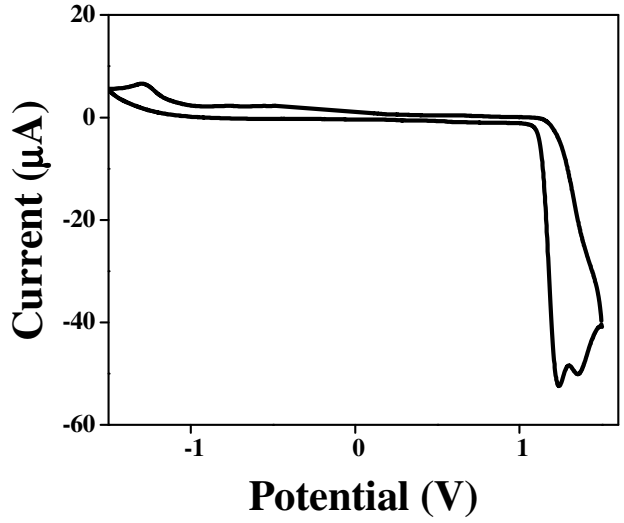

Figure 4.18. Cyclic volammogram of NMPtzO in ACN using tetrabutyl ammonium hexafluorophosphate as the supporting electrolyte. Potential is referenced to SCE.

Cyclic voltammogram shown in Figure 4.18 exhibited irreversible oxidation and reduction behaviour and hence we have taken the peak potentials as redox potentials and used these values in equation 4.2 to obtain ΔG^0 values for oxidative and reductive PET quenching in Ru-PtzO. For the oxidative quenching E_{ox} of $Ru(bpy)_3^{2+}$ (= 1.3 V)[14] and E_{red} of NMPtzO (= -1.27 V vs SCE, from Figure 4.18) are relevant and we obtained ΔG^0 = +0.40 eV. For reductive quenching, E_{red} of $Ru(bpy)_3^{2+}$ (= -1.33 V)[18] and E_{ox} of NMPtzO (= 1.28 V vs SCE, from Figure 4.18) are relevant and we obtained ΔG^0 = + 0.44 eV. ΔG^0 values are positive for both reactions and hence the emission of

$Ru(bpy)_3^{2+}$ core will not be quenched by the attached PtzO moiety. In other words, Ru-PtzO is expected to exhibit emission similar to the model compound **Ru-Ph**. This is the basis for the emission enhancement of **Ru-Ptz** in the presence of excess of Cu^{2+} and the situation is shown in Scheme 4.8.

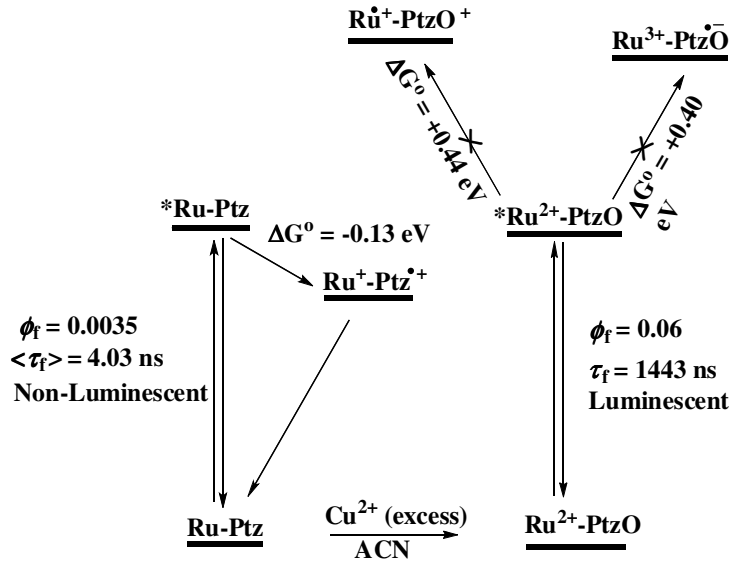

Scheme 4.8. Possible luminescence quenching pathways in **Ru-Ptz** and Ru-PtzO.

It may be noted that the luminescence quantum yield and lifetime of Ru-PtzO are somewhat higher than the model compound **Ru-Ph** (Figure 4.12 and 4.13). We attribute this to the differences in ligand structure. It is known that changes in ligand structure can lead to changes in emission quantum yield and lifetime for $Ru(bpy)_3^{2+}$ derivatives.[19]

4.3.2. Detection of Cu^{2+} from Biological Samples

Studies described so far in this chapter regarding the sensing of Cu^{2+} by **Ru-Ptz** were carried out in acetonitrile. Such studies have very limited scope. Ability of

the system to perform in aqueous or in mixtures of water and organic solvents is an important criterion for applying the dosimeter to biological samples. In pure water Cu^{2+} is incapable of oxidizing Ptz and the sensing mechanism will not work. We observed that in aqueous ACN containing less than 30% water, the sensing mechanism still works. This is illustrated in Figure 4.19 which shows the emission spectra of **Ru-Ptz/**Cu^{2+} in ACN at different water composition. It can be seen that the fluorescence intensity decreases with increase in water content, but considerable luminescence is exhibited even when the water content is 20%. Figure 4.19 clearly shows that **Ru-Ptz** can be used as a chemodosimeter for Cu^{2+} present in aqueous medium. Small amounts of aqueous Cu^{2+} samples can be added to sample solutions of **Ru-Ptz** in ACN and luminescence enhancements will be observed if the water content of the medium is less than 20%. Luminescence enhancement of 6 fold is observed in the presence of 20% water and this is sufficient for visual observation of the $Ru(bpy)_3^{2+}$ luminescence.

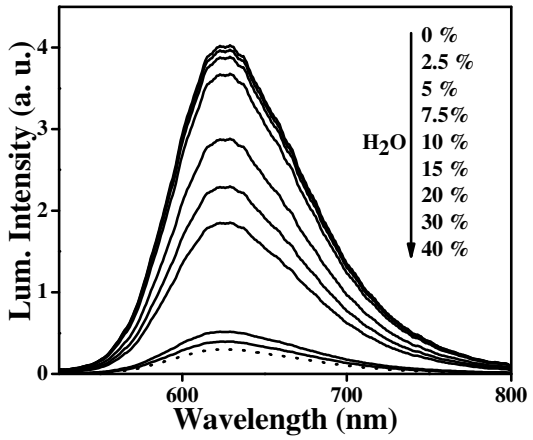

Figure 4.19. Emission spectra of **Ru-Ptz** (7×10^{-6} M)/Cu^{2+} (5×10^{-5} M) in ACN in the presence of different amounts of water.

4.3.3. Electrochemical Studies

Figure 4.19 clearly illustrates the effect of higher percentage of water, which critically affects the sensing mechanism. In order to ascertain the underlying mechanistic details, we have carried out electrochemical studies of Cu^{2+}/ACN system at different water compositions. We observed that the redox potential of Cu^{2+}/Cu^{+} couple in ACN exhibits considerable variation in the presence of water. Figure 4.20 shows the cyclic viltammograms of Cu^{2+}/Cu^{+} reduction in ACN in the presence of 0 – 30% water. Figure 4.21 shows the variation of Cu^{2+} reduction potential as a function of increasing water concentration.

It can be seen from these figures that the reduction potential of Cu^{2+} undergoes a gradual decrease from 0.96 V to 0.52 V as the percentage of water in ACN is varied from 0 to 30%. Once the reduction potential of Cu^{2+} is below 0.5 V oxidation of Ptz to $Ptz^{\bullet+}$ by Cu^{2+} would be endergonic (equation 4.1). This value of reduction potential of Cu^{2+} (0.5 V) corresponds to a 15-20% water composition in ACN. Thus the inability of **Ru-Ptz** to detect Cu^{2+} in pure aqoues medium is due to the low value of Cu^{2+}/Cu^{+} reduction potential in water. Presence of water inhibits the oxidation of Ptz to PtzO which in turn inhibits the luminescence enhancement. Thus we could correlate the changes in the luminescence enhancement factor with the changes in the redox potential of Cu^{2+}/Cu^{+} couple. It is to be mentioned here that the effect of water on the redox potential of Cu^{2+}/Cu^{+} was reported previously by others.[20]

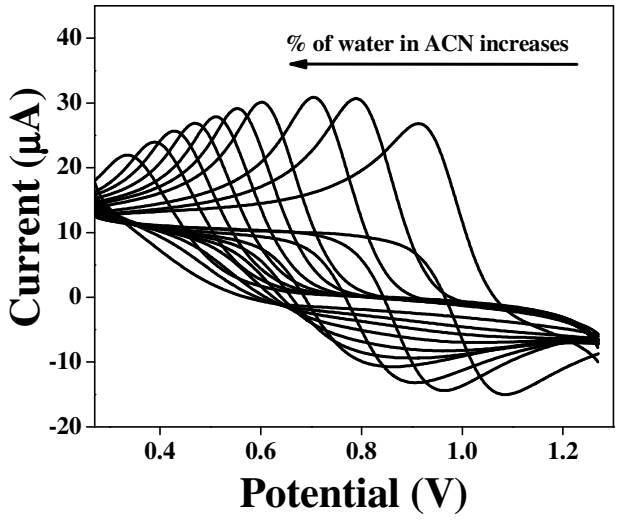

Figure 4.20. Cyclic voltammograms of Cu^{2+} in ACN medium with a gradually increasing percentage of water.

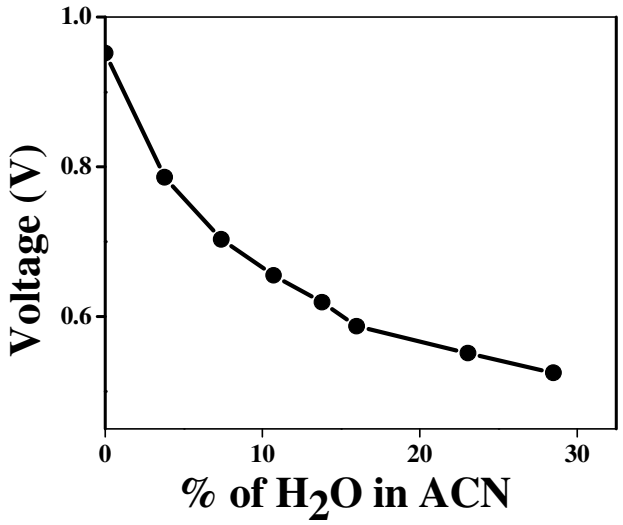

Figure 4.21. Variation of the reduction potential of Cu^{2+} with the percentage of water in the medium.

4.3.4. Metal Sensing Studies with Ru-Ptz$_2$, Ru-Ptz$_3$

We have extended the metal sensing studies to **Ru-Ptz$_2$** and **Ru-Ptz$_3$** dyads for which the photophysical aspects were studied in Chapter 2. As in the case of **Ru-**

Ptz, these systems also exhibited very selective "turn-ON" luminesecnce detection of Cu^{2+}. In these systems the 'onset' of luminescence enhancement in the presence of Cu^{2+} happens at relatively higher concentrations of Cu^{2+} as shown in Figures 4.22 and 4.23. For a Ru-Ptz_n system to exhibit luminescence enhancement all the Ptz units must get oxidized to PtzO and this requires higher Cu^{2+} concentration. Maximum luminescence enhancement for these systems were observed at 50 - 60 μM Cu^{2+} as in the case of **Ru-Ptz**. **Ru-Ptz_2** and **Ru-Ptz_3** also did not exhibit luminescence enhancement in the presence of other metal ions such as Li^+, Na^+, K^+, Mg^{2+}, Ca^{2+}, Ba^{2+}, Zn^{2+}, Cd^{2+}, Hg^{2+}, Pb^{2+}, and Cr^{3+}. These results are also shown in Figures 4.22 and 4.23.

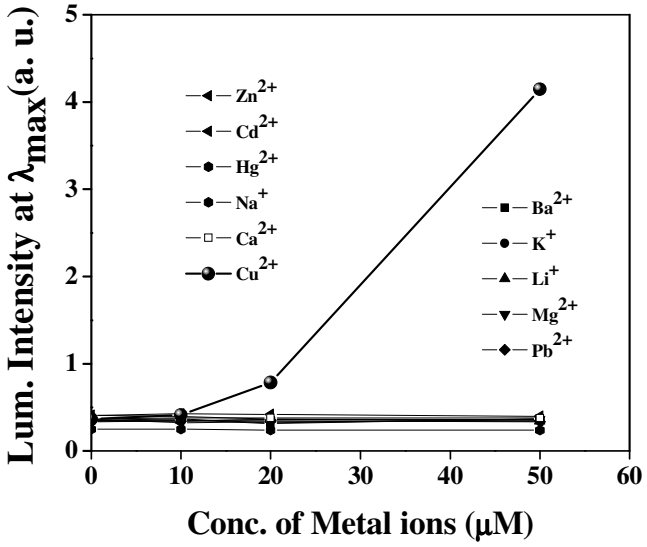

Figure 4.22. Luminescence studies of **Ru-Ptz_2** (7×10^{-6}) in ACN with the metal ions Li^+, Na^+, K^+, Mg^{2+}, Ca^{2+}, Ba^{2+}, Zn^{2+}, Cd^{2+}, Hg^{2+}, Pb^{2+} and Cu^{2+} (5×10^{-5} M each)

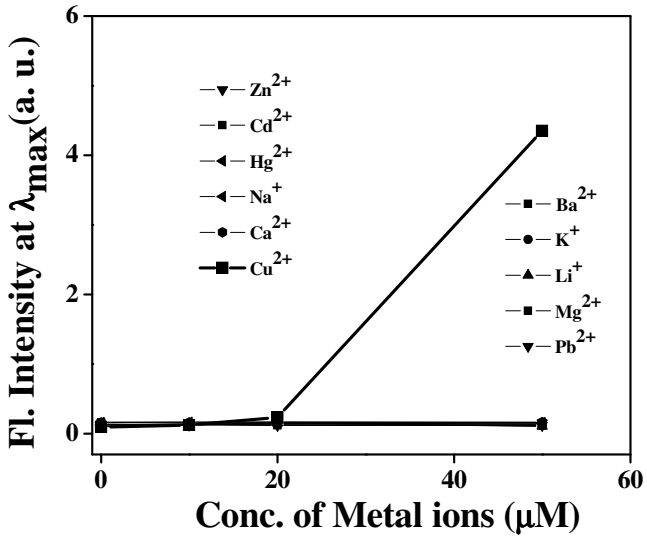

Figure 4.23. Luminescence studies of **Ru-Ptz$_3$** (7×10^{-6}) in ACN with the metal ions Li^+, Na^+, K^+, Mg^{2+}, Ca^{2+}, Ba^{2+}, Zn^{2+}, Cd^{2+}, Hg^{2+}, Pb^{2+} and Cu^{2+} (5×10^{-5} M each).

Absorption spectra of **Ru-Ptz$_2$** and **Ru-Ptz$_3$** in the presence of Cu^{2+} were recorded to confirm the mechanism of "turn-ON" luminescence. In both cases depletion in the region of Ptz absorption and enhancement in the region of $Ptz^{\bullet+}$ absorption were observed, which suggested that oxidation of Ru-Ptz_n to Ru-$(PtzO)_n$ is the reason behind the luminescence enhancement.

4.3.5. Metal sensing studies with Ru-Ptz$_{2(S)}$

As a continuation of these studies we have examined the photophysical properties of **Ru-Ptz$_{2(S)}$** in the presence of Cu^{2+} in ACN (photophysical studies of this compound is reported in Chapter 3). Luminescence of this compound was enhanced 25 times in the presence of Cu^{2+}. The onset of luminescence in this case was delayed until nearly 25 μM Cu^{2+} was added and luminescence intensity reached

a maximum at 300 mM Cu^{2+}, as shown in Figure 4.24(a) and (b).

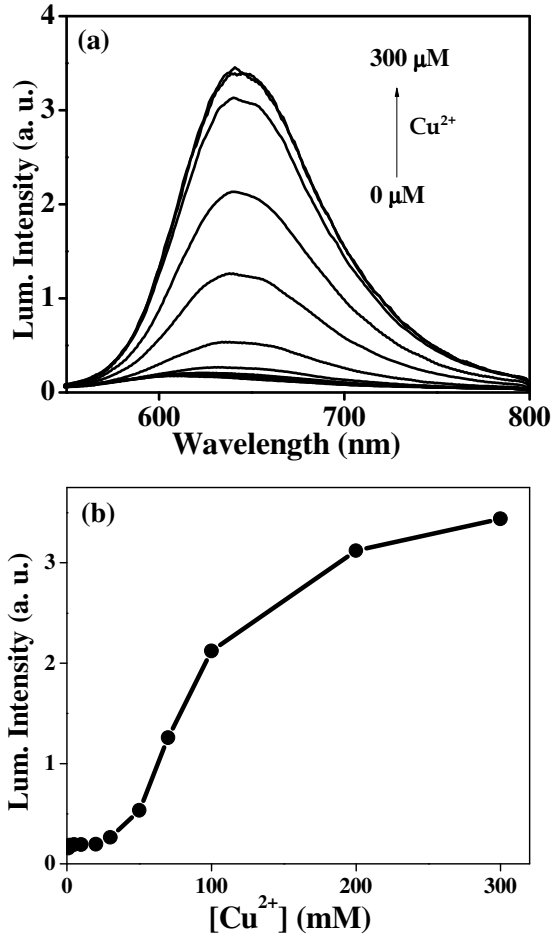

Figure 4.24.(a) Emission spectra of **Ru-Ptz$_{2(s)}$** in ACN in the presence of gradually increasing concentration of Cu^{2+}. All spectra were recorded 30 minutes after adding Cu^{2+}. (b) Plot of emission intensity of **Ru-Ptz$_{2(S)}$** at 620 nm *vs* [Cu^{2+}] in ACN.

In order to ascertain the mechanism of luminescence enhancement, absorption spectra of **Ru-Ptz$_{2(S)}$** was recorded in the absence and presence of Cu^{2+} in ACN and the results are presented in Figure 4.25. In the presence of Cu^{2+}, depletion of Ptz absorption in the 255 nm region and formation of $Ptz^{\bullet+}$ absorptions in the 272 and 524 nm regions are noted. Like in the case of Ru-Ptz derivatives, the oxidation of the Ptz moieties to

PtzO could be responsible for the observed luminescence enhancement in this system also.

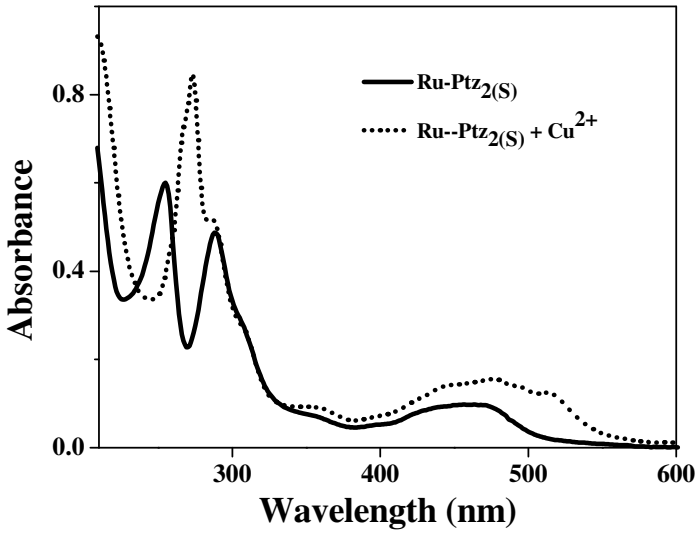

Figure 4.25. Absorption spectra of **Ru-Ptz$_{2(S)}$** (8.5×10^{-6} M) and **RuPtz$_{2(S)}$**/Cu^{2+} (8.5×10^{-6} / 2×10^{-5} M) in ACN.

4.3.6. "Turn-ON" luminescence sensing of Fe^{3+}

Cu^{2+} induced emission enhancements of Ru-Ptz systems occur only in acetonitrile medium and this is attributed to the enhancement of the oxidative ability of Cu^{2+} in this solvent. In order to see if other metals are capable of inducing emission enhancements in solvents other than ACN, we have examined the emission behavior of **Ru-Ptz** in the presence of several metal ions in water and methanol (MeOH). We observed that Fe^{3+} induces emission enhancement for **Ru-Ptz** in MeOH at higher concentrations as shown in Figure 4.26 A. Fe^{3+} is the most abundant metal ion in the human body.[2c] Fe^{3+} also is toxic at higher concentrations.

For example, accumulation of iron in the central nervous system has been implicated in Huntington's, Parkinson's and Alzheimer's diseases, all of which correlate with increased amounts of iron in the brain.[21] Hence selective sensing methodologies of Fe^{3+} are extremely important.[22] Fe^{3+} being paramagnetic, exhibits luminescence quenching behavior.[23] As a result, only few reports on "turn-ON" luminescence chemodosimeters for Fe^{3+} are available.[24] Our studies show that **Ru-Ptz** in MeOH can serve as a chemodosimeter for Fe^{3+}, although high concentrations of Fe^{3+} (0.5 – 1.0 mM) are requied to observe the visible glow (Figure 4.26 B). It is to be mentioned that **Ru-Ptz** in MeOH will not show luminescence enhancement in the presene of Cu^{2+} (Figure 4.26 B).

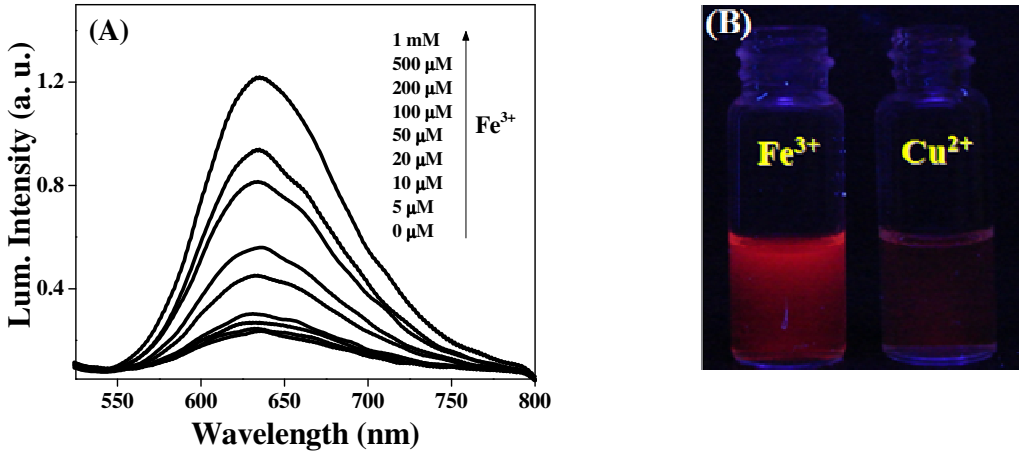

Figure 4.26. (A) Emission spectra of **Ru-Ptz** in MeOH in the presence of Fe^{3+} (0 to 1 mM, each spectrum recorded 1 h after mixing). **(B)** Photograph of **Ru-Ptz** in MeOH in the presence of Fe^{3+} and Cu^{2+} (1 mM) under illumination.

In the case of Fe^{3+}, maximum luminescence enhancement observed is only six fold. The selectivity of Fe^{3+} over Cu^{2+} for the **Ru-Ptz/**MeOH system is also presented in

the form of a bar graph in Figure 4.27. Cu^{2+} resulted in a nominal enhancement of luminescence in MeOH.

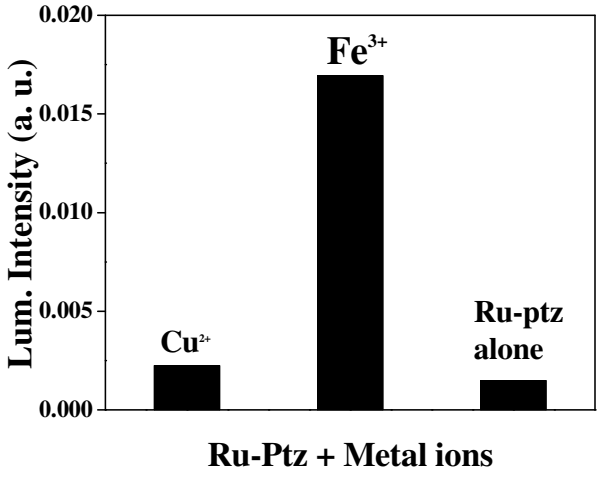

Figure 4.27. Bar graph showing the emission intensity of **Ru-Ptz** in the presence of Cu^{2+} and Fe^{3+} in MeOH.

Detection of Fe^{3+} in this manner suffers from three major disadvantages. (1) maximum luminescence intensity was observed at > 1 mM Fe^{3+}, which is about 20 times higher than in the case of Cu^{2+} in ACN; (2) the reaction is very slow and even at 1 mM Fe^{3+} maximum intensity was observed 2-3 h after mixing and (3) the luminescence enhancement for **Ru-Ptz**/Fe^{3+} in MeOH was nearly three times smaller than that of **Ru-Ptz**/Cu^{2+} in ACN. Because of these reasons, **Ru-Ptz** in MeOH is not a good dosimeter for Fe^{3+}.

We confirmed from absorption spectral studies that in the case of Fe^{3+} in MeOH also, the luminescence enhancement occurs through the two-electron oxidation of the Ptz moiety to PtzO. Figure 4.28 shows the absorption spectra of **Ru-Ptz** in MeOH in the

absence and presence of Fe^{3+}. The difference spectrum in the 300-600 nm, shown in the inset of Figure 4.28, is identical to $Ptz^{\bullet+}$ absorption suggesting the oxidation of Ptz by Fe^{3+} in this solvent medium. This absorption decays with time as in the case of **Ru-Ptz**/Cu^{2+} in ACN suggesting the conversion of $Ptz^{\bullet+}$ to stable PtzO. We thus conclude that luminescence enhancement of **Ru-Ptz** in the presence of Fe^{3+} in MeOH is due to the oxidation of **Ru-Ptz** to Ru-PtzO by Fe^{3+}.

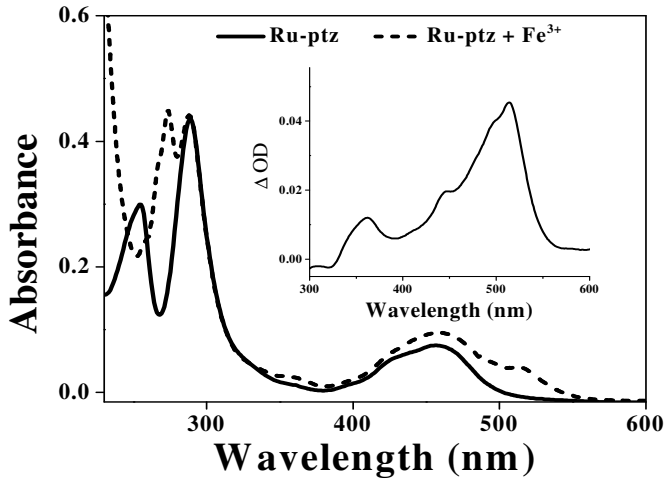

Figure 4.28. Absorption spectra of **Ru-Ptz** (7×10^{-6} M) and **Ru-Ptz**/Fe^{3+} (7×10^{-6} / 1.4×10^{-5} M) in MeOH. The difference spectrum in the 350-600 nm region is shown in the inset.

4.4. Conclusions

In summary, we have demonstrated potential applications for **Ru-Ptz** dyads in the metal sensing area. Design of metal ion sensors or dosimeters based on $Ru(bpy)_3^{2+}$ is highly desirable because of its excellent photochemical and redox behaviours. A hitherto unused strategy, namely the enhancement of oxidative ability of Cu^{2+} in ACN by nearly 1 eV compared to that in water, was exploited here to design dosimeters for

Cu^{2+}. Although this property of Cu^{2+} was known for several years, it was seldom used for any applications in organic chemistry. Only Cu^{2+} is capable of this reaction and hence the chemodosimeter is very selective. In principle, the strategy offers a general approach to "turn-ON" luminescence detection of Cu^{2+} in that any fluorophore that can be quenched reductively by NMPtz could be employed in place of $Ru(bpy)_3^{2+}$, making it possible to tune the emission color and detection limit. We also showed that the same probe can act as a chemodosimeter for the detection of Fe^{3+} in MeOH, though the sensitivity and the luminescence enhancement factors were smaller.

4.5. Experimental Section

4.5.1. Materials. All metal salts were commercial samples and used as received. Metal perchlorates were used except for Fe^{3+}, for which the chloride salt was used. Acetonitrile and methanol used were of spectroscopic grade.

Synthesis and characterization of **Ru-Ptz**, **Ru-Pt$_2$** and **Ru-Ptz$_3$** were reported in Chapter 2 of this thesis. Synthesis of **Ru-Ptz$_{2(S)}$** was reported in Chapter 3. Model compounds **Ru-Ph**[25] and NMPtz[26] were prepared and purified by reported procedures. Reaction of NMPtz with Cu^{2+} was carried out as follows.

To a solution of NMPtz (0.1 g, 0.47 mM) in ACN (10 mL), copper(II) perchlorate hexahydrate (0.87 g, 2.35 mM) was added and the solution was stirred overnight. The mixture was diluted with dichloromethane and filtered through a neutral alumina column. Solvent was then evaporated and the residue was recrystallized from 1:8 dichloromethane-hexane mixture to get NMPtzO, 0.96 g (89%); mp 184-85°C

(reported mp 191.5-192.5 °C);[27] FT-IR (KBr) ν = 3093, 2918, 2868, 1575, 1530, 1454, 1216, 1159, 1130, 1099, 871, 769 cm^{-1}; ^1H NMR (300 MHz, $CDCl_3$): δ 3.77 (s, 3H), 7.25 (t, 2H), 7.39 (d, 2H), 7.62 (t, 2H), 7.93 (d, 2H); Elemental Analysis: Calcd for $C_{13}H_{11}NOS$: C, 68.09; H, 4.84; N, 6.11. Found: C, 67.72; H, 4.62; N, 5.94.

4.5.2. Measurements. A 1 cm path quartz cell was used for spectroscopic and luminescence measurements. UV-Vis spectra were recorded on a Shimadzu UV-3101 PC NIR Scanning Spectrometer. Steady-state luminescence experiments were performed on a spectrofluorimeter SPEX Fluorolog F112X with a 450 W xenon lamp. For all measurements optically dilute solutions (optical density < 0.1 at the excitation wavelength 440 nm) were used. Emission quantum yields were obtained using $[Ru(bpy)_3]Cl_2$ as reference.[14] Luminescence titration experiments were performed by progressive addition of aliquots of 10 mM solutions of metal salts to solutions of Ru-Ptz systems. Emission lifetime measurements were performed using an IBH picosecond single photon counting system employing a 440 nm nano-LED excitation source and a Hamamatsu C4878-02 MCP detector. Cyclic voltammograms were obtained using voltammetric analyzer BAS 50W in argon purged ACN solutions with 0.1 M tetra-*n*-butylammonium hexafluorophosphate as supporting electrolyte.

4.6. References

(1) (a) Czarnik, A. W. in *Frontiers in Supramolecular Organic Chemistry and Photochemistry*, Schneider, H.-J. ; Dürr, H. Eds. ; VCH Weinheim, **1991**, pp 109-122. (b) *Fluorescent Chemosensors for Ion and Molecule Recognition*; Czarnik,

A. W. Ed.; ACS Symposium Series 538; American Chemical Society: Washington, DC, 1993. (c) de Silva, A. P.; Gunaratne, H. Q. N.; Gunnlaugsson, T.; Huxley, A. J. M.; McCoy, C. P.; Rademacher, J. T.; Rice, T. E. *Chem. Rev*. **1997**, *97*, 1515-1566. (d) *Chemosensors for Ion and Molecule Recognition*; Desvergne, J. P.; Czarnik, A. W. Eds.; Kluwer Academic Publishers: Dordrecht, The Netherlands, **1997**. (e) Prodi, L.; Bolletta, F.; Montalti, M.; Zaccheroni, N. *Coord. Chem. Rev*. **2000**, *205*, 59-83. (f) Rogers, C. W.; Wolf, M. O. *Coord. Chem. Rev*. **2002**, *233-234*, 341-350. (g) de Silva, A. P.; McCaughan, B.; McKinney, B. O. F.; Querol, M. *Dalton Trans.* **2003**, 1902-1913. (h) Anslyn, E. V. *J. Org. Chem.* **2007**, *72*, 687-699.

(2) (a) *Metal Ions in Biological Systems, Properties of Copper*; Sigel, H. Ed.; Marcel Dekker, Inc.: New York, **1981**; vol.12. (b) da Silva, J. J. R. F.; Williams, R. J. P. *The Biological Chemistry of the Elements*: *The Inorganic Chemistry of Life*; Clarendon: Oxford, **1991**. (c) Barceloux, D. G. *J. Toxicol-Clin. Toxicol*. **1999**, *37*, 217-230.

(3) Georgopoulos, P. G.; Roy, A.; Yonone-Lioy, M. J.; Opiekun, R. E.; Lioy, P. J. *J. Toxicol. Env. Health, B* **2001**, 4, 341-394.

(4) (a) Forstner, U.; Wittmann, G. T. *Metal pollution in the aquatic environment*; Springer, Berlin Heidelberg: New York, **1981**; p. 8. (b) Merian, E. *Metals and their compounds in the environment: Occurrence, Analysis and Biological Relevance*; VCH: Weinheim**, 1991**; p. 893.

(5) (a) Kramer, R. *Angew. Chem., Int. Ed*. **1998**, *37*, 772-773. (b) Torrado, A.; Walkup, G. K.; Imperiali, B. *J. Am. Chem. Soc*. **1998**, *120*, 609-610. (c) Grandini, P.; Mancin, F.; Tecilla, P.; Scrimin, P.; Tonellato, U. *Angew. Chem., Int. Ed.* **1999**, *38*, 3061-3064. (d) Bhattacharya, S.; Thomas, M. *Tetrahedron Lett*. **2000**, *41*, 10313-10317. (e) Beltramello, M.; Gatos, M.; Mancin, F.; Tecilla, P.; Tonellato, U. *Tetrahedron Lett*. **2001**, *42*, 9143-9146. (f) Zheng, Y.; Gattas-Asfura, K. M.; Konka, V.; Leblanc, R. M. *Chem. Commun*. **2002**, 2350-2351. (g) Zheng, Y.; Orbulescu, J.; Ji, X.; Andreopoulos, F. M.; Pham, S. M.; Leblanc, R. M. *J. Am. Chem. Soc.* **2003**, *125*, 2680-2686. (h) Gattas-Asfura, K. M.; Leblanc, R. M. *Chem. Commun*. **2003**, 2684-2685. (i) Zeng, H.-H.; Thompson, R. B.; Maliwal, B. P.; Fones, G. R.; Moffett, J. W.; Fierke, C. A. *Anal. Chem.* **2003**, *75*, 6807-6812. (j) Gunnlaugsson, T.; Leonard, J. P.; Murray, N. S. *Org. Lett*. **2004**, *6*, 1557- 1560. (k) Royzen, M.; Dai, Z.; Canary, J. W. *J. Am. Chem. Soc*. **2005**, *127*, 1612-1613. (l) Banthia, S.; Samanta, A. *New J. Chem.* **2005**, *29*, 1007-1010. (m) Shervedani, R. K.; Mozaffari, S. A. *Anal. Chem.* **2006**, *78*, 4957-4963. (n) Qi, X.; Jun, E. J.; Kim, S.-J.; Hong, J. J. S.; Yoon, Y. J.; Yoon, J. *J. Org. Chem.* **2006**, *71*, 2881-2884. (o) Xie, J.; Menand, M.; Maisonneuve, S.; Metivier, R. *J. Org. Chem.* **2007**, *72*, 5980-5985.

(6) (a) Yoon, J.; Ohler, N. E.; Vance, D. H.; Aumiller, W. D.; Czarnik, A. W. *Tetrahedron Lett*. **1997**, *38*, 3845-3848. (b) Bodenant, B.; Weil, T.; Businelli-Pourcel, M.; Fages, F.; Barbe, B.; Pianet I.; Laguerre, M. *J. Org. Chem*. **1999**, *64*, 7034-7039. (c) Klein, G.; Kaufmann, D.; Schurch S.; Reymond, J.-L. *Chem.*

Commun. **2001**, 561-562. (d) Zheng, Y.; Huo, Q.; Kele, P.; Andreopoulos, F. M.; Pham S. M.; Leblanc, R. M. *Org. Lett.* **2001**, *3*, 3277-3280. (e) Boiocchi, M.; Fabbrizzi, L.; Licchelli, M.; Sacchi, D.; Vazquez, M.; Zampa, C. *Chem. Commun*. **2003**, 1812-1813. (f) Zheng, Y.; Cao, X.; Orbulescu, J.; Konka, V.; Andreopoulos, F. M.; Pham, S. M.; Leblanc, R. M. *Anal. Chem.* **2003**, *75*, 1706-1712. (g) Roy, B. C.; Chandra, B.; Hromas, D.; Mallik, S. *Org. Lett.* **2003**, *5*, 11-14. (h) Kaur, S.; Kumar, S. *Tetrahedron Lett.* **2004**, *45*, 5081-5085. (i) Mei, Y.; Bentley, P. A.; Wang, W. *Tetrahedron Lett.* **2006**, *47*, 2447-2449. (j) Zhang, X.-B.; Peng, J.; He, C.-L.; Shen, G.-L.; Yu, R.-Q. *Anal. Chim. Acta* **2006**, *567*, 189-195. (k) Comba, P.; Kramer, R.; Mokhir, A.; Naing, K.; Schatz, E. *Eur. J. Inorg. Chem.* **2006**, 4442-4448. (l) Kim, S. H.; Kim, J. S.; Park, S. M.; Chang, S.-K. *Org. Lett.* **2006**, *8*, 371-374. (m) White, B. R.; Holcombe, J. A. *Talanta* **2007**, *71*, 2015-2020. (n) Oter, O.; Ertekin, K.; Kirilmis, C.; Koca, M. *Anal. Chim. Acta* **2007**, *584*, 308-314. (o) Ghosh, P.; Bharadwaj, P. K.; Mandal, S.; Ghosh, S. *J. Am. Chem. Soc*. **1996**, *118*, 1553-1554. (p) Kaur, S.; Kumar, S. *Chem. Commun.* **2002**, 2840-2841.

(7) (a) Ghosh, P.; Bharadwaj, P. K.; Mandal, S.; Ghosh, S. *J. Am. Chem. Soc*. **1996**, *118*, 1553-1554. (b) Ghosh, P.; Bharadwaj, P. K.; Roy, J.; Ghosh, S. *J. Am. Chem. Soc.* **1997**, *119*, 11903-11909.

(8) (a) Kaur, S.; Kumar, S. *Chem. Commun.* **2002**, 2840-2841. (b) Qi, X.; Jun, E. J.; Xu, L.; Kim, S.-J.; Hong, J. S. J.; Yoon, Y. J.; Yoon, J. *J. Org. Chem.* **2006**, *71*, 2881-2884. (c) Zeng, L.; Miller, E. W.; Pralle, A. Isacoff, E. Y.; Chang, C. J. *J. Am. Chem. Soc.* **2006**, *128*, 10-11. (d) Zheng, Y.; Orbulescu, J.; Ji, X.;

Andreopoulos, F. M.; Pham, S. M.; Leblanc, R. M. *J. Am. Chem. Soc.* **2003**, *125*, 2680-2686. (e) Xu, Z.; Xiao, Y.; Qian, X.; Cui, J.; Cui, D. *Org. Lett.* **2005**, *7*, 889-892. (f) Xu, Z.; Qian, X.; Cui, J. *Org. Lett.* **2005**, *7*, 3029-3032.

(9) (g) Dujols, V.; Ford, F.; Czarnik, A. W. *J. Am. Chem. Soc.* **1997**, *119*, 7386-7387.

(10) (a) Xiang, Y.; Li, Z.; Chen, X.; Tong, A. *Talanta* **2008**, *74*, 1148-1153. (b) Zhang, X.; Shiraishi, Y.; Hirai, T. *Org. Lett.* **2007**, *9*, 5039-5042. (c) Mei, L.; Xiang, Y.; Li, N.; Tong, A. *Talanta* **2007**, *72*, 1717-1722. (d) Martinez, R.; Zapata, F.; Caballero, A.; Espinosa, A.; Tarraga, A.; Molina, P. *Org. Lett.* **2006**, *8*, 3235-3238.

(11) Ramachandram, B.; Samanta, A. *J. Chem. Soc., Chem. Commun.* **1997**, 1037-1038.

(12) (a) Martinez, R.; Zapata, F.; Caballero, A.; Espinosa, A.; Tarraga, A.; Ramachandram, B.; Samanta, A. *J. Phys. Chem. A* **1998**, *102*, 10579–10587. (b) Mitchell, K. A.; Brown, R. G.; Yuan, D.; Chang, S.-C.; Utecht, R. E.; Lewis, D. E. *J. Photochem. Photobiol., A* **1998**, *115*, 157–161. (c) Ramachandram, B.; Saroja, G.; Sankaran, N. B.; Samanta, A. *J. Phys. Chem. B* **2000**, *104*, 11824–11832. (d) Yang, J.-S.; Lin, C.-S.; Hwang, C.-Y. *Org. Lett.* **2001**, *3*, 889-892. (e) Wu, Q.; Anslyn, E. V. *J. Am. Chem. Soc.* **2004**, *126*, 14682-14683. (f) Wen, Z.-C.; Yang, R.; He, H.; Jiang, Y.-B. *Chem. Commun.* **2006**, 106-108. (g) Yang, H.; Liu, Z.-Q.; Zhou, Z.-G.; Shi, E.-X.; Li, F.-Y.; Du, Y.-K.; Yi, T.; Huang, C.-H. *Tetrahedron Lett.* **2006**, *47*, 2911-2914.

(13) Sumalekshmy, S.; Gopidas, K. R. *Chem. Phys. Lett.* **2005**, *413*, 294-299.

(14) Kirchgessner. M.; Sreenath, K.; Gopidas, K. R. *J. Org. Chem*. **2006**, *71*, 9849-9852.

(15) Sreenath, K.; Suneesh, C. V.; Kumar, V. K. R.; Gopidas, K. R. *J. Org. Chem.* **2008**, *73*, 3245-3251.

(16) (a) Warren, R. J.; Eisdorfer, I. B.; Thompson, W. E.; Zarembo, J. E. *J. Pharm. Sci.* **1966**, *55*, 144-150. (b) *Advances in Heterocyclic Chemistry*; Katritzky, A. R.; Boulton, A. J. Eds.; Academic Press: New York, 1968; vol. 9, p. 321-460.

(17) (a) Parker, A. J. *Pure Appl. Chem.* **1981**, *53*, 1437-1445. (b) Persson, I. *Pure Appl. Chem.* **1986**, *58*, 1153-1161. (c) Cox, B. G.; Jedral, W.; Palou, J. *J. Chem. Soc. Dalton Trans.* **1988**, 733-740. (d) Kamau, P.; Jordan, R. B. *Inorg. Chem.* **2001**, *40*, 3879-3883.

(18) Mann, C. K.; Barnes, K. K. *Electrochemical Reactions in Nonaqueous Systems*; Marcel Dekker, Inc., New York, 1970, p. 312.

(19) Juris, A.; Balzani, V.; Barigeletti, F.; Campagna, S.; Belser, P.; von Zelewsky, A. *Coord. Chem. Rev.* **1988**, *84*, 85-277.

(20) Bard, A. J. (Ed.), *Encyclopedia of Electrochemistry of the Elements*, Dekker, New York, 1974.

(21) Burdo, J. R.; Connor, J. R. *Biometals* **2003**, *16*, 63-75.

(22) (a) Pehkonen, S. *Analyst* **1995**, *120*, 2655-2663. (b) Tumambac, G. E.; Rosencrance, C. M.; Wolf, C. *Tetrahedron* **2004**, *60*, 11293-11297. (c) Bricks, J. L.; Kovalchuk, A.; Trieflinger, C.; Nofz, M.; Büschel, M.; Tolmachev, A. I.; Daub, J.; Rurack, K. *J. Am. Chem. Soc.* **2005**, *127,* 13522-13529. (d) Wallace, K. J.; Gray, M.; Zhong, Z.; Lynch, V. M.; Anslyn, E. V. *Dalton Trans.* **2005**, 2436-2441.

(23) (a) Weizman, H.; Ardon, O.; Mester, B.; Libman, J.; Dwir, O.; Hadar, Y.; Chen, Y.; Shanzer, A. *J. Am. Chem. Soc*. **1996**, *118*, 12368-12375. (b) Hankovszky, O. H.; Kalai, T.; Hideg, E.; Jeko, J.; Hideg, K. *Synth. Commun*. **2001**, *31*, 975-986. (c) Liu, J.-M.; Zhenng, Q.-Y.; Yang, J.-L.; Chen, C.-F.; Huang, Z.-T. *Tetrahedron Lett*. **2002**, *43*, 9209-9212. (d) Wolf, C.; Mei, X.; Rokadia, H. K. *Tetrahedron Lett*. **2004**, *45*, 7867-7871 . (e) Ma, L.; Luo, W.; Quinn, P. J.; Liu, Z.; Hider, R. C. *J. Med. Chem.* **2004**, *47*, 6349-6362. (f) Sumner, J. P.; Kopelman, R. *Analyst* **2005**, *130*, 528-533.

(24) (a) Guo, X.; Zhang, D.; Zhu, D. *Adv. Mater.* **2004**, *16*, 125-130. (b) Hua, J.; Wang, Y.-G. *Chem. Lett.* **2005**, *34*, 98-99. (c) Xiang, Y.; Tong, A. J. *Org. Lett*. **2006**, *8*, 1549-1552. (d) Zhang, M.; Gao, Y.; Li, M.; Yu, M.; Li, F.; Li, L.; Zhu, M.; Zhang, J.; Yi, T.; Huang, C. *Tetrahedron Lett*. **2007**, *48*, 3709-3712. (e) Bae, S.; Tae, J. *Tetrahedron Lett.* **2007**, *48*, 5389-5392.

(25) Gehlen, M. H.; de Carvalho, I. M. M.; de Sousa Moreira, I. *Inorg. Chem.* **2003***, 42,* 1525-1531.

(26) Sakaguchi, M.; Hu, M.; Kevan, L. *J. Phy. Chem.* **1990**, *94*, 870-874.

(27) Brown, G. P.; Cole, J. W.; Crowell, T. I. *J. Org. Chem.* **1955**, *20*, 1772-1776.

List of Publications

1. Phenothiazine substituted $Ru(bpy)_3^{2+}$ derivative as highly selective "turn-ON" luminescence chemodosimeter for Cu^{2+}.
   Ajayakumar, G.; Sreenath, K.; Gopidas, K. R.
   Dalton Trans., DOI: 10.1039/b813765j (**2008**) (**Accepted for publication**).

2. Long-Lived Photoinduced Charge Separation in new $Ru(bipyridine)_3^{2+}$ - Phenothiazine dyads.
   Ajayakumar, G.; Gopidas, K. R.
   Photochem. Photobiol. Sci., **7**, 826-833 (**2008**).

3. Structure Absorption Spectra Correlation in a Series of 2,6-Dimethyl-4-arylpyrylium Salts.
   Manoj, N.; **Ajayakumar, G.**; Gopidas, K. R.; Suresh, C. H.
   J. Phys. Chem. A, **110**, 11338-11345 (**2006**).

Posters Presented at Conferences

1. Long-lived Photoinduced Charge Separation in new $Ru(bipyridine)_3^{2+}$-Phenothiazine Dyads.
   G. Ajayakumar and K. R. Gopidas
   In ***"10th National Symposium in Chemistry"*** by CRSI held at IISc, Bangalore, February 01-03, 2008.

2. Photoinduced Electron Transfer in Covalently Linked $Ru(bipyridine)_3^{2+}$-Phenothiazine Systems.
   G. Ajayakumar and K. R. Gopidas
   In ***"Indo-Japan Cooperative Science Programme"***, held at Trivandrum, January, 20-22, 2008.